第60回　物性若手夏の学校講義
2015年7月28-30日
@ぎふ長良川温泉ホテルパーク
良光殿

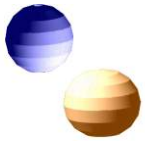

メタマテリアルの世界

東北大学大学院理学研究科物理学専攻
石原照也

メタマテリアルとは

（電磁場に対する）特異な応答がその構成物質の性質でなく、その構造に由来する人工複合構造体

μετα=beyond

特异介质 (te yi jie zhi) = 特異介質

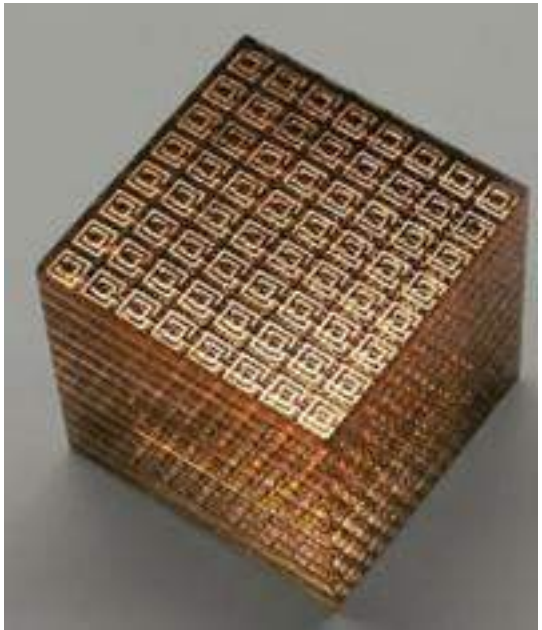

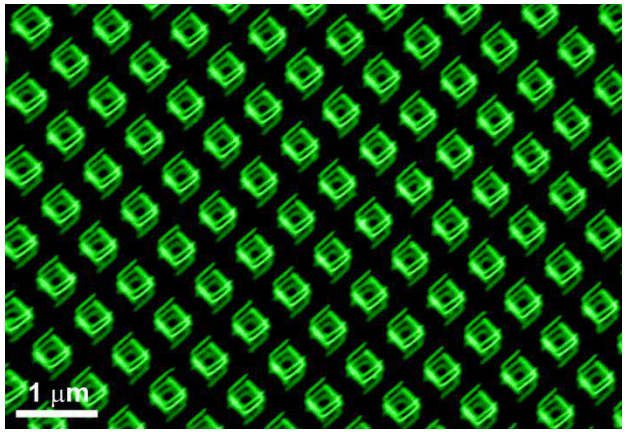

マイクロ波および
光領域のメタマテリアルの実例

メタマテリアルに関係する論文数の推移

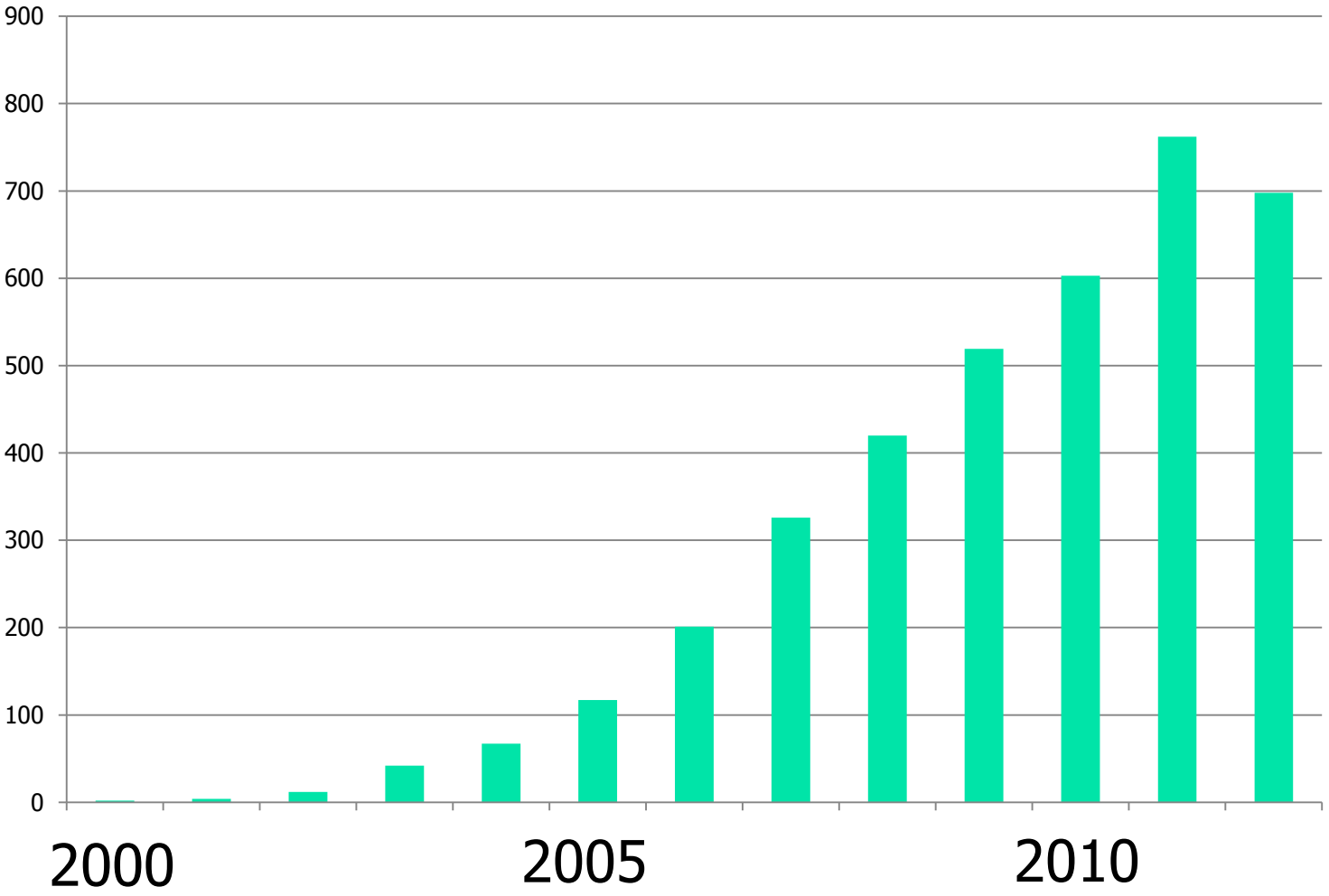

*From ISI database: keyword=metamaterial**

講義の予定

1） イントロ、負の屈折率

2） メタマテリアルの波動伝搬、近接場

3） メタマテリアルにおける光物性

着目点：

どのように常識は打ち破られたか？

従来の壁は何だったのか？

1） 負の屈折率

負屈折率の条件
負透磁率を実現する方法
実験的な検証
種々の反論
有効媒質理論
短波長化
有効誘電率･透磁率
伝送線路理論
非フォスター回路

負屈折率の条件

Maxwellの方程式
Veselagoが考えたこと
Maxwell方程式と波動伝搬
負の屈折率をもつ薄板の光学応答
εとμによる物質の分類
メタマテリアルとは
複合構造の均質化
電磁気学を考える
金属円柱配列の透磁率
分割リング共振器の磁気共鳴
金属細線配列の電磁応答

Maxwellの方程式

$$\nabla \times \vec{H} = \frac{\partial \vec{D}}{\partial t}, \qquad \nabla \times \vec{E} = -\frac{\partial \vec{B}}{\partial t}$$

$$\nabla \cdot \vec{D} = \rho, \qquad \nabla \cdot \vec{B} = 0$$

$$\vec{D} = \varepsilon \vec{E}, \qquad \vec{B} = \mu \vec{H}$$

$$\nabla \equiv \begin{pmatrix} \frac{\partial}{\partial x} \\ \frac{\partial}{\partial y} \\ \frac{\partial}{\partial z} \end{pmatrix}$$

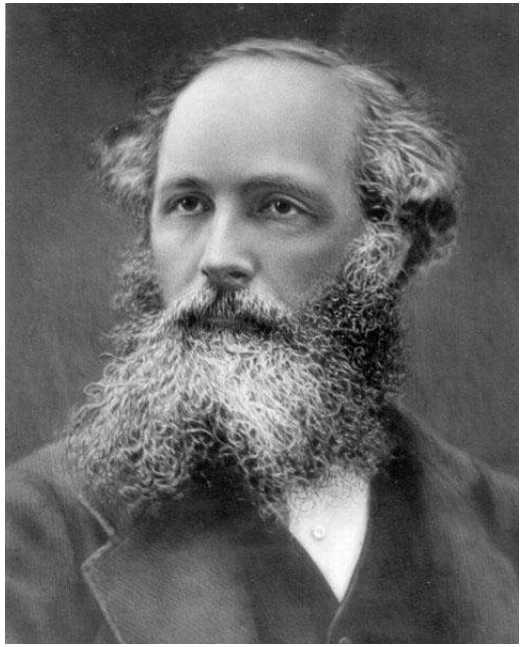

電気的な量：電場 E, 電束密度　D
磁気的な量: 磁場　H, 磁束密度　B
ε: 誘電率, μ: 透磁率

J. C. Maxwell
電気磁気論考(1873).

Veselagoが考えたこと(1967)

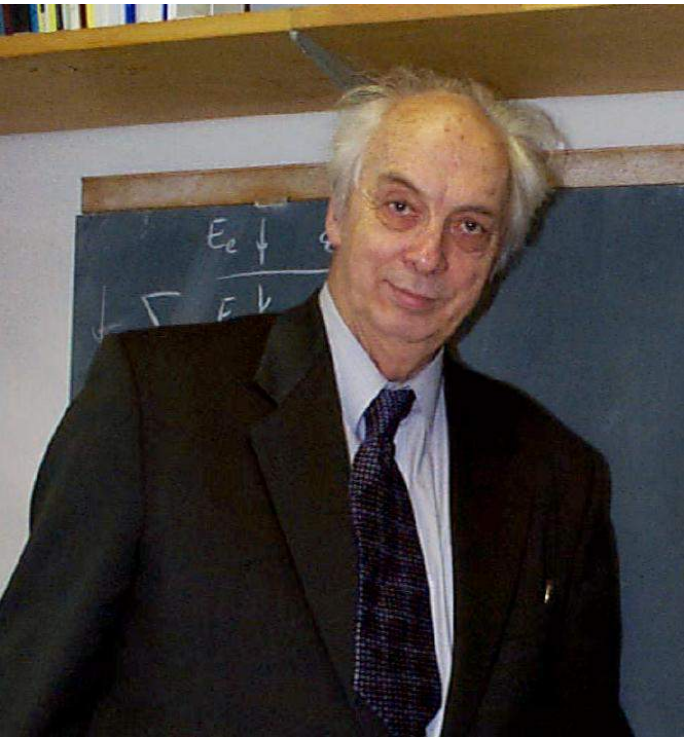

誘電率εと透磁率μが同時に
負であったら何が起こる？

1) 何も変わらない
2) 自然の基本法則によって
そのようなことは起こらない
3)通常の物質とは
異なった性質をもつ

Veselago's paper

1967 г. Июль *Том 92, вып. 3*

УСПЕХИ ФИЗИЧЕСКИХ НАУК

538.30

ЭЛЕКТРОДИНАМИКА ВЕЩЕСТВ С ОДНОВРЕМЕННО ОТРИЦАТЕЛЬНЫМИ ЗНАЧЕНИЯМИ ε И μ

В. Г. Веселаго

I. ВВЕДЕНИЕ

Диэлектрическая проницаемость ε и магнитная проницаемость μ являются основными характеристиками, которые определяют распространение электромагнитных волн в веществе. Это связано с тем, что они являются единственными параметрами вещества, входящими в дисперсионное уравнение

$$\left| \frac{\omega^2}{c^2} \varepsilon_{il} \mu_{lj} - k^2 \delta_{ij} + k_i k_j \right| = 0, \qquad (1)$$

Maxwell方程式と波動伝搬

ε<0, μ<0;
左手系

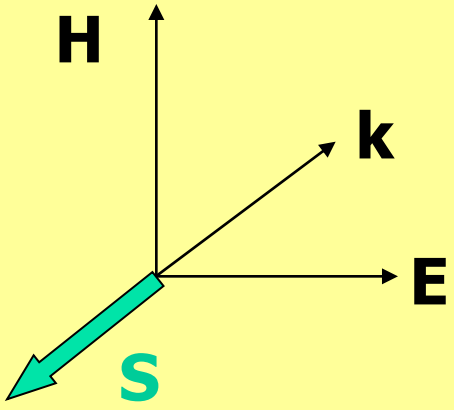

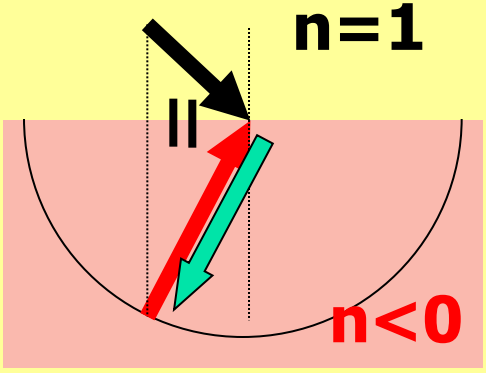

負の屈折

Maxewll 方程式

$$\vec{k}\times\vec{E}=-\omega\mu\mu_0\vec{H}$$

$$\vec{k}\times\vec{H}=+\omega\varepsilon\varepsilon_0\vec{E}$$

分散関係

$$\left(\frac{ck}{\omega}\right)^2\equiv n^2=\varepsilon\mu$$

$$n=\pm\sqrt{|\varepsilon||\mu|}$$

エネルギーの流れ

$$\vec{S}=\vec{E}\times\vec{H}$$

ε>0, μ>0;
右手系

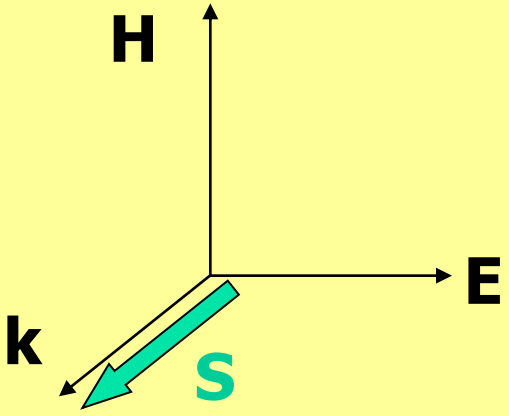

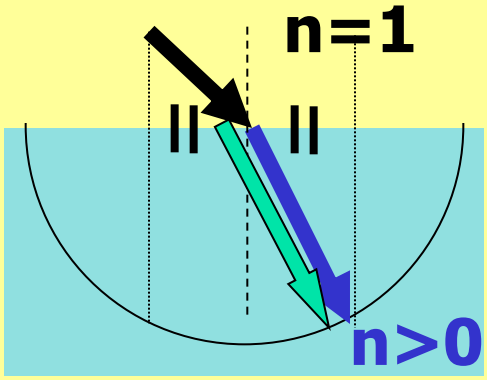

正の屈折

負の屈折率をもつ薄板の光学応答

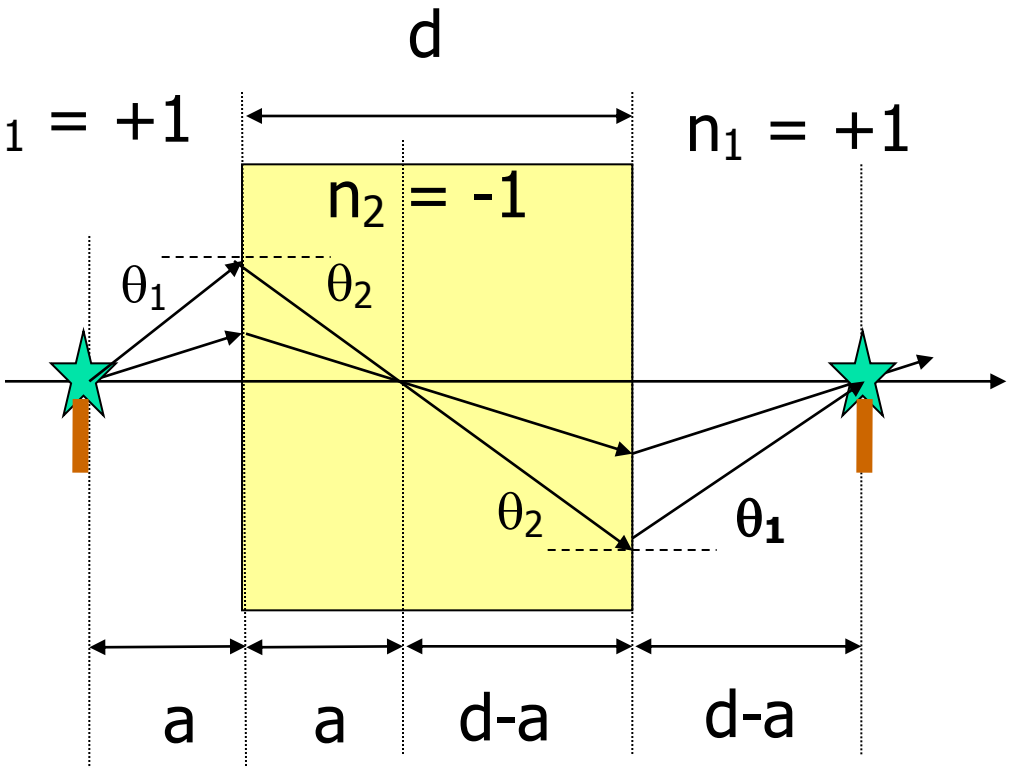

Veselagoレンズ

$$\frac{\sin\theta_1}{\sin\theta_2} = \frac{n_2}{n_1} = \frac{-1}{1} = -1$$

- 正立像を作る
- 遠くにあるものは結像できない

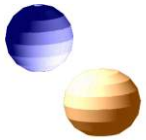

その他のVeselagoの論点

負のチェレンコフ

負のドップラー

負の輻射圧

電磁エネルギーは？

ε と μ による物質の分類

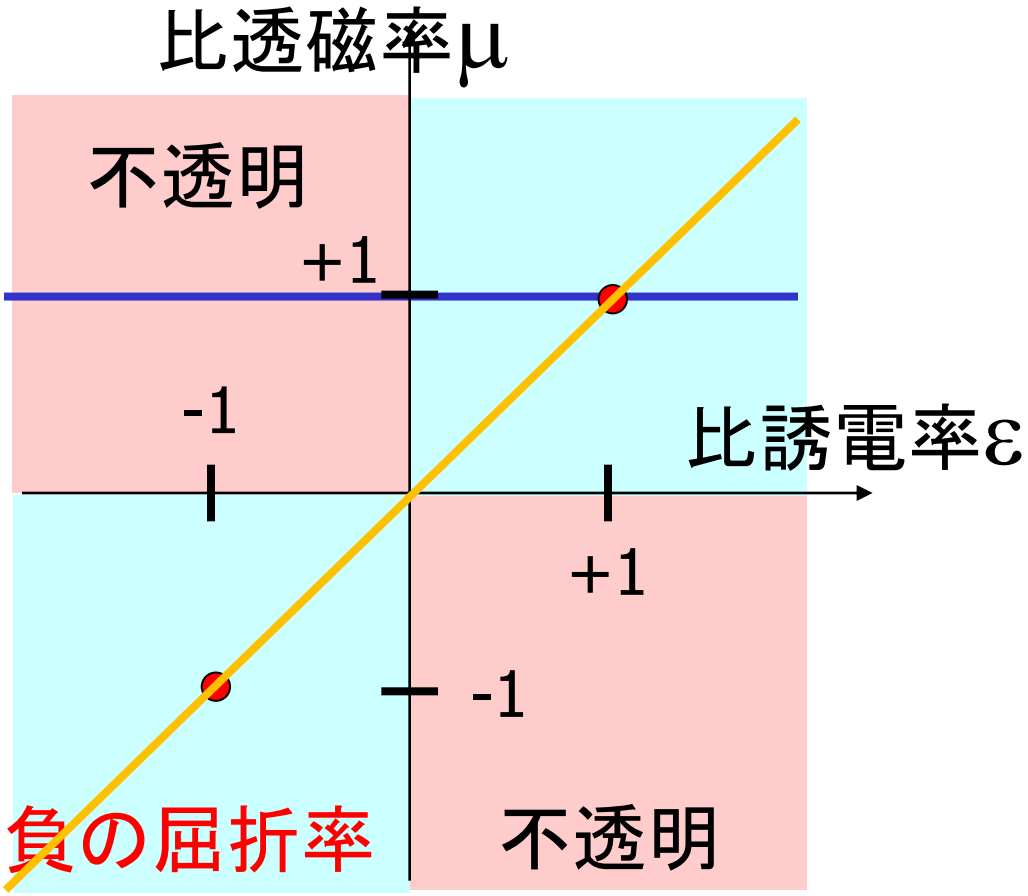

光の周波数では
比透磁率はほとんど1

$$n \equiv \frac{k}{k_0} = \frac{k}{\omega / c} = \sqrt{\varepsilon\mu};$$

$$z = \sqrt{\frac{\mu}{\varepsilon}}; \qquad R = \left(\frac{z-1}{z+1}\right)^2$$

z=1なら反射はない。

複合構造の均質化

IN A SENSE, every material is a composite, even if the individual ingredients consist of atoms and molecules. The original objective in defining a permittivity and permeability was to present an homogeneous view of the electromagnetic properties of a medium. Therefore, it is only a small step to replace the atoms of the original concept with structure on a larger scale.
"Magnetism from Conductors and Enhanced Nonlinear Phenomena" (1999)

$$rot\vec{H} = \frac{\partial \vec{D}}{\partial t}, \qquad rotE = -\frac{\partial \vec{B}}{\partial t}$$

$$\oint_C \vec{H} \cdot d\vec{\ell} = -i\omega \int_S \vec{D} d\sigma$$

$$\oint_C \vec{E} \cdot d\vec{\ell} = +i\omega \int_S B d\sigma$$

Sir. J. B. Pendry

E, Hは縦平均; D, Bは横平均

複合構造の均質化

$$rot\vec{H} = \frac{\partial \vec{D}}{\partial t}, \qquad rotE = -\frac{\partial \vec{B}}{\partial t}$$

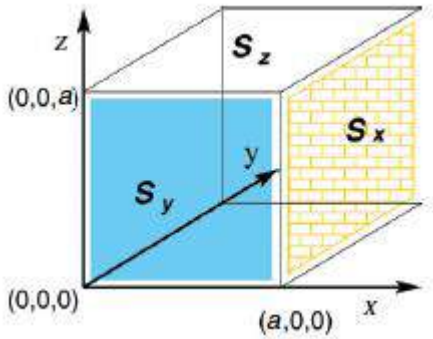

$$\oint_C \vec{H} \cdot d\vec{\ell} = -i\omega \int_S \vec{D} d\sigma$$

$$\oint_C \vec{E} \cdot d\vec{\ell} = +i\omega \int_S B d\sigma$$

$$E_{eff}^{(x)} = \frac{1}{a}\int_{(0,0,0)}^{(a,0,0)} E_x dx, \quad H_{eff}^{(x)} = \frac{1}{a}\int_{(0,0,0)}^{(a,0,0)} H_x dx,$$

$$D_{eff}^{(x)} = \frac{1}{a^2}\int_{S_x} D_x d\sigma_x, \quad B_{eff}^{(x)} = \frac{1}{a^2}\int_{S_x} B_x d\sigma_x, \ldots$$

電磁気学を考える

物質中の電磁場を平均的に表す基本量として、D，B，E，Hの4種のベクトルを定義する。D，Bはそれぞれ、電気力線および磁力線の幾何学的性質を平均的に代表するものである。また、E，Hはそれぞれ力学的性質を代表する。D，Bは微視的な場の‘横の平均’であり、E，Hは対応する微視的な量の‘縦の平均‘である。(p.113)
「電磁気学を考える」(1989)

今井功(1914-2004)
ロゲルギスト I_2

金属円柱配列の透磁率μ

First proposed by J. Pendry (1999)

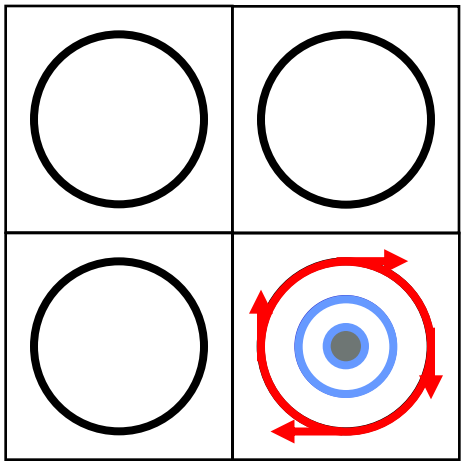

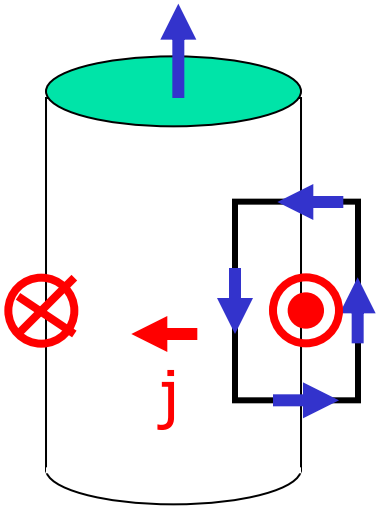

$$H_{in} = H_0 - j + \frac{\pi r^2}{a^2} j < H_0$$

$$H_{out} = H_0 + \frac{\pi r^2}{a^2} j > H_0$$

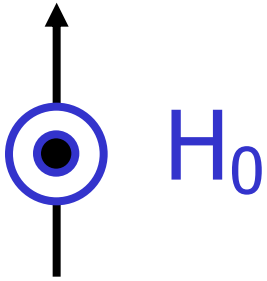

$$\mu_{eff} = \frac{B_{eff}}{\mu_0 H_{eff}} = 1 - \frac{\pi r^2 / a^2}{1 + i2\rho/(\mu_0 \omega r)} < 1$$

分割リング共振器の磁気共鳴

First proposed by J. Pendry (1999)

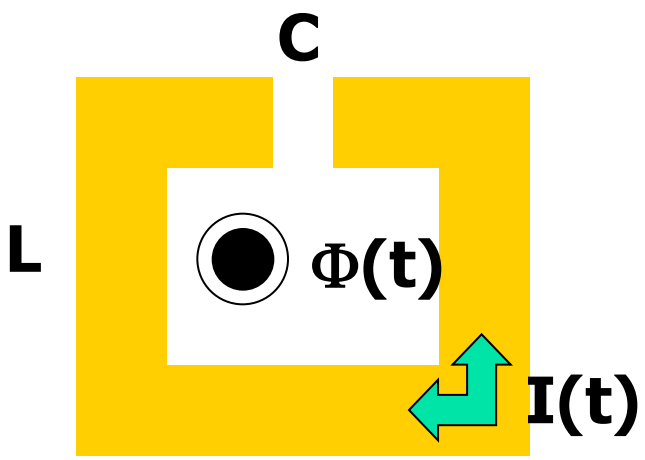

$$L\dot{I} + \frac{1}{C}\int I dt = -\frac{d\Phi}{dt}$$

$$\Phi = \mu_0 HS$$

$$\ddot{I} + \frac{1}{LC} I = \omega^2 \frac{\mu_0 S}{L} H$$

$$M = \frac{N}{V} IS = \chi_m H$$

$$\mu = 1 + \chi_m = 1 + \frac{f\omega^2}{\omega_{LC}^2 - \omega^2}$$

金属細線配列の電磁応答

First proposed by J. Pendry et al. (1998)

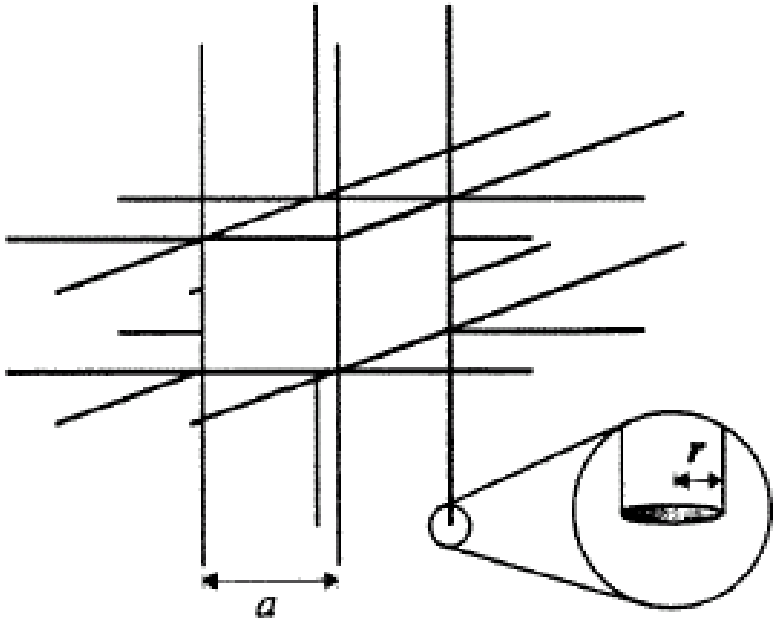

$$\varepsilon(\omega) = 1 - \frac{{\omega_P}^2}{\omega(\omega + i\gamma)}$$

$${\omega_P}^2 = \frac{n_{eff} e^2}{\varepsilon_0 m_{eff}} = \frac{2\pi {c_0}^2}{a^2 \ln(a/r)}$$

実験的検証

最初のメタマテリアル

メタマテリアルに関する最初の論文

負の屈折に関する最初の実験報告

最初のメタマテリアル

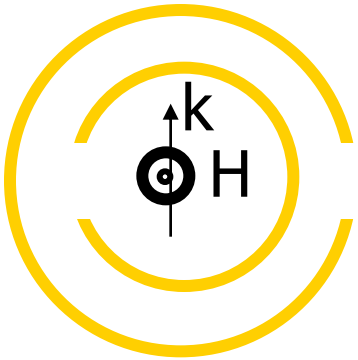

分割リング共振器:
透磁率の共鳴

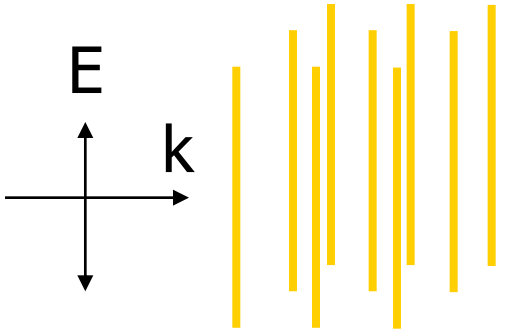

金属細線:
負の誘電率

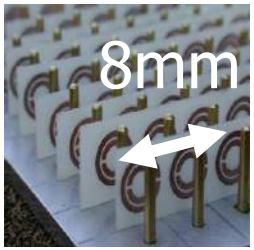

負の屈折率をもった
最初のメタマテリアル
@5GHz (λ = 6cm)
Smith et al. (2000)

メタマテリアルに関する最初の論文

Composite Medium with Simultaneously Negative Permeability and Permittivity

D. R. Smith,* Willie J. Padilla, D. C. Vier, S. C. Nemat-Nasser, and S. Schultz

Department of Physics, University of California, San Diego, 9500 Gilman Drive, La Jolla, California 92093-0319

(Received 2 December 1999)

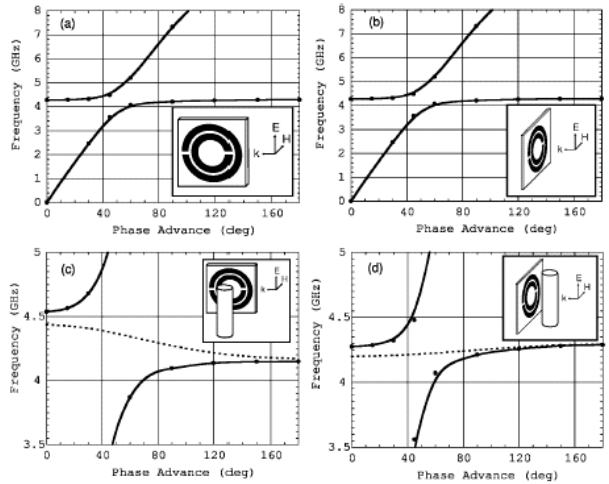

FIG. 2. (a) Dispersion curve for the parallel polarization $H_{\parallel}$. The lines with the solid circles correspond to the split ring resonators only. The inset shows the orientation of the split ring with respect to the incident radiation. The horizontal axis is the phase advance per unit cell, or kd, where k is the wave number. (b) Dispersion curve for the perpendicular polarization $H_{\perp}$. The lines with the solid circles correspond to the split ring resonators only. The inset shows the orientation of the split ring with respect to the incident radiation. (c) Expanded view of the dispersion curve shown in (a). The dashed line corresponds to the split ring resonators with wires placed uniformly between split rings. (d) Expanded view of the dispersion curve shown in (b). The dashed line corresponds to the split ring resonators with wires placed uniformly between split rings. The insets to (c) and (d) show the orientations of the split rings with respect to the wires.

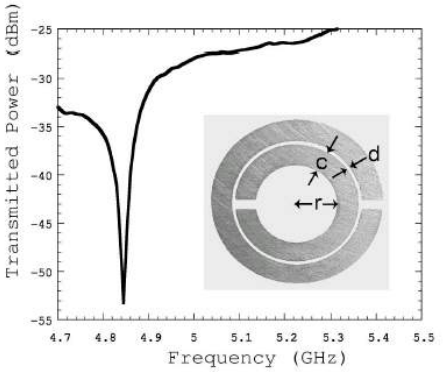

FIG. 1. Resonance curve of an actual copper split ring resonator (SRR). $c = 0.8$ mm, $d = 0.2$ mm, and $r = 1.5$ mm. The SRR has its resonance at about 4.845 GHz, and the quality factor has been measured to be $Q = f_0/\Delta f_{3dB} > 600$, consistent with numerical simulations.

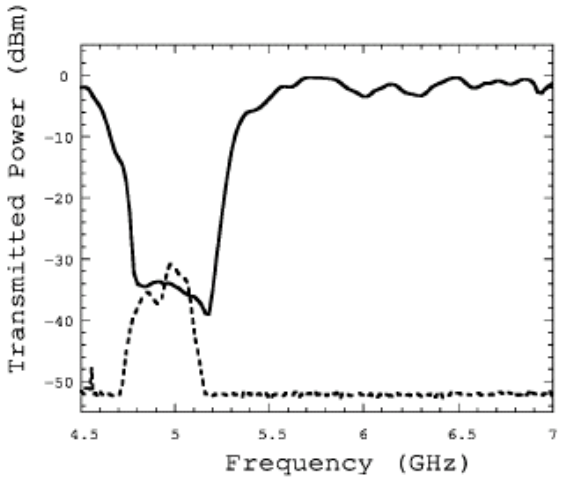

FIG. 3. A transmission experiment for the case of $H_{\parallel}$. The upper curve (solid line) is that of the SRR array with lattice parameter $a = 8.0$ mm. By adding wires uniformly between split rings, a passband occurs where μ and ε are both negative (dashed curve). The transmitted power of the wires alone is coincident with that of the instrumental noise floor (-52 dB).

負の屈折に関する最初の実験報告

Shelby, Smith et al. 2001

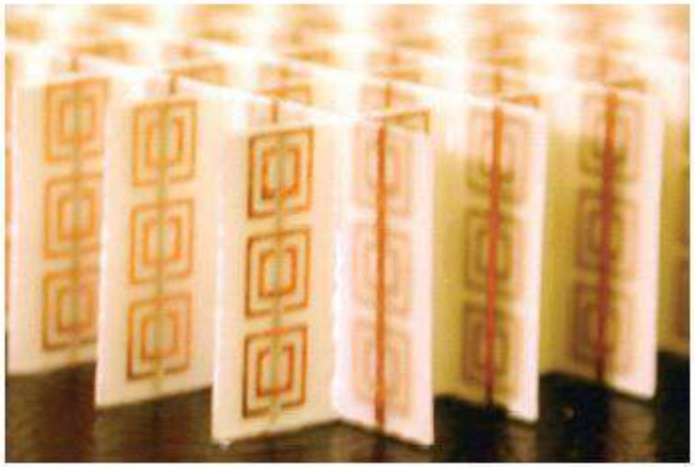

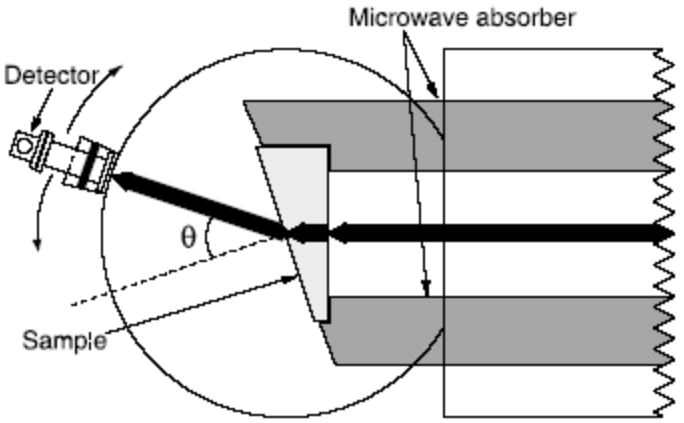

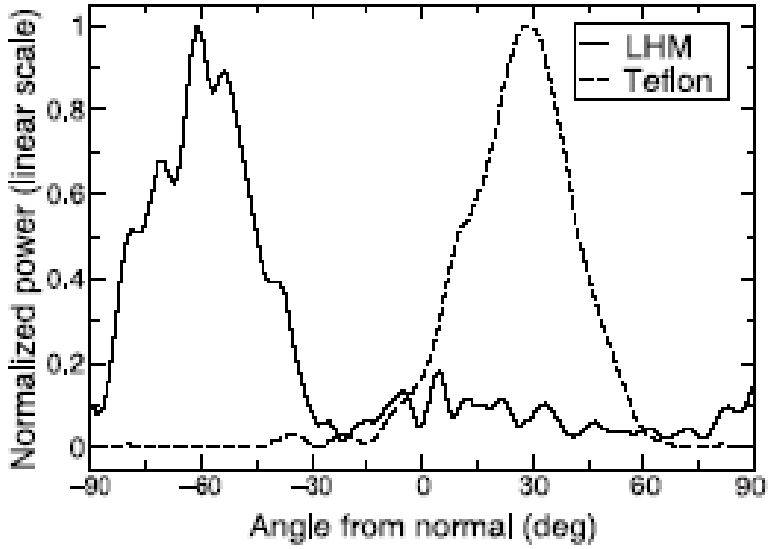

メタマテリアルシンポジウム
2011.3.11@東大本郷

種々の批判

負の屈折が生じるには光速を越えなくてはならない！？

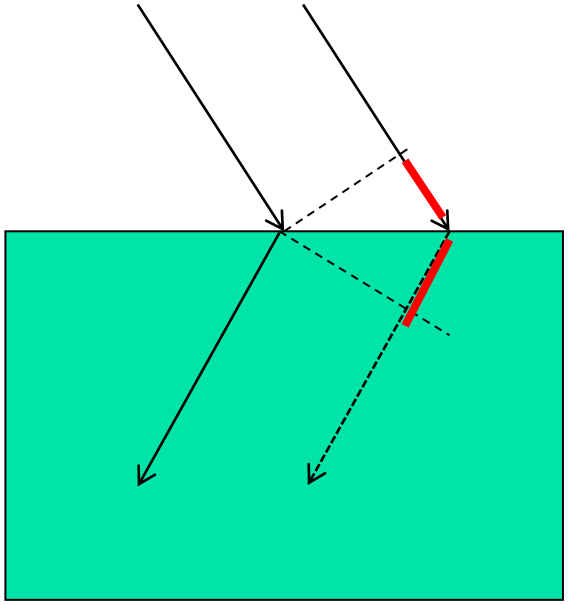

負の屈折が確立するには時間がかかる。
See a movie at Youtube:
https://www.youtube.com/watch?v=PP6HCpIaeKQ

光領域の透磁率

Landau&Lifshitz「連続媒質の電気力学」
光領域（GHz領域ですでに）の透磁率は意味がない。

R. Merlin（PNAS 106(2009)1693.）
PNAS =*proceedings of national academy of sciences of USA*

$$\mathrm{Im}\sqrt{\varepsilon_S} >> \lambda/\ell \quad \text{or} \quad \mathrm{Re}\sqrt{\varepsilon_S} \approx \lambda/\ell$$

の場合、ランダウの議論は成り立たない

電磁エネルギー

誘電率と透磁率が同時に負なら、エネルギー密度は負？

$$u = \frac{\varepsilon}{2} E^2 + \frac{\mu}{2} H^2 \quad < 0 \quad ?$$

誘電率、透磁率が分散をもつ場合には
以下の式が正しいエネルギー密度を与える。

$$u = \frac{1}{2} \frac{\partial(\varepsilon\omega)}{\partial\omega} E^2 + \frac{1}{2} \frac{\partial(\mu\omega)}{\partial\omega} H^2 \quad > 0$$

人工電磁媒質の粗視化：1

$$B_{ave} = \mu\ \mu_0 H_{ave}$$

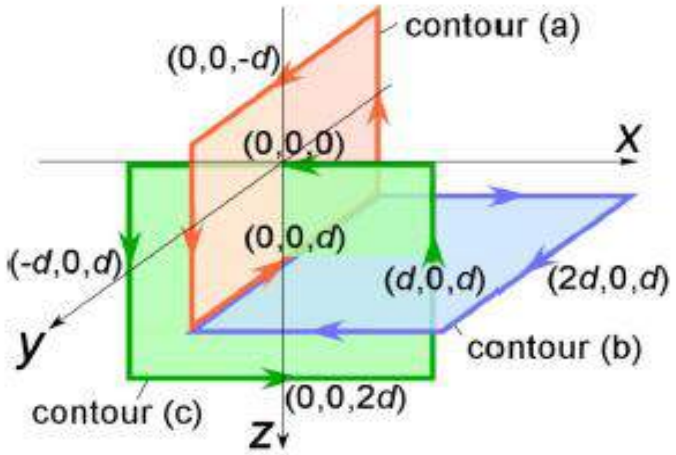

$$\oint \mathbf{E} \cdot d\ell = i\omega \int \mathbf{B} \cdot d\mathbf{S}; \quad \oint \mathbf{H} \cdot \mathrm{d}\ell = -\mathrm{i}\omega \int \mathbf{D} \cdot \mathrm{d}\mathbf{S}$$

人工電磁媒質の粗視化：2

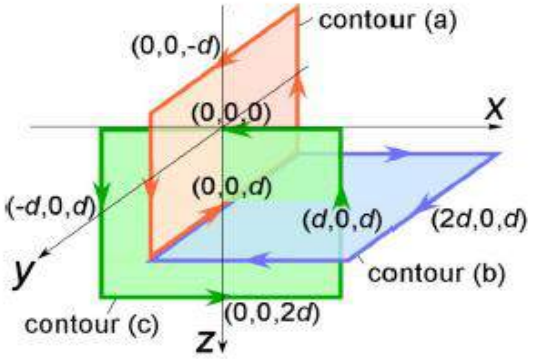

$$\int_{-d}^{d} H_z(0,d,z)dz - \int_{d}^{-d} H_y(0,y,d)dy - \int_{d}^{-d} H_z(0,-d,z)dz + \int_{-d}^{d} H_y(0,y,-d)dy$$

$$= -i\omega \int_{-d}^{d} dy \int_{-d}^{d} dz D_x(0,y,z)$$

$$\overline{H}_z(0,d,0) \equiv \int_{-d}^{d} H_z(0,d,z)dz/(2d), \quad \overline{D}_x(0,0,0) \equiv \int_{-d}^{d} dx \int_{-d}^{d} dz D_x(0,y,z)/(2d)^2$$

$$2d\left\{\overline{H}_z(0,d,0) - \overline{H}_y(0,0,d) - \overline{H}_z(0,-d,0) + \overline{H}_y(0,0,-d)\right\} = i\omega(2d)^2 \overline{D}_x(0,0,0)$$

人工電磁媒質の粗視化：3

$$2d\left\{-\overline{H}_y(0,0,0)e^{ikd}+\overline{H}_y(0,0,0)e^{-ikd}\right\}=-i\omega(2d)^2\overline{D}_x(0,0,0)$$

$$\bar{\varepsilon}\equiv\frac{\overline{D}_x(0,0,0)}{\varepsilon_0\overline{E}_x(0,0,0)}=\frac{\int_{-d}^{d}dy\int_{-d}^{d}dz\varepsilon(0,y,z)E_x(0,y,z)/(2d)^2}{\int_{-d}^{d}E_x(x,0,0)/(2d)}$$

$$\overline{H}_y\sin(kd)=\omega d\bar{\varepsilon}\varepsilon_0\overline{E}_x$$

$$\overline{E}_x\sin(kd)=\omega d\bar{\mu}\mu_0\overline{H}_y$$

$$\frac{\sin^2(kd)}{(\omega d)^2}=\bar{\varepsilon}\bar{\mu}\varepsilon_0\mu_0=\bar{\varepsilon}\bar{\mu}/c^2$$

$$\varepsilon_{eff}\equiv\frac{kd}{\sin(kd)}\bar{\varepsilon};\quad\mu_{eff}\equiv\frac{kd}{\sin(kd)}\bar{\mu}$$

短波長化

考慮すべき事項

- 金属の誘電率の周波数依存
- 微細加工の困難

短波長化への挑戦

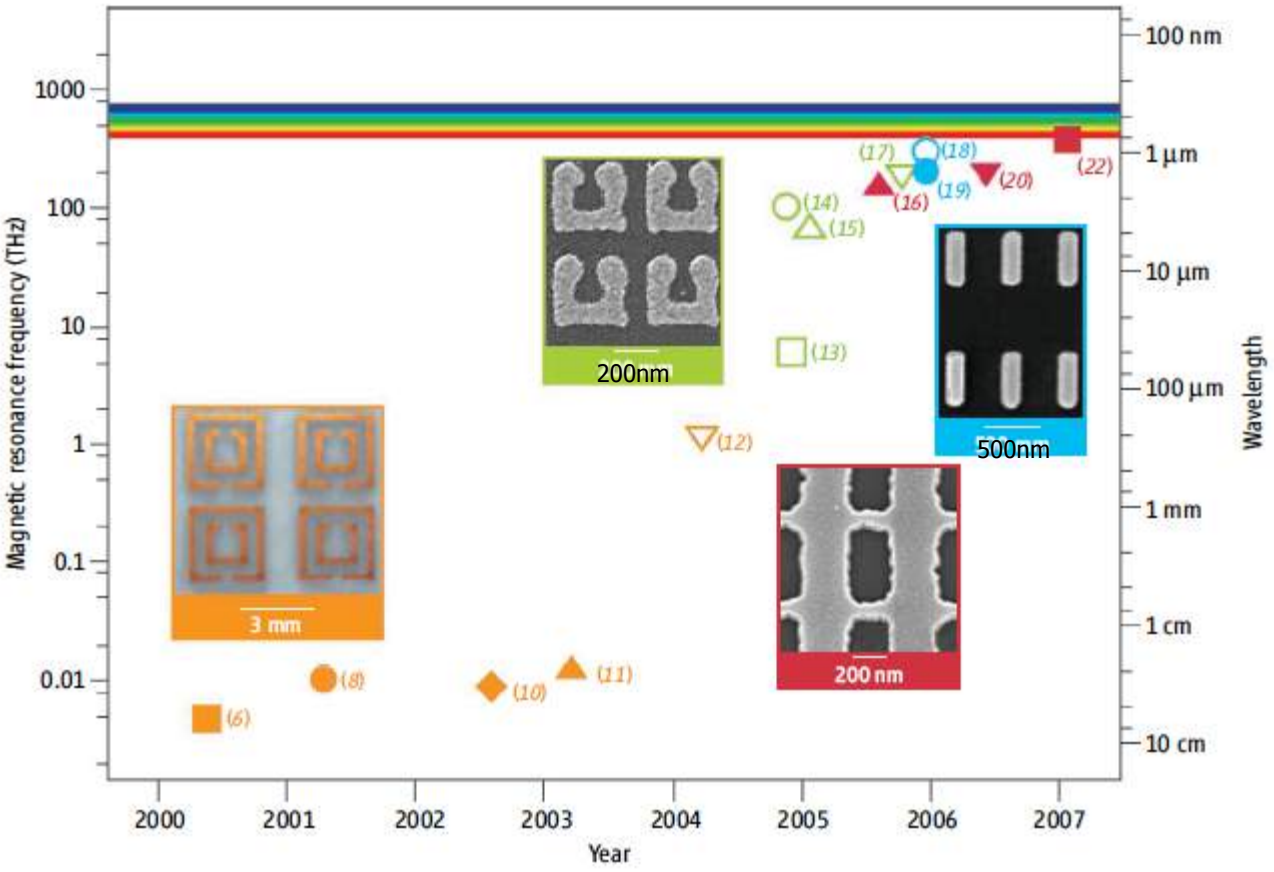

Advances in metamaterials. The solid symbols denote $n < 0$; the open symbols denote $\mu < 0$. Orange: data from structures based on the double split-ring resonator (SRR); green: data from U-shaped SRRs; blue: data from pairs of metallic nanorods; red: data from the "fishnet" structure. The four insets give pictures of fabricated structures in different frequency regions.

C. Soukoulis et al. , Science, Jan.5 (2007)

カットワイアペア構造

可視光領域の磁気応答　　Cai, …, Shalaev;
Rainbow magnetism (Opticsl Express, March 2007)

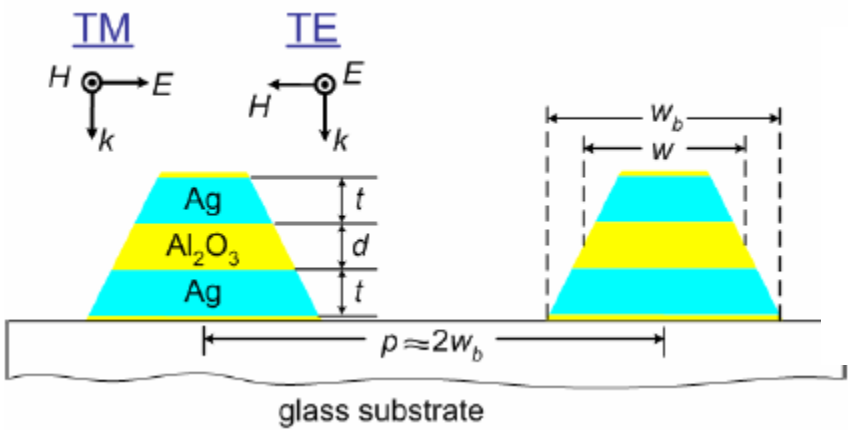

Table 1. Geometric parameters of the magnetic nanostrip samples

Sample #	Bottom Width w_b	Average Width w	Periodicity p	Coverage % *
A	95	50	191	0.50
B	118	69	218	0.54
C	127	83	245	0.52
D	143	98	273	0.52
E	164	118	300	0.55
F	173	127	300	0.58

* Cover ratio is calculated by the ratio of bottom width w_b to the periodicity p.

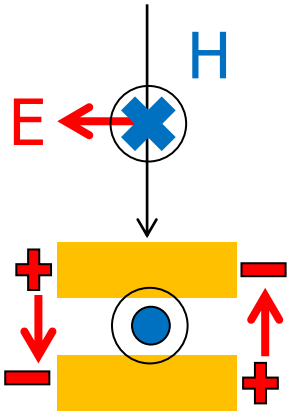

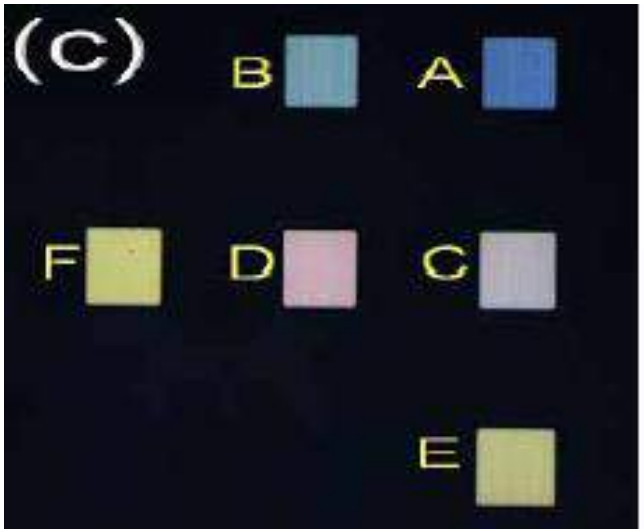

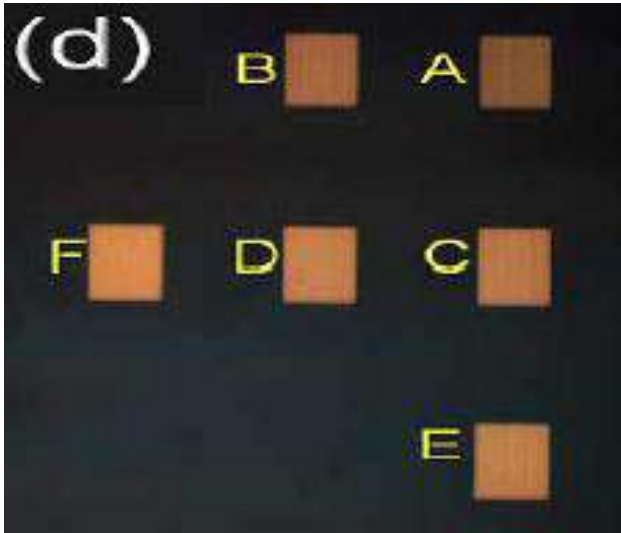

二重魚網(ダブルフィッシュネット)構造

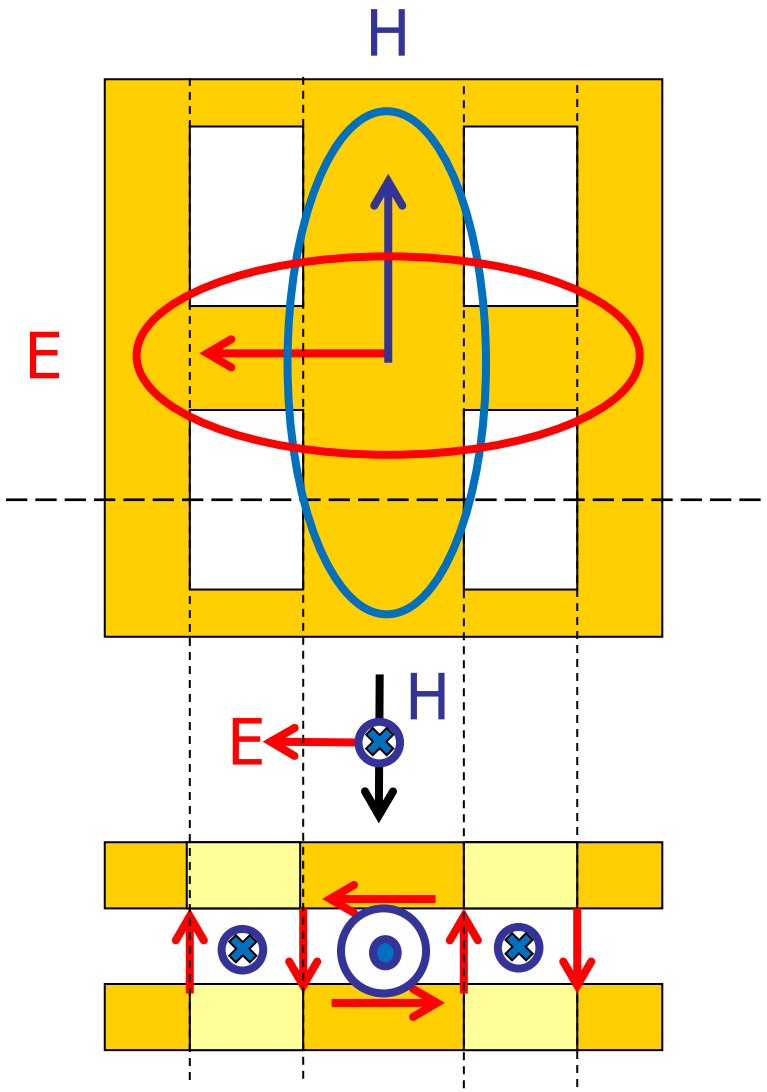

単純な構造に磁気応答
と電気応答の両方を内在
Shuang Zhang et al. (2005)

n = -0.6 @ 780nm

Dolling, Wegener, Soukoulis, Linden
Opt. Lett. 32(2007)53.

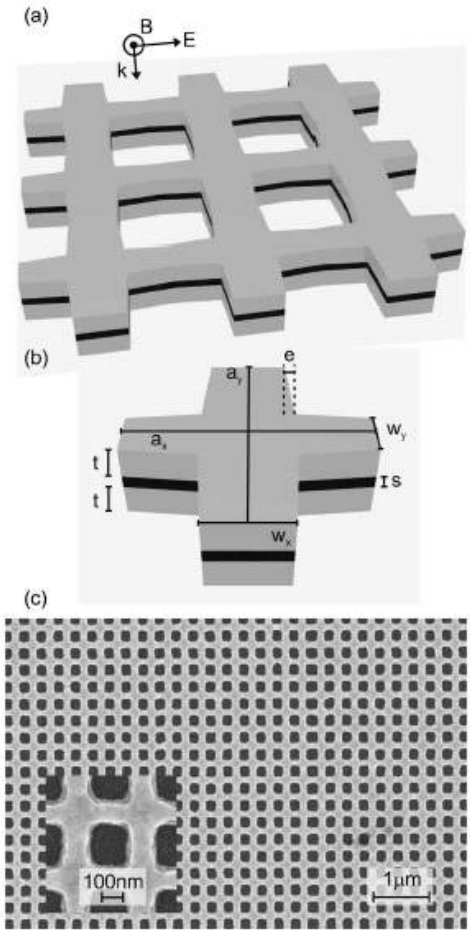

Ag/MgF_2/Ag
ax=ay=300nm
t=40nm
s=17nm

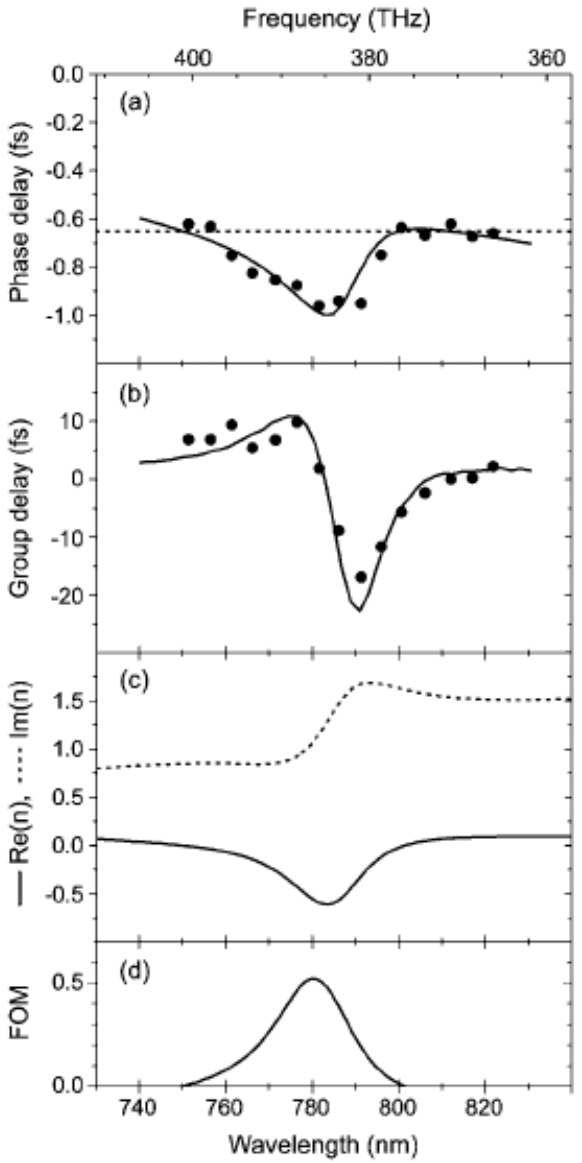

二重魚網構造:Ez

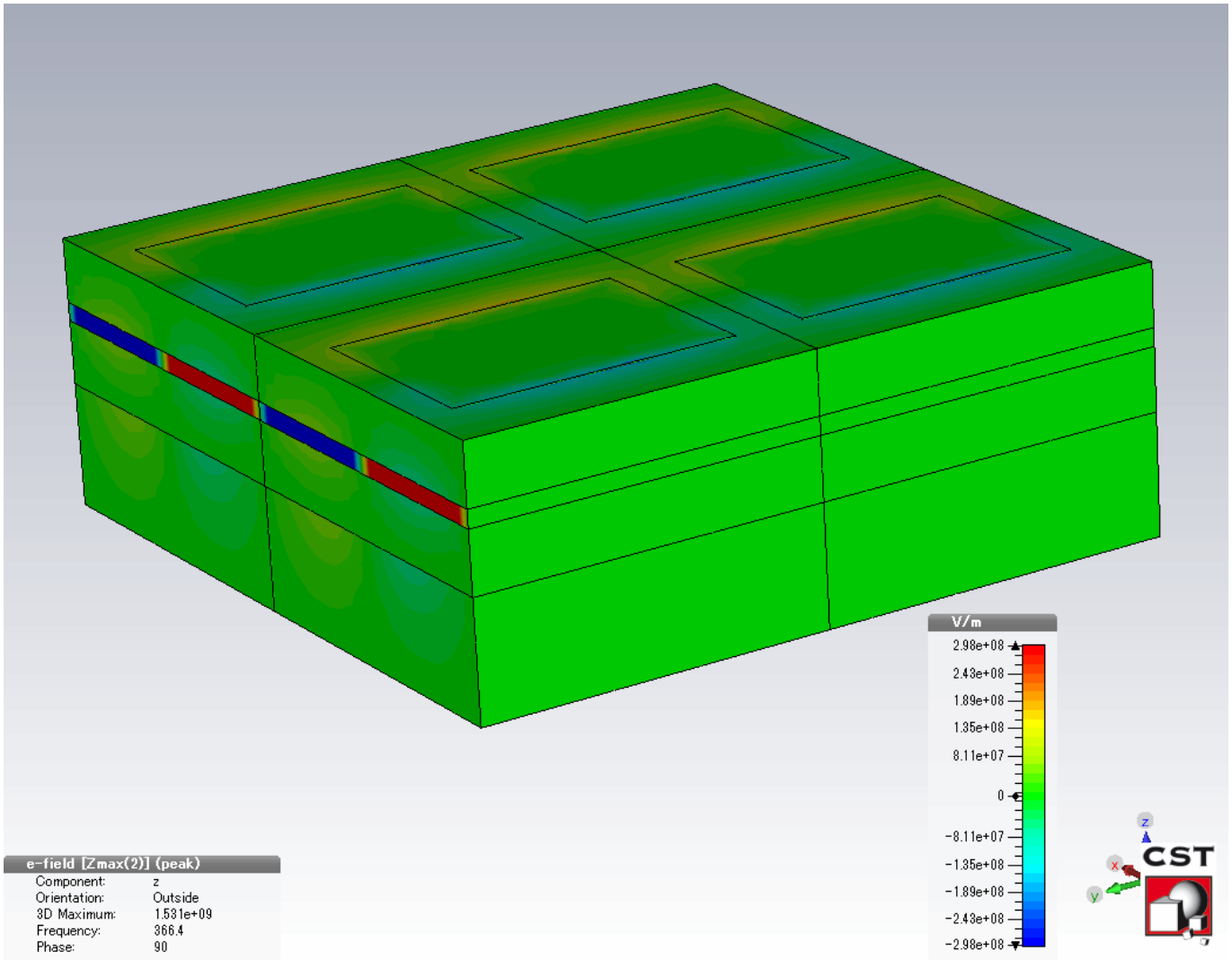
V/m
2.98e+08
2.43e+08
1.89e+08
1.35e+08
8.11e+07
0
-8.11e+07
-1.35e+08
-1.89e+08
-2.43e+08
-2.98e+08
e-field [Zmax(2)] (peak)
Component: z
Orientation: Outside
3D Maximum: 1.531e+09
Frequency: 366.4
Phase: 90
CST

二重魚網構造:Hy

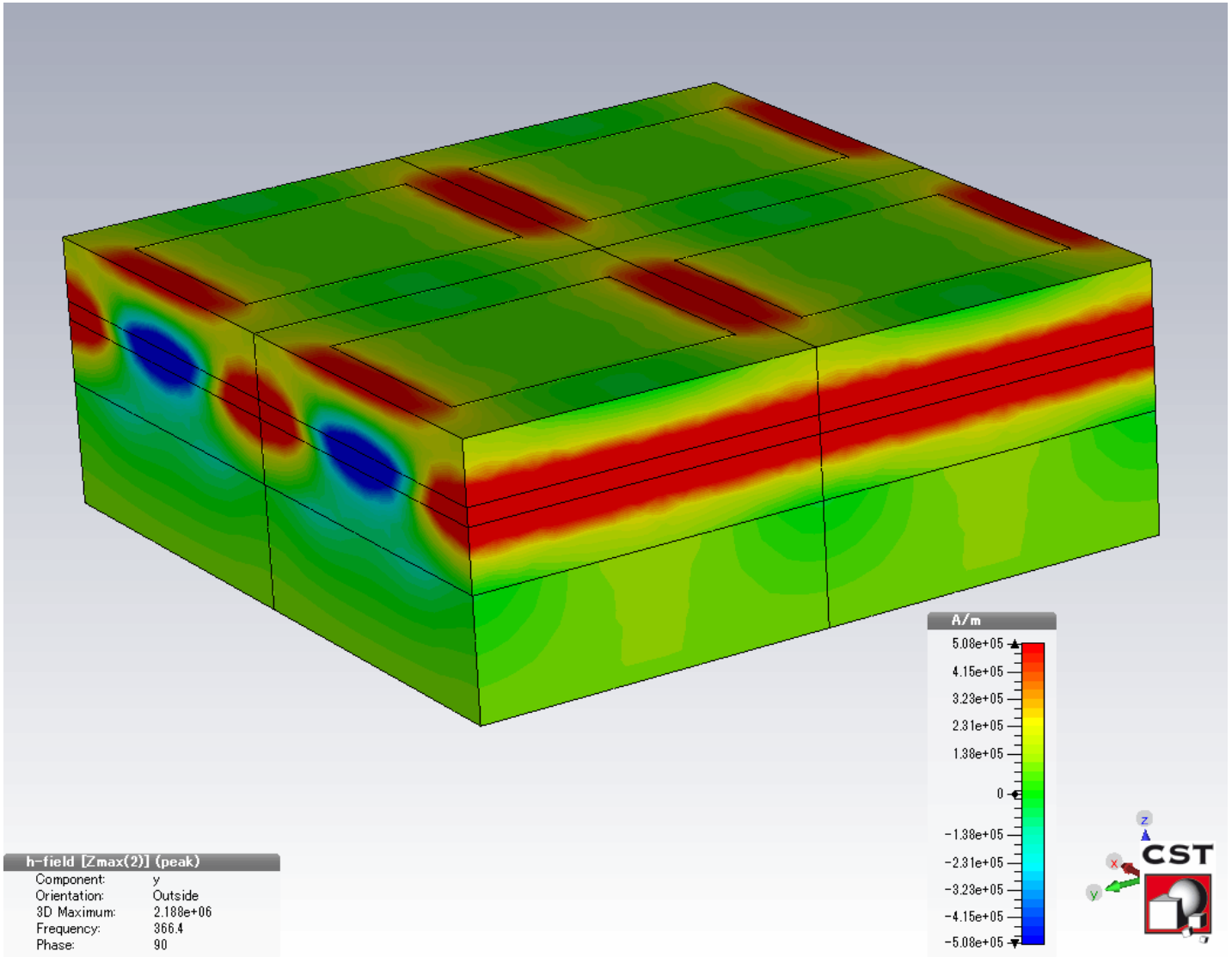
A/m
5.08e+05
4.15e+05
3.23e+05
2.31e+05
1.38e+05
0
-1.38e+05
-2.31e+05
-3.23e+05
-4.15e+05
-5.08e+05
h-field [Zmax(2)] (peak)
Component: y
Orientation: Outside
3D Maximum: 2.188e+06
Frequency: 366.4
Phase: 90
CST

メタマテリアル分子の設計

DFNは周期構造なので、ランダムに分散させるのは困難。
単位構造内で磁気応答と電気応答を共存させる工夫が必要:

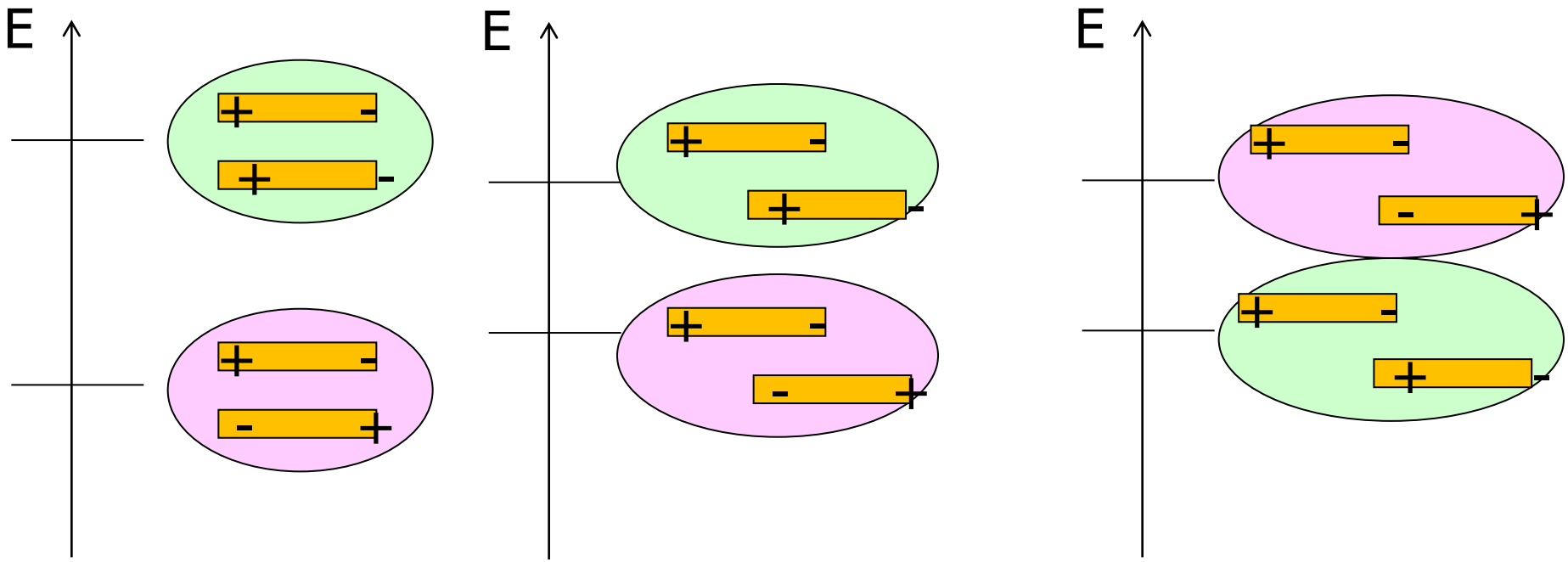

カットワイア対をずらして電気的反発を減らし、共鳴を重ねればよい！
シフトバー構造

Reference: Proposed isotoropic negative index
in three-dimensional optical metamaterials
Boubacar KANTE , …, Xiang ZHANG, PRB, 041103(R) (2012)

シフトバー構造の ε と μ

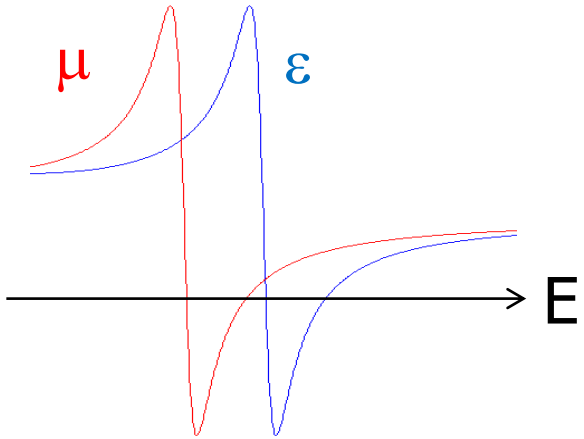

シフトなし

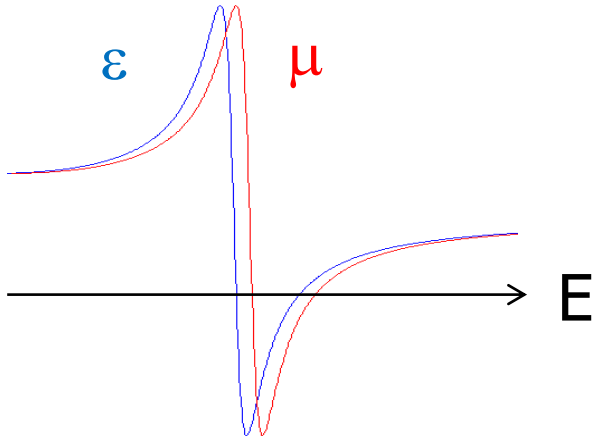

シフトあり

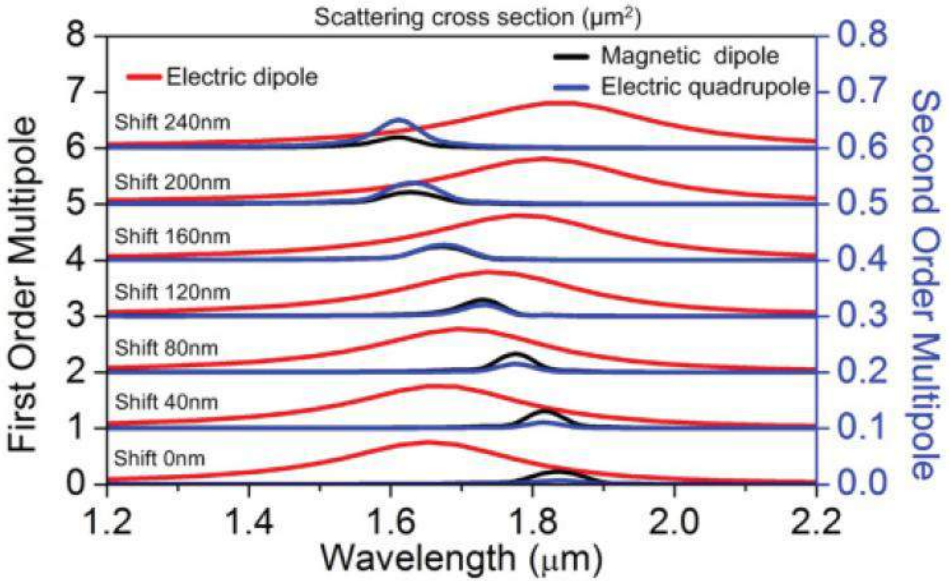

有効誘電率･透磁率

複素透過率、反射率から
有効誘電率、透磁率をもとめる
定式化について

境界条件

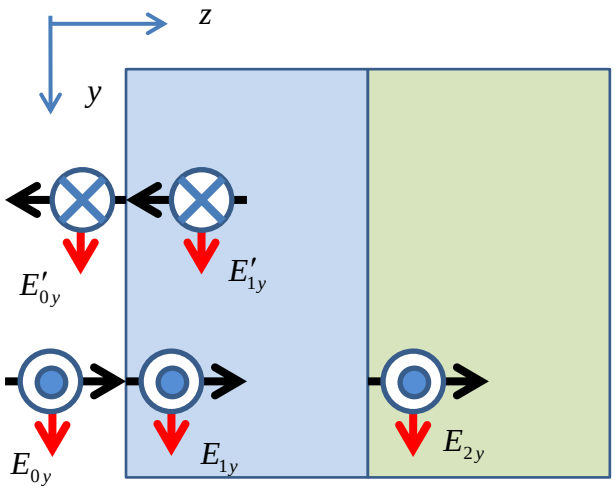

$$E_{0y} + E'_{0y} = E_{1y} + E'_{1y}$$

$$-H_{0x} + H'_{0x} = -H_{1x} + H'_{1x}$$

$$rot\mathbf{E} = -\frac{\partial \mathbf{B}}{\partial t} \therefore \mathbf{k} \times \mathbf{E} = i\omega\mu\mathbf{H}$$

$$\begin{pmatrix} k_x \\ k_y \\ k_z \end{pmatrix} \times \begin{pmatrix} 0 \\ E_y \\ 0 \end{pmatrix} = \begin{pmatrix} -k_z E_y \\ 0 \\ k_x E_y \end{pmatrix} = i\omega\mu \begin{pmatrix} H_x \\ 0 \\ H_z \end{pmatrix} \qquad \therefore H_x = \frac{-k_z}{i\omega\mu} E_y$$

$$a \equiv \frac{k_{1z}}{k_{0z}\mu} = \frac{1}{Z} \qquad a' \equiv \frac{k_{2z}}{k_{0z}\mu} = \frac{1}{Z_2} = n_s$$

$$t = \frac{2Z}{(1+n_s)Z\cos(k_z d) - i(1+n_s Z^2)\sin(k_z d)}$$

$$r = \frac{(1-n_s)Z\cos(k_z d) + i(1-n_s Z^2)\sin(k_z d)}{(1+n_s)Z\cos(k_z d) - i(1+n_s Z^2)\sin(k_z d)}$$

境界条件を行列で表現

$$\begin{pmatrix}1 & 1\\ 1 & -1\end{pmatrix}\begin{pmatrix}E_{0y}\\ E'_{0y}\end{pmatrix}=\begin{pmatrix}1 & 1\\ a & -a\end{pmatrix}\begin{pmatrix}E_{1y}\\ E'_{1y}\end{pmatrix}$$

$$\begin{pmatrix}e^{ik_zd} & e^{-ik_zd}\\ ae^{ik_zd} & -ae^{-ik_zd}\end{pmatrix}\begin{pmatrix}E_{1y}\\ E'_{1y}\end{pmatrix}=\begin{pmatrix}b & 1/b\\ ab & -a/b\end{pmatrix}\begin{pmatrix}E_{1y}\\ E'_{1y}\end{pmatrix}=\begin{pmatrix}1 & 0\\ a' & 0\end{pmatrix}\begin{pmatrix}E_{2y}\\ 0\end{pmatrix}$$

$$\begin{pmatrix}E_{0y}\\ E'_{0y}\end{pmatrix}=\begin{pmatrix}1 & 1\\ 1 & -1\end{pmatrix}^{-1}\begin{pmatrix}1 & 1\\ a & -a\end{pmatrix}\begin{pmatrix}b & 1/b\\ ab & -a/b\end{pmatrix}^{-1}\begin{pmatrix}1 & 0\\ a' & 0\end{pmatrix}\begin{pmatrix}E_{2y}\\ 0\end{pmatrix}$$

$$=\frac{1}{2}\begin{pmatrix}1 & 1\\ 1 & -1\end{pmatrix}\begin{pmatrix}1 & 1\\ a & -a\end{pmatrix}\frac{1}{2a}\begin{pmatrix}b & 1/b\\ ab & -a/b\end{pmatrix}\begin{pmatrix}1 & 0\\ a' & 0\end{pmatrix}\begin{pmatrix}E_{2y}\\ 0\end{pmatrix}$$

$$=\frac{1}{2}\begin{pmatrix}1+a & 1-a\\ 1-a & 1+a\end{pmatrix}\begin{pmatrix}1 & 1\\ a & -a\end{pmatrix}\frac{1}{2a}\begin{pmatrix}(a+a')/b & 0\\ (a-a')/b & 0\end{pmatrix}\begin{pmatrix}E_{2y}\\ 0\end{pmatrix}$$

$$=\frac{1}{4a}\begin{pmatrix}(1-a)(a-a')b+(1+a)(a+a')/b\\ (1+a)(a-a')b+(1-a)(a+a')/b\end{pmatrix}E_{2y}$$

$$=\frac{1}{4a}\begin{pmatrix}a(1+a')(b+1/b)-(a^2+a')(b-1/b)\\ a(1-a')(b+1/b)+(a^2-a')(b-1/b)\end{pmatrix}E_{2y}$$

$$=\frac{1}{2}\begin{pmatrix}(1+a')\cos(k_zd)-i(a+a'/a)\sin(k_zd)\\ (1-a')\cos(k_zd)+i(a-a'/a)\sin(k_zd)\end{pmatrix}E_{2y}$$

$$\begin{pmatrix}1\\ r\end{pmatrix}=\frac{1}{2}\begin{pmatrix}(1+a')\cos(k_zd)-i(a+a'/a)\sin(k_zd)\\ (1-a')\cos(k_zd)+i(a-a'/a)\sin(k_zd)\end{pmatrix}t$$

$$t\equiv\frac{E_{2y}}{E_{0y}}=\frac{2}{(1+a')\cos(k_zd)-i(a+a'/a)\sin(k_zd)}$$

$$r\equiv\frac{E'_{0y}}{E_{0y}}=\frac{(1-a')\cos(k_zd)+i(a-a'/a)\sin(k_zd)}{2}t$$

$$=\frac{(1-a')\cos(k_zd)+i(a-a'/a)\sin(k_zd)}{(1+a')\cos(k_zd)-i(a+a'/a)\sin(k_zd)}$$

$$t=\frac{2Z}{(1+n_s)Z\cos(k_zd)-i(1+n_sZ^2)\sin(k_zd)}$$

$$r=\frac{(1-n_s)Z\cos(k_zd)+i(1-n_sZ^2)\sin(k_zd)}{(1+n_s)Z\cos(k_zd)-i(1+n_sZ^2)\sin(k_zd)}$$

有効パラメタを複素反射・透過で表現

$$\begin{pmatrix}1\\ r\end{pmatrix}=\frac{1}{2}\begin{pmatrix}(1+a')\cos(k_z d)-i(a+a'/a)\sin(k_z d)\\ (1-a')\cos(k_z d)+i(a-a'/a)\sin(k_z d)\end{pmatrix}t$$

$$\begin{pmatrix}(1+a') & -i(a+a'/a)\\ (1-a') & +i(a-a'/a)\end{pmatrix}\begin{pmatrix}\cos(k_z d)\\ \sin(k_z d)\end{pmatrix}=\begin{pmatrix}2/t\\ 2r/t\end{pmatrix}$$

$$\begin{pmatrix}\cos(k_z d)\\ \sin(k_z d)\end{pmatrix}=\begin{pmatrix}(1+a') & -i(a+a'/a)\\ (1-a') & +i(a-a'/a)\end{pmatrix}^{-1}\begin{pmatrix}2/t\\ 2r/t\end{pmatrix}$$

$$=\begin{pmatrix}(1+n_s) & -i(1/Z+n_s Z)\\ (1-n_s) & +i(1/Z-n_s Z)\end{pmatrix}^{-1}\begin{pmatrix}2/t\\ 2r/t\end{pmatrix}$$

$$=\frac{1}{2/Z-2{n_s}^2 Z}\begin{pmatrix}+i(1/Z-n_s Z) & i(1/Z+n_s Z)\\ -(1-n_s) & (1+n_s)\end{pmatrix}\begin{pmatrix}2/t\\ 2r/t\end{pmatrix}$$

$$=\frac{1}{1/Z-{n_s}^2 Z}\begin{pmatrix}(1+r)/Z-(1-r)n_s Z\\ -i(n_s-1+(1+n_s)r)\end{pmatrix}\frac{1}{t}$$

$$1=\frac{((1+r)/Z2-(1-r)n_s Z)^2+(-i(n_s-1+(1+n_s)r))^2}{(1/Z-{n_s}^2 Z)^2 t^2}$$

$$(1/Z-{n_s}^2 Z)^2 t^2=((1+r)/Z-(1-r)n_s Z)^2-((n_s-1+(1+n_s)r))^2$$

$$(1/Z^2-2{n_s}^2+{n_s}^4 Z^2)t^2+((n_s-1+(1+n_s)r))^2$$

$$=(1+r)^2/Z^2-(1+r)(1-r)n_s+(1-r)^2{n_s}^2 Z^2$$

$${n_s}^2({n_s}^2 t^2-(1-r)^2)Z^4+({n_s}^2((1+r)^2-2t^2)+(r-1)^2)Z^2+t^2-(1+r)^2$$

$$=\left\{({n_s}^2 t^2-(1-r)^2)Z^2-t^2+(1+r)^2\right\}\left\{{n_s}^2 Z^2-1\right\}=0$$

$$\therefore\quad Z^2=\frac{(1+r)^2-t^2}{(1-r)^2-{n_s}^2 t^2}$$

$$\cos(k_z d)=\frac{(1+r)/Z-(1-r)n_s Z}{1/Z-{n_s}^2 Z}\frac{1}{t}$$

$$=\frac{(1+r)-(1-r)n_s Z^2}{1-{n_s}^2 Z^2}\frac{1}{t}$$

$$=\frac{(1+r)-(1-r)n_s\dfrac{(1+r)^2-t^2}{(1-r)^2-{n_s}^2 t^2}}{1-{n_s}^2\dfrac{(1+r)^2-t^2}{(1-r)^2-{n_s}^2 t^2}}\frac{1}{t}$$

$$=\frac{(1+r)(1-r)^2-{n_s}^2 t^2-(1-r)n_s((1+r)^2-t^2)}{((1-r)^2-{n_s}^2 t^2)-{n_s}^2((1+r)^2-t^2)}\frac{1}{t}$$

$$=\frac{{n_s}t^2+(1-r)(1+r)}{n_s(1+r)+(1-r)}\frac{1}{t}$$

$$=\frac{{n_s}t^2-r^2+1}{(n_s-1)r+n_s+1}\frac{1}{t}$$

$$k_z d=n\frac{\omega}{c}d=\cos^{-1}\left(\frac{{n_s}t^2-r^2+1}{(n_s-1)r+n_s+1}\frac{1}{t}\right)$$

$$\therefore\quad n=\frac{c}{\omega d}\cos^{-1}\left(\frac{{n_s}t^2-r^2+1}{(n_s-1)r+n_s+1}\frac{1}{t}\right)$$

赤外領域のダブルフィッシュネット構造

Dolling et al. Opt.Lett.31(2006)1800.

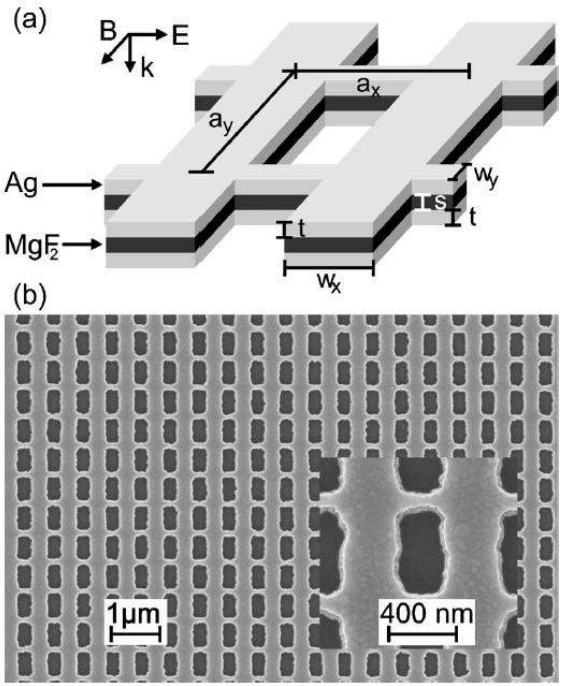

Fig. 1. (a) Scheme of the negative-index metamaterial design and polarization configuration. The sample parameters used in Figs. 2 and 3 are given: w_x=316 nm, w_y =100 nm, t=45 nm, s=30 nm, and lattice constant a_x=a_y =600 nm. (b) Top-view electron micrograph of the silver-based structure. Inset, magnified view.

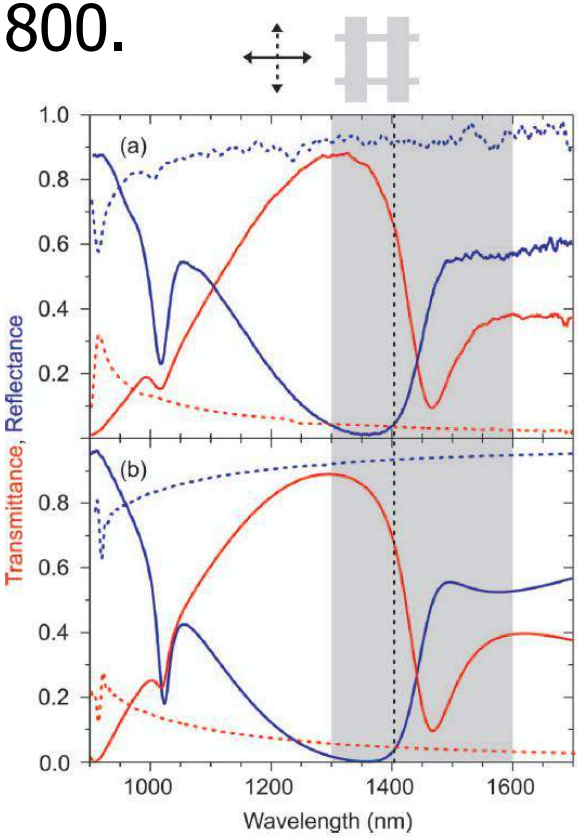

Fig. 2. (a) Measured normal-incidence transmittance (red) and reflectance (blue) spectra for the incident polarization configuration (solid curves) depicted in Fig. 1(a); dashed curve, orthogonal linear polarization. (b) Corresponding calculated spectra. Gray area, spectral region shown in Fig. 3; dashed vertical line, position of Re(n)=−1, where the FOM is ~3.

電磁場シミュレーション

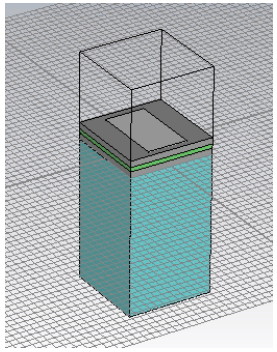

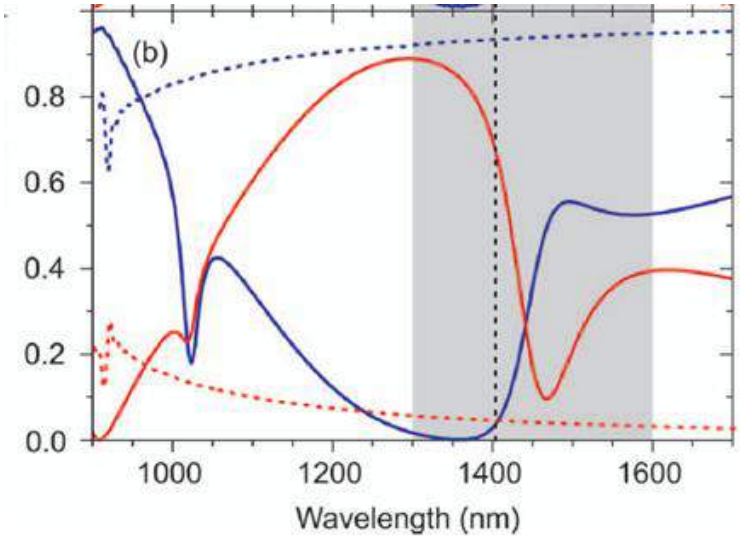

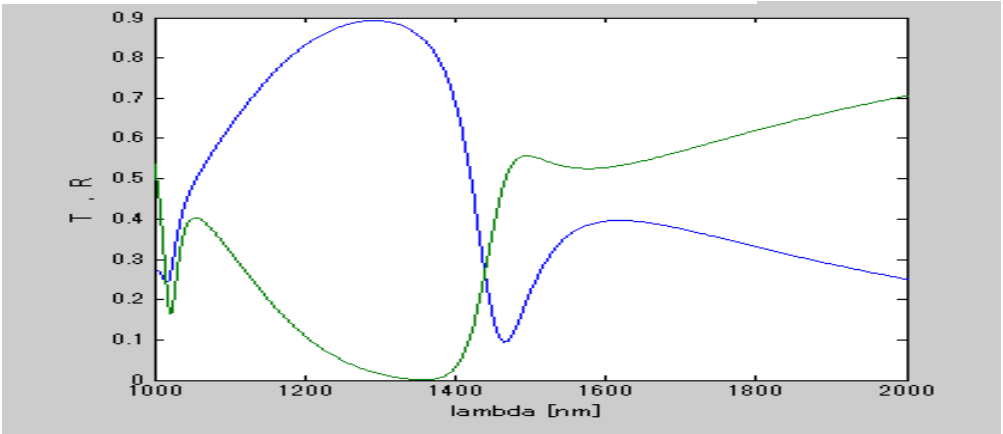

Dollingらの計算結果を再現

単純に計算すると...

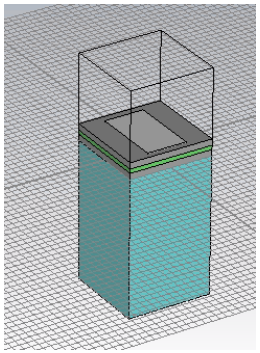

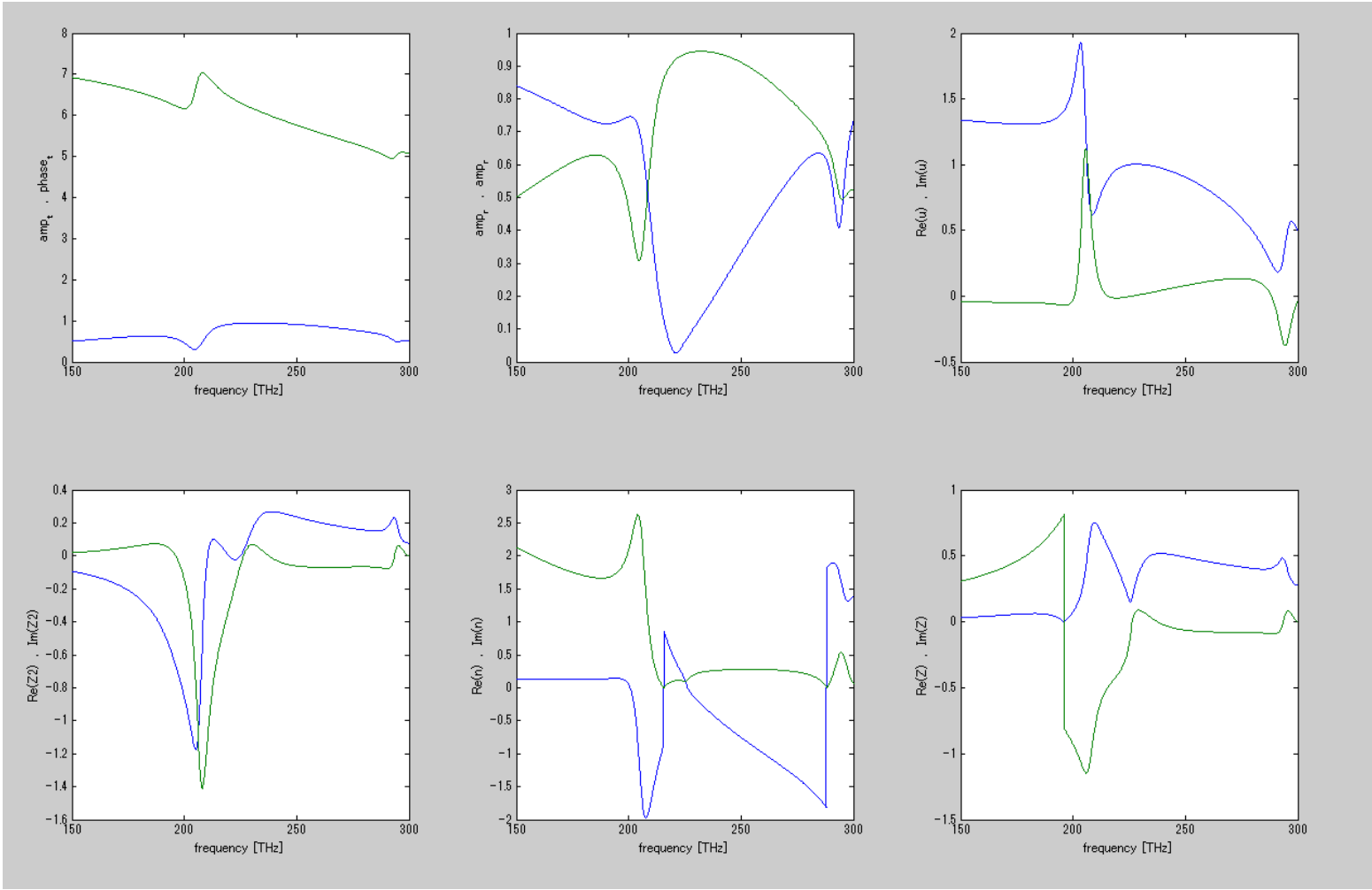

ところどころでジャンプが生じる。

(u′, u″); u′(f), u″(f)

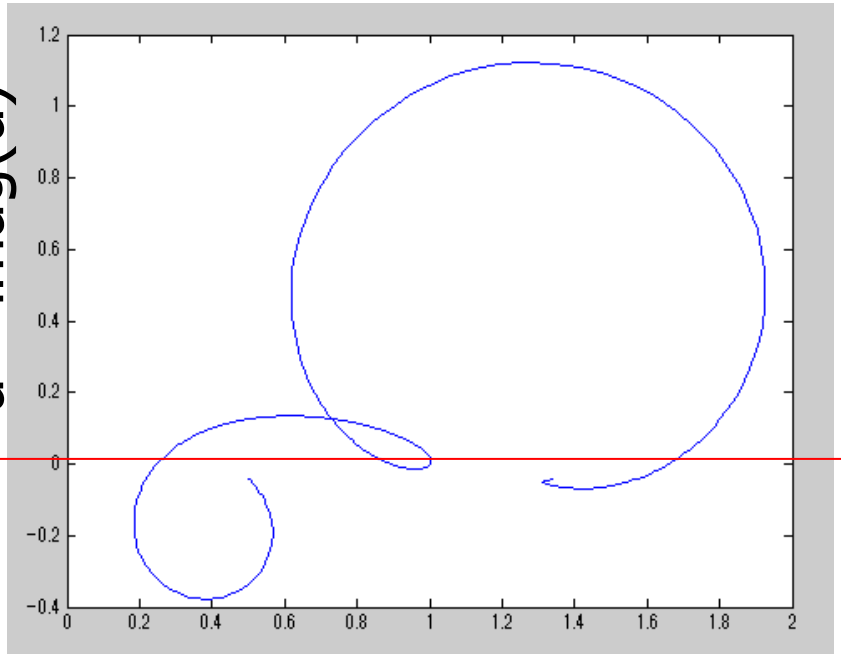
u″=imag(u)
u′=real(u)
1.2
1
0.8
0.6
0.4
0.2
0
−0.2
−0.4
0
0.2
0.4
0.6
0.8
1
1.2
1.4
1.6
1.8
2

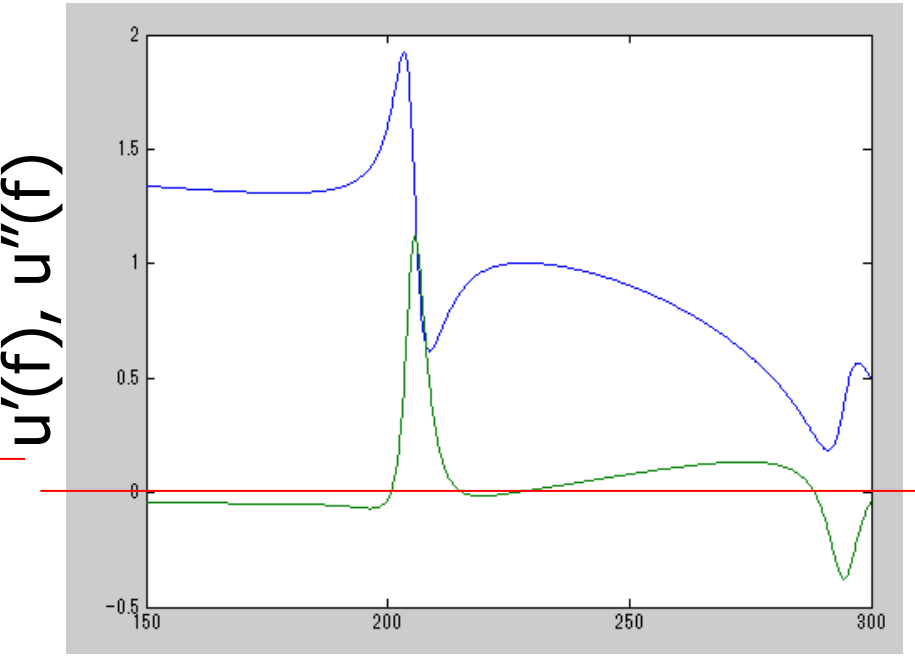
u′(f), u″(f)
f [THz]
2
1.5
1
0.5
0
−0.5
150
200
250
300

MATLABにおける acos(z)の変域

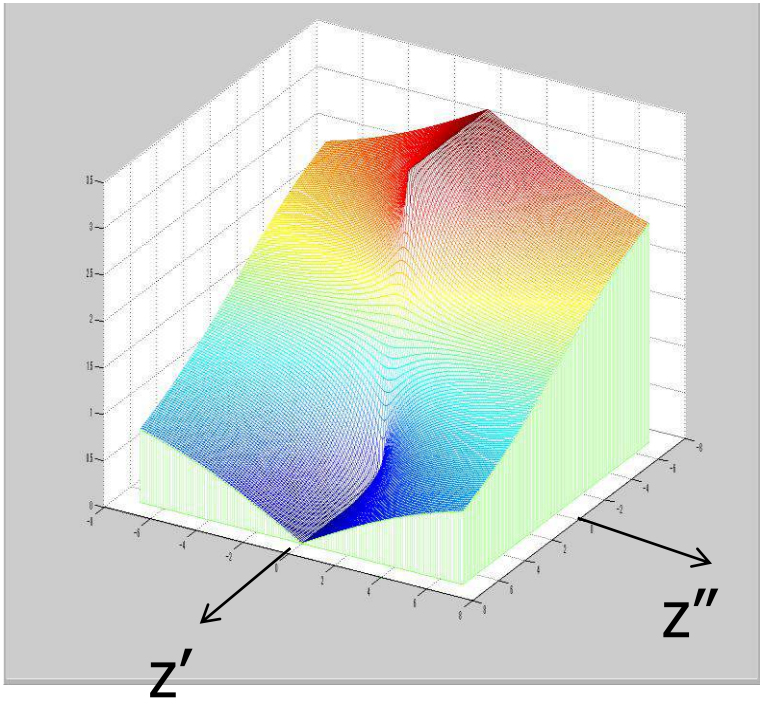

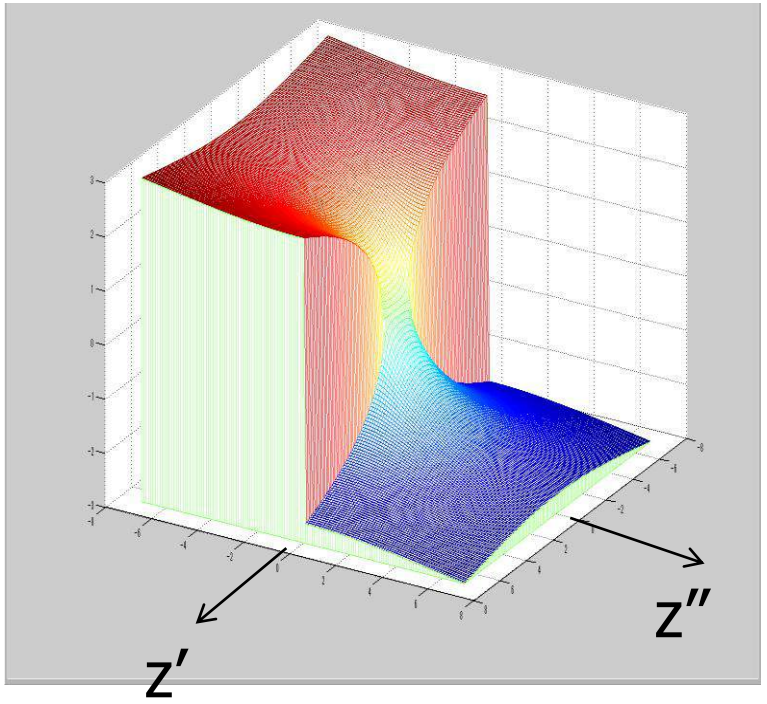

解析： DFN@IR 基板なし

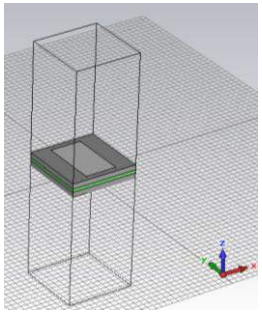

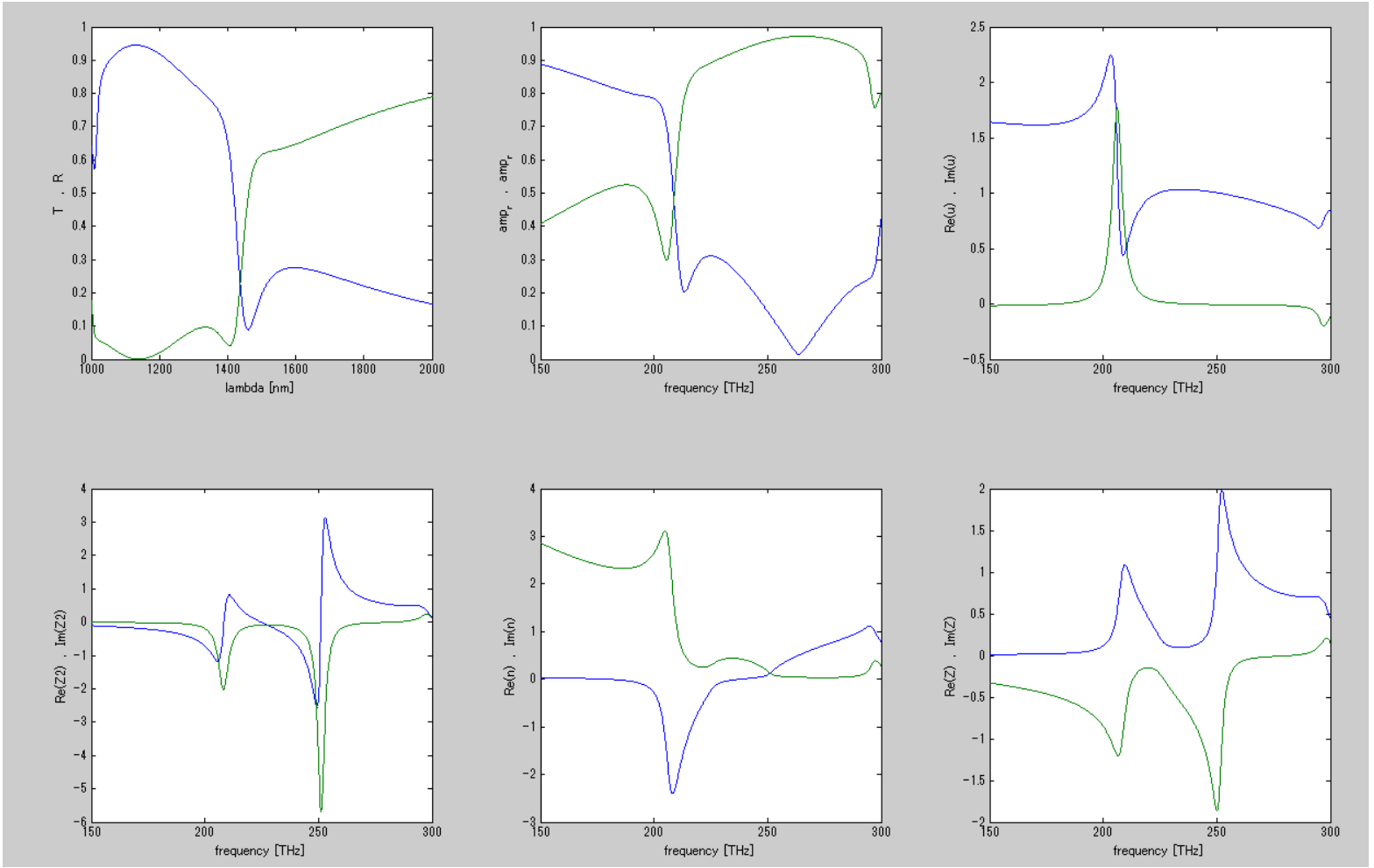

特定の周波数領域で負の屈折率が実現される！

DollingIR without substrate
t1=45, t2=30, t3=316, t4=100, L1=1000,L2=100000,nsub=1,n_MgF2=1.38

解析： DFN@IR 基板なし

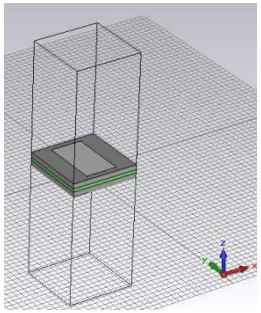

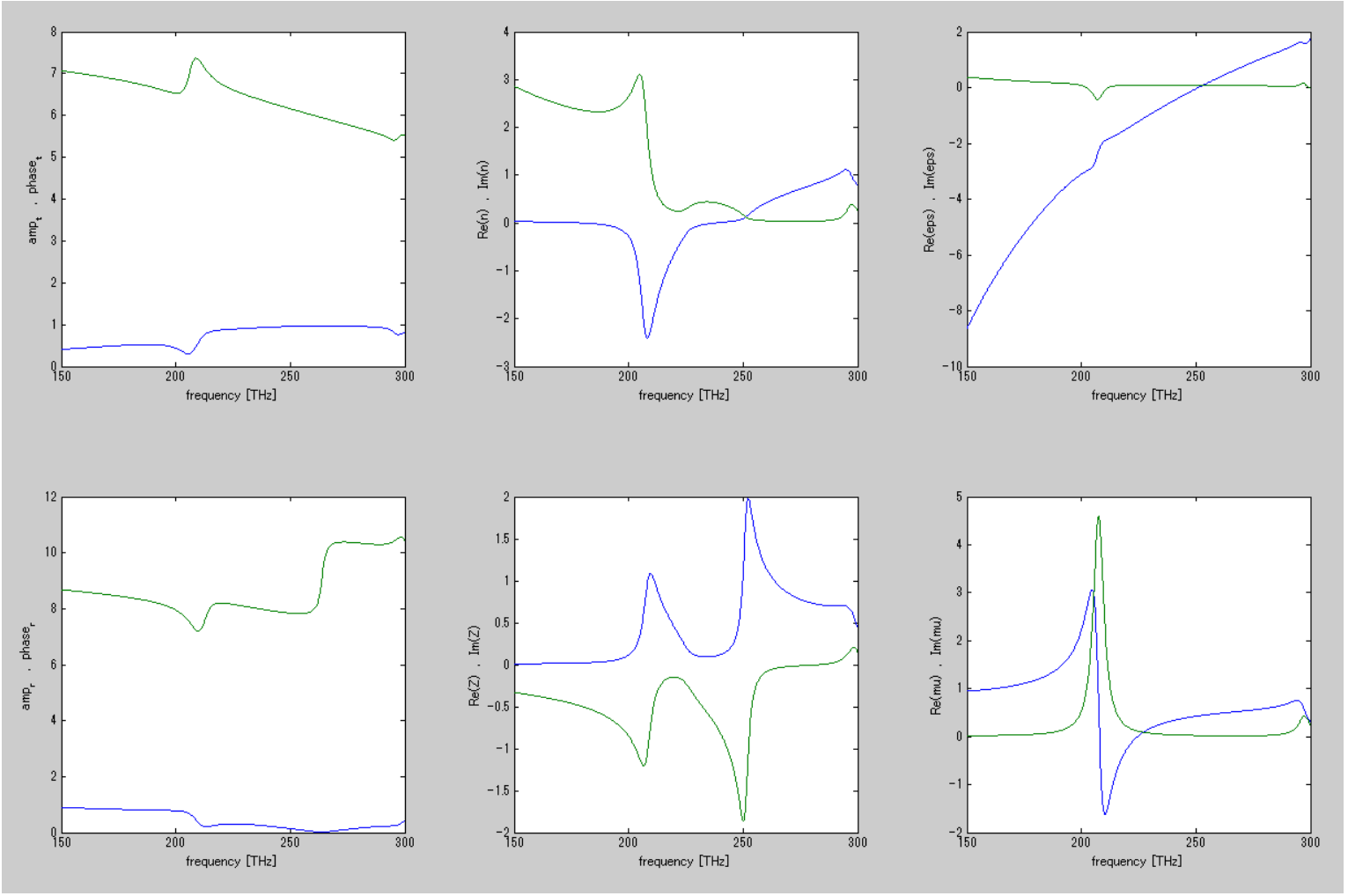

誘電率と透磁率が同時に負の領域で負の屈折率が実現できている。

DFN@IR　基板あり　解析接続

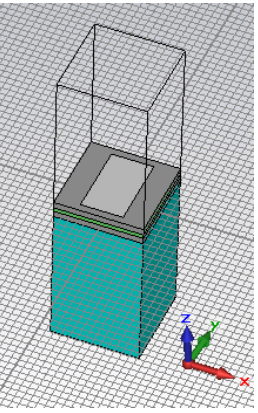

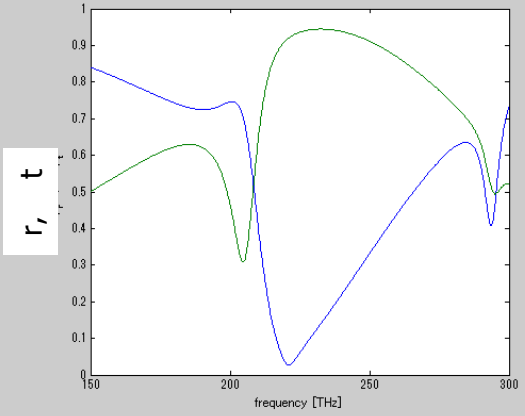

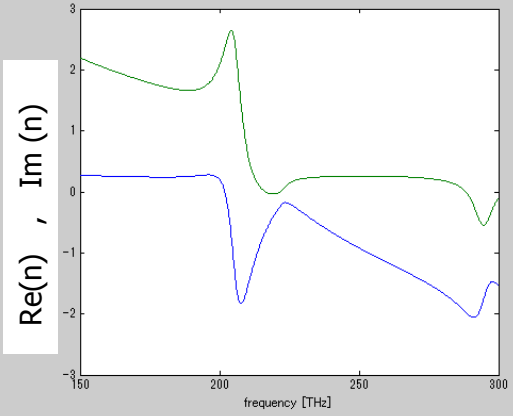

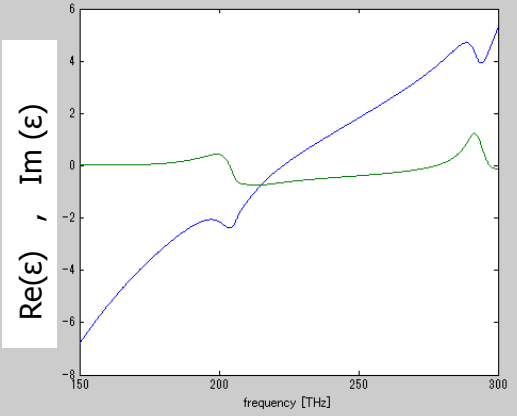

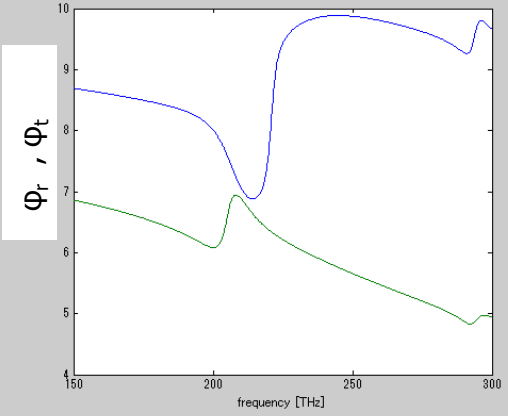

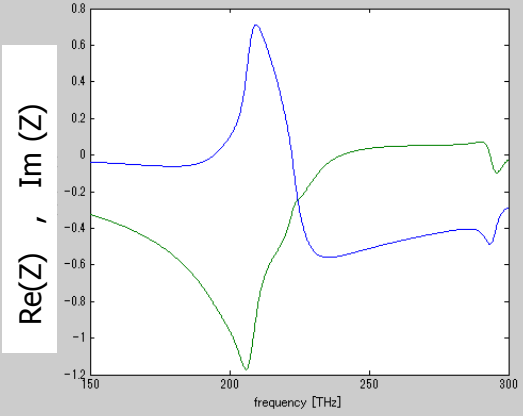

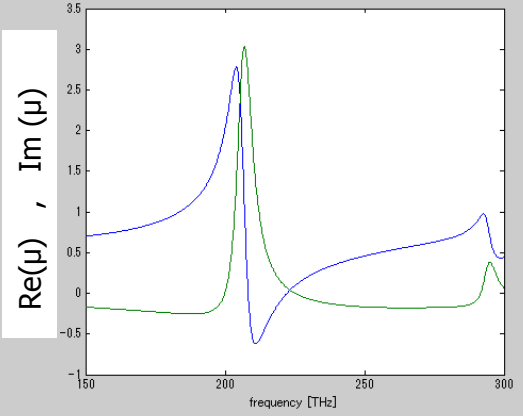

伝送線路理論

$$V = RI \quad \therefore Z = \frac{V}{I} = R$$

$$V = L\frac{dI}{dt} \Rightarrow V = j\omega LI \quad \therefore Z = \frac{V}{I} = j\omega L$$

$$CV = \int Idt : C\dot{V} = I \Rightarrow j\omega CV = I \quad \therefore Z = \frac{V}{I} = \frac{1}{j\omega C}$$

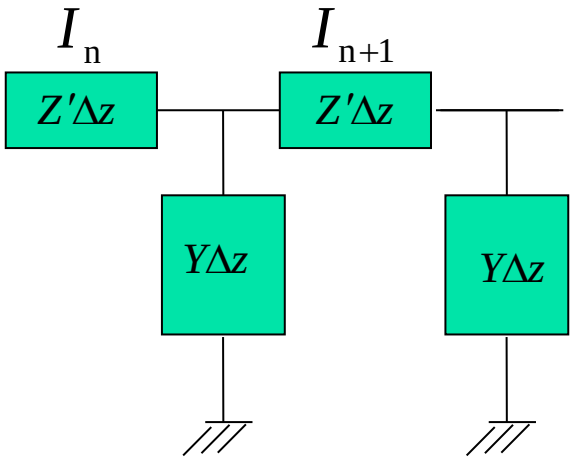

$$\left.\begin{aligned} I_n - I_{n+1} &= Y'\Delta z V_n \\ V_n - V_{n+1} &= Z'\Delta z I_{n+1} \end{aligned}\right\} \Rightarrow \left\{\begin{aligned} \frac{dI}{dz} &= -Y'V \\ \frac{dV}{dz} &= -Z'I \end{aligned}\right. \Rightarrow \left\{\begin{aligned} \frac{d^2I}{dz^2} &= Y'Z'I \\ \frac{d^2V}{dz^2} &= Z'Y'V \end{aligned}\right.$$

$$I, V \propto e^{\gamma x} \Rightarrow \gamma^2 = Y'Z'$$

$$-\frac{dH_y}{dz} = j\omega\varepsilon E_x ; \frac{dE_x}{dz} = -j\omega\mu H_y$$

$$\begin{pmatrix} E_x \\ H_y \end{pmatrix} \Leftrightarrow \begin{pmatrix} V \\ I \end{pmatrix}; \quad \begin{pmatrix} Z' \\ Y' \end{pmatrix} \Leftrightarrow \begin{pmatrix} j\omega\mu \\ j\omega\varepsilon \end{pmatrix}$$

$$\left(\frac{ck}{\omega}\right)^2 = \varepsilon\mu = \frac{Z'Y'}{(j\omega)^2}$$

伝送線路理論

$$I, V \propto \exp(\gamma z) \Rightarrow \gamma^2 = Y'Z'$$

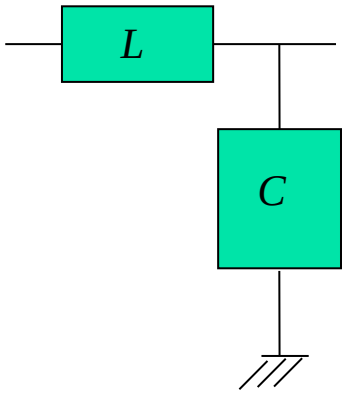

$$Z' = j\omega L', Y' = j\omega C'$$

$$\gamma = j\beta = j\omega\sqrt{L'C'}$$

$$\therefore \beta = \omega\sqrt{L'C'}$$

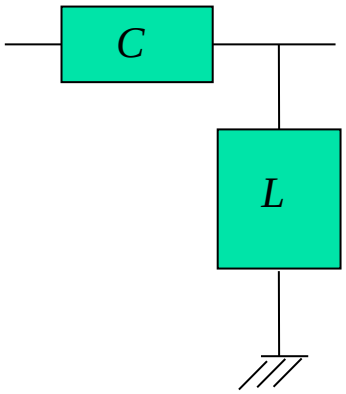

$$Z' = 1/\, j\omega L', Y' = 1/\, j\omega C$$

$$Z' = j\omega L', Y' = j\omega C'$$

$$\gamma = j\beta = j\omega\sqrt{L'C'}$$

$$\therefore \beta = \omega\sqrt{L'C'}$$

伝送線路理論

負の屈折率を得るための戦略は？

戦略1： CとLを入れ替える！
これに物理的な効果（有限の距離、浮遊容量）を加える。
⇒ Composite Right-Left Handed (CRLH) Transmission Line

負の屈折を示す伝送線路網の構成

Planar Distributed Structures With Negative Refractive Index

Atsushi Sanada, *Member, IEEE*, Christophe Caloz, *Member, IEEE*, and Tatsuo Itoh, *Fellow, IEEE*

***Abstract*—Planar distributed periodic structures of microstrip-line and stripline types, which support left-handed (LH) waves are presented and their negative refractive index (NRI) properties are shown theoretically, numerically, and experimentally. The supported LH wave is fully characterized based on the composite right/left-handed transmission-line theory and the dispersion characteristics, refractive indexes, and Bloch impedance are derived theoretically. In addition, formulas to extract equivalent-circuit parameters from full-wave simulation are given. Open (microstrip) and closed (stripline) structures with a 5×5 mm^2 unit cell operating at approximately 4 GHz are designed and characterized by full-wave finite-element-method simulations. A 20×6 unit-cell NRI lens structure interfaced with two parallel-plate waveguides is designed. The focusing/refocusing effect of the lens is observed by both circuit theory and full-wave simulations. Focusing in the NRI lens is also observed experimentally in excellent agreement with circuit theory and numerical predictions. This result represents the first experimental demonstration of NRI property using a purely distributed planar structure.**

mensional (1-D) TL implementations with practical applications such as backward-to-forward leaky-wave antennas [8], [9], tight/dual-band couplers [10], and zeroth-order resonators [11] using microstrip lines or coplanar waveguides (CPWs).

Two-dimensional (2-D) TL-based metamaterials have also been presented by extending 1-D LH TLs to 2-D TL circuit networks. A 2-D LH TL circuit using *LC lumped-element* components has been implemented [7] and its NRI focusing property [1], [12] has been shown experimentally by an NRI slab lens. A *purely distributed* 2-D NRI structure would be more desirable because it would provide flexibility in design and fabrication and scalability to any frequency. Such a distributed structure would also be closer to real material than circuit-type lumped-element configuration. Thus far, only a few structures of the 2-D distributed LH TL have been proposed [13], [14] and demonstrated numerically, however, no experimental result showing

構成要素

Fig. 2. Open hexagonal structure. (a) General view. (b) Unit cell.

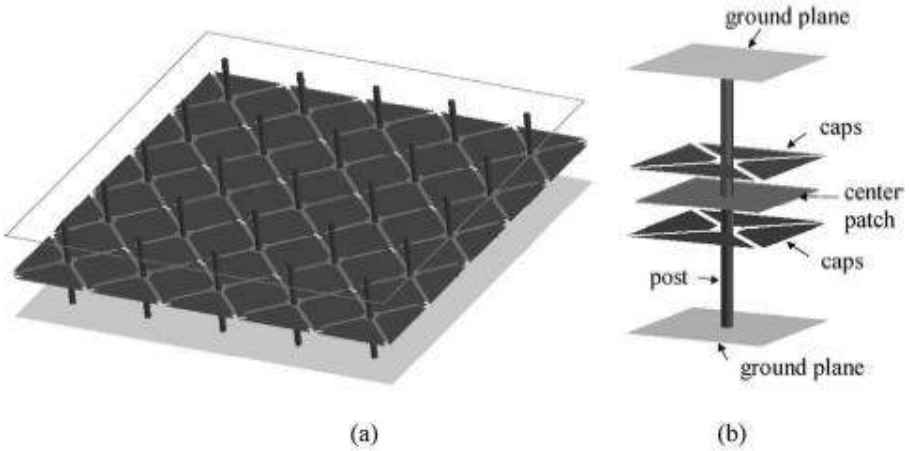

Fig. 3. Closed (stripline) structure. (a) General view. The top ground plane is drawn transparently for easy view. (b) Unit cell.

II. Planar LH Distributed Structures

Although the mode guided by the structure is microscopically hybrid, it is essentially compatible with the TEM mode and can

等価回路と分散関係

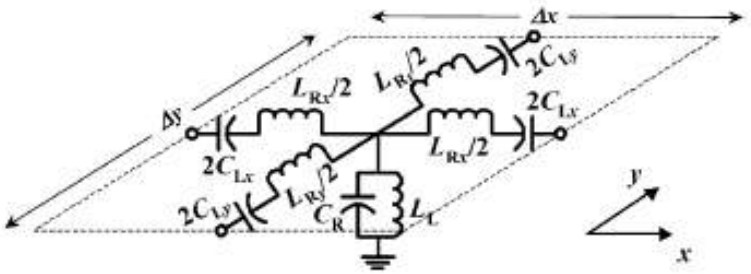

Fig. 4. Equivalent circuit of the unit cell of the 2-D CRLH TL.

since this structure is *closed* by two ground planes, it supports a *pure* LH mode in the whole spectral domain, whereas the LH mode of the open structure couples with the RH surface wave mode in the long wavelength wave region where $\beta < k_0$. These characteristics will be shown in Section III.

III. Theory

A. Dispersion Relation

The equivalent circuit of the unit cell of the proposed 2-D structures is shown in Fig. 4. The unit cell consists of a series capacitance and a shunt inductance (LH components), as well as

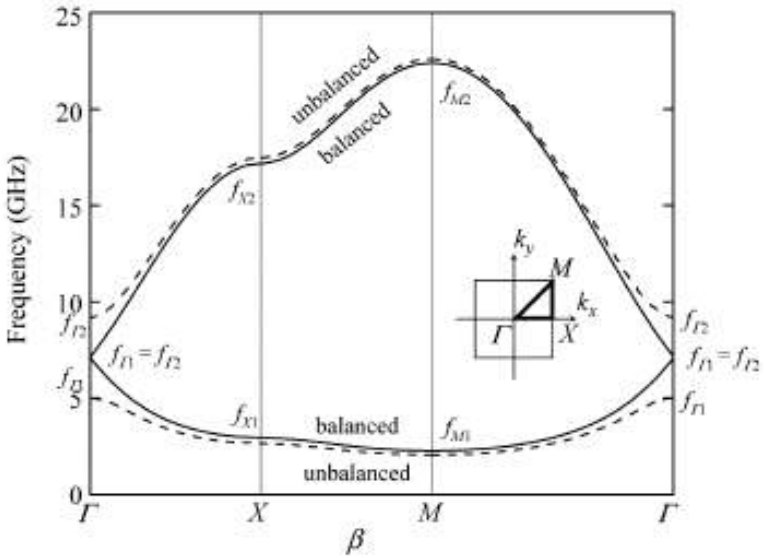

Fig. 5. Dispersion diagram of the structure. Solid line: balanced case ($L_L = 1.0$ nH, $C_L = 0.5$ pF, $L_L = 1.0$ nH, $C_L = 0.5$ pF). Dashed line: unbalanced case ($L_L = 0.6$ nH, $C_L = 1.0$ pF, $L_L = 1.0$ nH, $C_L = 0.5$ pF). The Γ, X, and M represent the high symmetry points ($k_x a = k_y a = 0$), ($k_x a = \pi, k_y a = 0$), and ($k_x a = k_y a = \pi$), respectively in the spectral domain.

$$k_i = \frac{1}{\cdot}\cos^{-1}\left\{1 - \frac{1}{\cdot}\left[\frac{\omega_L^2}{\cdot^2} + \frac{\omega^2}{\cdot^2} - \left(\frac{\omega_{sh}^2}{\cdot^2} + \frac{\omega_{se}^2}{\cdot^2}\right)\right]\right\},$$

Veselagoレンズの結像：位相分布

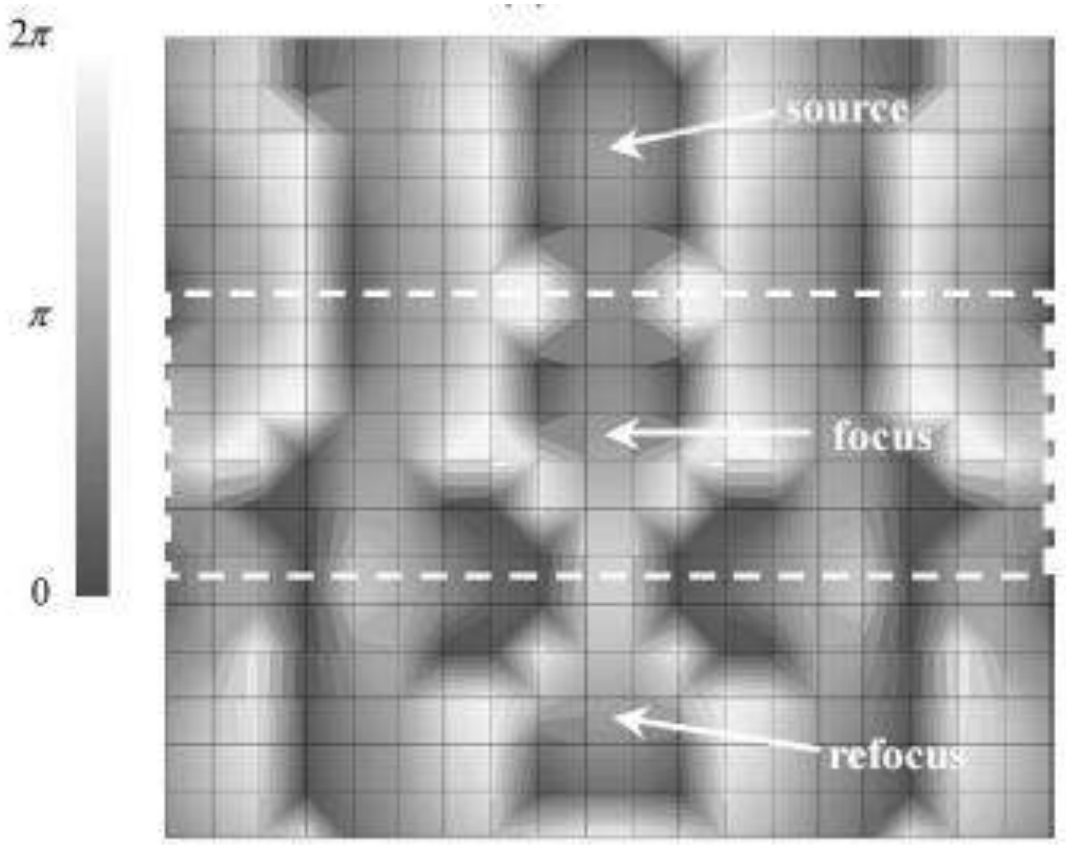

Non-Foster回路

戦略２:

LとCの符号を変えることで、

負の屈折を実現。

オペアンプによるNICの構成 I

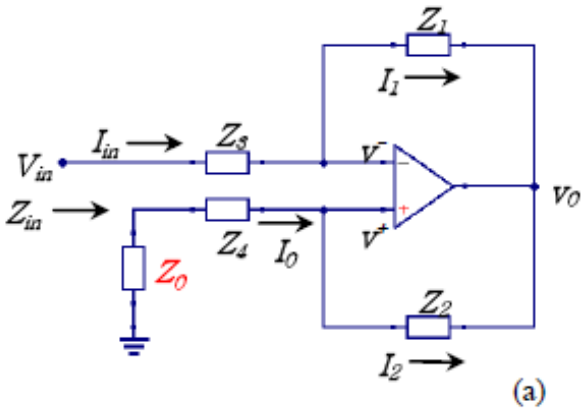

(a)

$$v^- - v_0 = Z_1 I_1$$
$$v^+ - v_0 = Z_2 I_2$$
$$V_{in} - v^- = Z_3 I_{in}$$
$$v^+ = -(Z_0 + Z_4) I_0$$
$$I_{in} = I_1$$
$$I_0 = I_2$$
$$v^+ = v^-$$

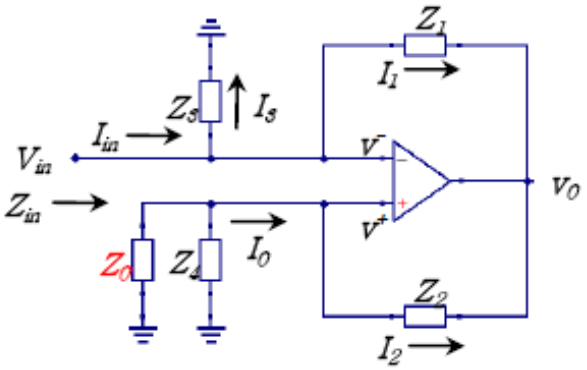

(b)

$$v^- - v_0 = Z_1 I_1$$
$$v^+ - v_0 = Z_2 I_2$$
$$V_{in} = Z_3 I_3$$
$$\left(\frac{1}{Z_0} + \frac{1}{Z_4}\right) v^+ = -I_0$$
$$I_{in} = I_1 + I_3$$
$$I_0 = I_2$$
$$v^+ = v^-$$

Fig. 1 Operational-amplifier-based NICs with symmetric architecture of impedance elements Z_1=Z_2 and Z_3=Z_4. The sign of an impedance Z_0 will be reversed as $-Z_0$ by the NIC. (a) NIC1. (b) NIC2.

オペアンプによるNICの構成 II

$$Z_{in} = \frac{V_{in}}{I_{in}} = Z_3 - (Z_0 + Z_4)\frac{Z_1}{Z_2}, \qquad \text{(NIC1)}$$

$$Z_{in} = \frac{V_{in}}{I_{in}} = Z_1 \Big/ \left(\frac{Z_1}{Z_3} - \frac{Z_2}{Z_0} - \frac{Z_2}{Z_4}\right) \qquad \text{(NIC2)}$$

By applying the symmetric conditions Z1=Z2 and Z3=Z4,

$$Z_{in} = \frac{V_{in}}{I_{in}} = -Z_0$$

第一日目のまとめ

- $\varepsilon, \mu < 0$ なら屈折率が負となる。
- $\varepsilon = \mu = -1$の平板は結像作用をもつ。
- 分割リング共振器やカットワイアペアに
  よって透磁率を負にすることができる。
- 伝送線路においても負屈折率が実現できる。
  LとCを入れ替える方法の他、符号を逆にする方法もある。
  後者は外部からエネルギーを供給することで可能となる。

第二日： 電磁場分布、作製、評価

金属の光学応答

表面プラズモン

完全レンズの結像作用

準定常極限

ハイパーレンズ

S偏光ブリュースター角

クローキング

光メタマテリアルの作製法（電子線描画、ナノインプリント、光リソ）

光メタマテリアルの評価法

電磁シミュレーション

金属の光学応答

自由電子の応答：Drude 模型

$$m\ddot{r} + \frac{m}{\tau}\dot{r} = qE_0 e^{-i\omega t}$$

$r = r_0 e^{-i\omega t}$とおいて代入すると

$$r = \frac{qE}{m(-\omega^2 - i\frac{1}{\tau}\omega)}$$

電流密度　$j = nq\dot{r}$

$$j = \frac{-i\omega nq^2 E}{m(-\omega^2 - i\frac{1}{\tau}\omega)} = \frac{nq^2 E}{m(-i\omega + \frac{1}{\tau})} \equiv \sigma(\omega)E$$

$$\sigma_0 \equiv \sigma(0) = \frac{nq^2\tau}{m}$$

$$\sigma(\omega) = \frac{\sigma_0}{1 - i\omega\tau}$$

$$D = \varepsilon E = E + 4\pi P = \varepsilon_b E$$

$$j_{cond} = \sigma E$$

$$\frac{\partial D}{\partial t} + 4\pi j_{cond} = -i\omega\varepsilon_b E + 4\pi\sigma E = -i\omega\tilde{\varepsilon}E$$

$$\tilde{\varepsilon} \equiv \varepsilon_b + i\frac{4\pi\sigma}{\omega} = \varepsilon_b + i\frac{4\pi\sigma_0}{\omega(1 - i\omega\tau)}$$

$$= \varepsilon_b + i\frac{4\pi\sigma_0(1 + i\omega\tau)}{\omega(1 + (\omega\tau)^2)}$$

$$= \varepsilon_b - \frac{4\pi\sigma_0\tau}{1 + (\omega\tau)^2} + i\frac{4\pi\sigma_0}{\omega(1 + (\omega\tau)^2)}$$

$$= \varepsilon_b - \frac{4\pi nq^2/m}{\omega^2 + \gamma^2} + i\gamma\frac{4\pi nq^2/m}{\omega(\omega^2 + \gamma^2)}$$

$$= \varepsilon_b - \frac{\omega_P{}^2}{\omega^2 + \gamma^2} + i\frac{\gamma\omega_P{}^2}{\omega(\omega^2 + \gamma^2)}$$

金属誘電率のエネルギー依存性(線形)

Drude 模型

$$\varepsilon(\omega) = \varepsilon_b - \frac{f\omega_P^2}{\omega(\omega + i\gamma)}$$

$$\varepsilon_b = 1;\ f = 1;\ \hbar\omega_P = 3eV;\ E = \hbar\omega$$

$$\gamma = 1\ [1\mathrm{meV}]$$

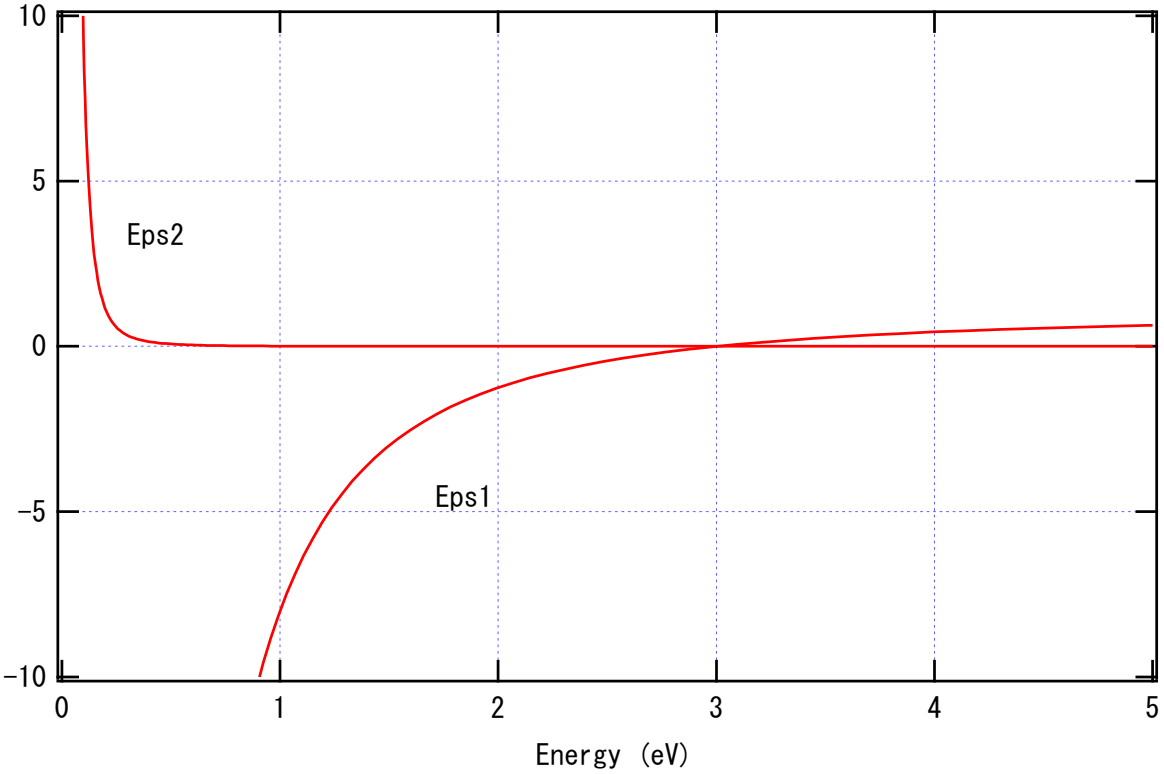

金属誘電率の周波数依存性(両対数)

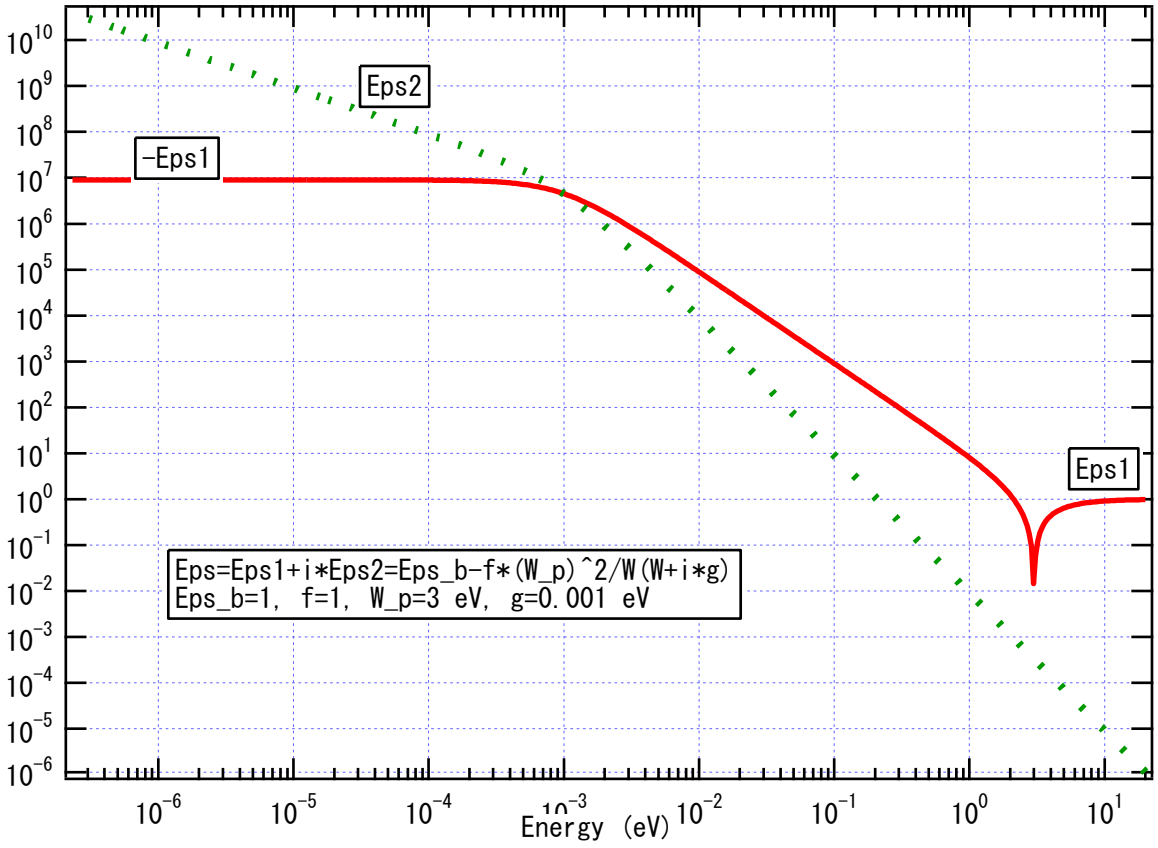

Hagen-Rubens領域:ω<<1/τ
誘電率は純虚数と見なせる。
完全導体として扱える領域
遷移領域 ：1/τ<< ω
誘電率が負であると見なせる
表面プラズモンが存在できる
透明領域 $\omega_P<\omega$
誘電率が正： 光が伝搬する

$$\tilde{\varepsilon}(\omega)=\varepsilon_b-\frac{\omega_P^2}{\omega(\omega+i\gamma)};\varepsilon_1(\omega)=\varepsilon_b-\frac{\omega_P^2}{\omega^2+\gamma^2};\varepsilon_2(\omega)=\frac{1}{\omega\gamma}\frac{\omega_P^2}{\omega^2+\gamma^2}$$

Ag & Au

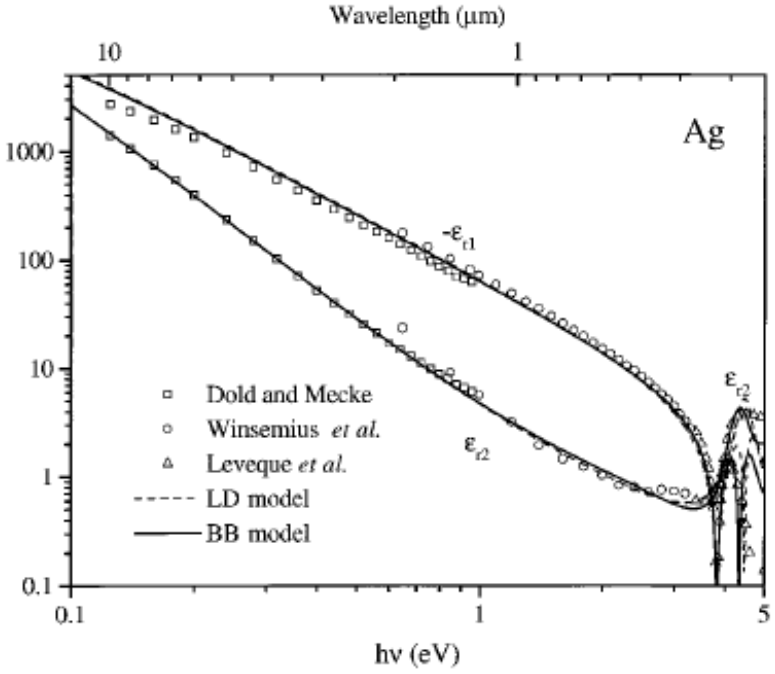

Fig. 1. Real and imaginary parts of the optical dielectric function of Ag: solid curves, values that we calculated using the BB model; dashed curves, the LD model. Also shown are the selected experimental data points from Dold and Mecke,[46] Winsemius *et al.*,[47] and Leveque *et al.*[48]

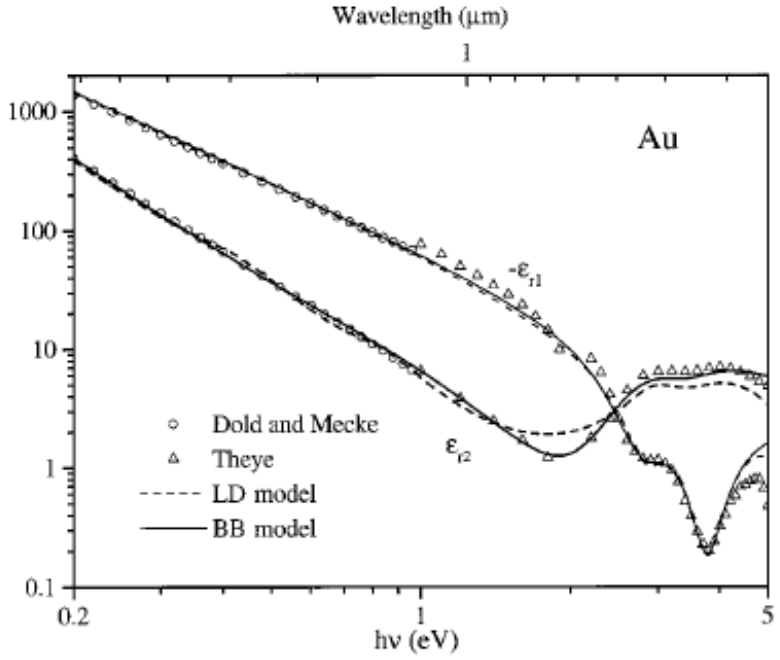

Fig. 2. Real and imaginary parts of the optical dielectric function of Au: solid curves, values that we calculated using the BB model; dashed curves, the LD model. Also shown are selected experimental data points from Dold and Mecke[46] and Thèye.[49]

Rakic, Applied Optics (1998).

Al & Cr

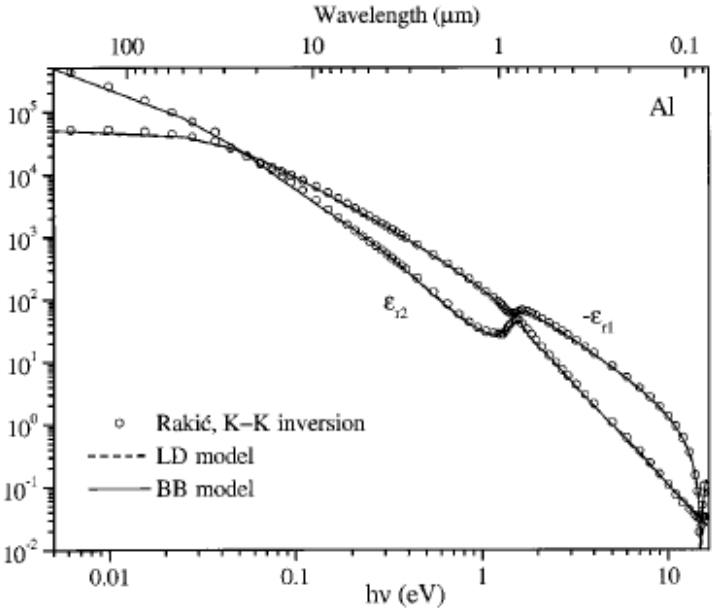

Fig. 4. Real and imaginary parts of the optical dielectric function of Al: solid curves, values that we calculated using the BB model; dashed curves, the LD model. Also shown are selected data from Rakić.[18]

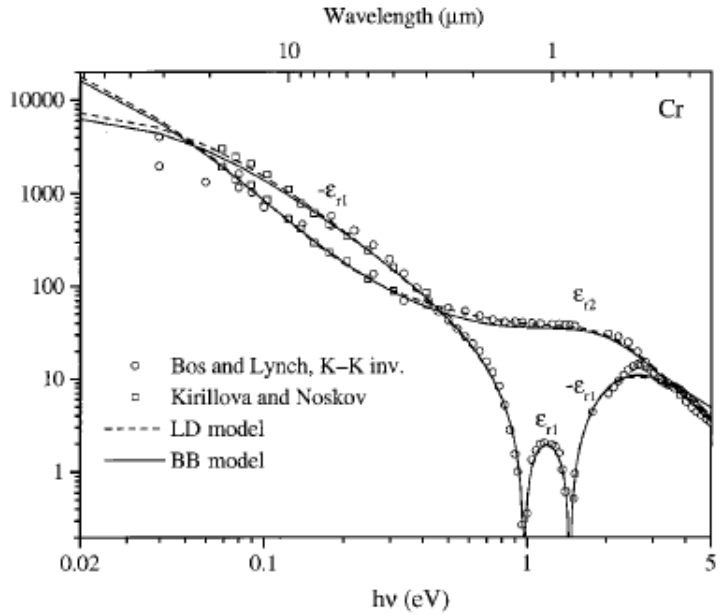

Fig. 6. Real and imaginary parts of the optical dielectric function of Cr: solid curves, values that we calculated using the BB model; dashed curves, the LD model. Also shown are tabulated data

Rakic, Applied Optics (1998).

表面プラズモン Ⅰ

$$\nabla \times E = -\frac{\partial B}{\partial t} = -\mu \frac{\partial H}{\partial t};$$

$$\nabla \times H = \frac{\partial D}{\partial t} = \varepsilon \frac{\partial E}{\partial t};$$

$$\nabla \times \nabla \times \vec{H} = \varepsilon \frac{\partial}{\partial t} \nabla \times E = -\varepsilon\mu \frac{\partial^2 \vec{H}}{\partial t^2} = -\frac{\varepsilon_r}{c^2} \frac{\partial^2 \vec{H}}{\partial t^2}; \ \mu_r = 1$$

$$\nabla \times \nabla \times \vec{H} = \nabla\nabla \cdot \vec{H} - \nabla^2 \vec{H}$$

$$\nabla^2 \vec{H} = \frac{\varepsilon_r}{c^2} \frac{\partial^2 \vec{H}}{\partial t^2}$$

$$\vec{H} = (0, H, 0)$$

$$H = \begin{cases} H_0 e^{+\alpha z + i\beta x - i\omega t} \ldots z < 0 \\ H_0 e^{-\gamma z + i\beta x - i\omega t} \ldots z > 0 \end{cases}$$

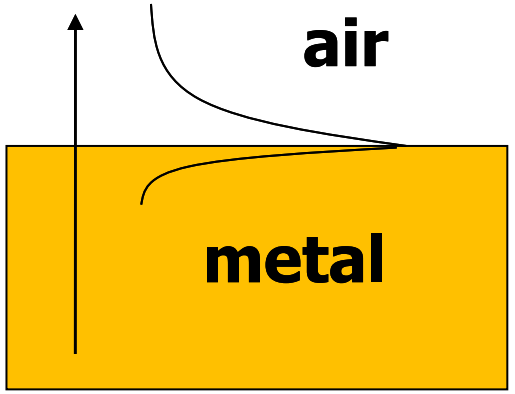

表面プラズモン II

$$\beta^2 - \alpha^2 = \varepsilon_d \omega^2 / c^2$$
$$\beta^2 - \gamma^2 = \varepsilon_m \omega^2 / c^2$$

$$-i\omega\varepsilon E = \nabla \times H = \begin{pmatrix} \partial_x \\ \partial_y \\ \partial_z \end{pmatrix} \times \begin{pmatrix} 0 \\ H \\ 0 \end{pmatrix} = \begin{pmatrix} -\partial_z H \\ 0 \\ \partial_x H \end{pmatrix}$$

$$E_x = \frac{1}{i\omega\varepsilon}\partial_z H = \frac{1}{i\omega}\begin{cases} \frac{\alpha}{\varepsilon_d} H_0 \ldots z < 0 \\ \frac{-\gamma}{\varepsilon_m} H_0 \ldots z > 0 \end{cases}$$

$$\therefore \frac{\alpha}{\varepsilon_d} = \frac{-\gamma}{\varepsilon_m} \qquad \therefore \varepsilon_m = \frac{-\gamma}{\alpha}\varepsilon_d < 0$$

$$\varepsilon_m \omega^2 / c^2 = \beta^2 - \gamma^2 = \beta^2 - (\alpha\varepsilon_m / \varepsilon_d)^2$$
$$\varepsilon_d \omega^2 / c^2 = \beta^2 - \alpha^2$$

$$((\varepsilon_d / \varepsilon_m)^2 - 1)\beta^2 = \varepsilon_d(\varepsilon_d / \varepsilon_m - 1)\frac{\omega^2}{c^2}$$

$$\beta^2 = \frac{\varepsilon_m \varepsilon_d}{\varepsilon_m + \varepsilon_d}\frac{\omega^2}{c^2}$$

$$= \begin{cases} \frac{\omega^2}{c^2} \ldots (\varepsilon_m \to -\infty) \\ \infty \ldots (\varepsilon_m \to -\varepsilon_d) \end{cases}$$

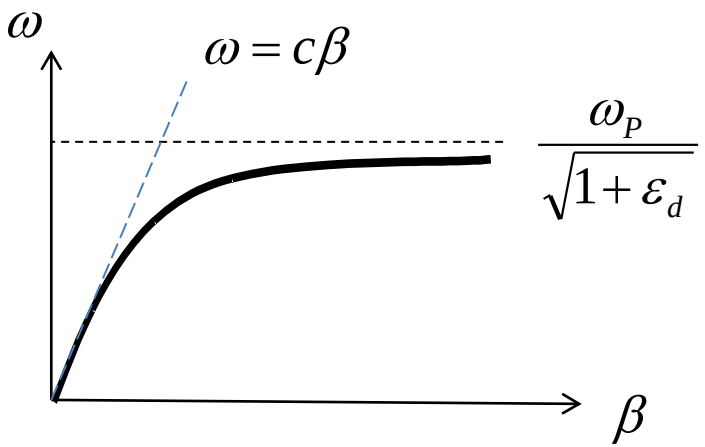

表面プラズモンの磁場分布

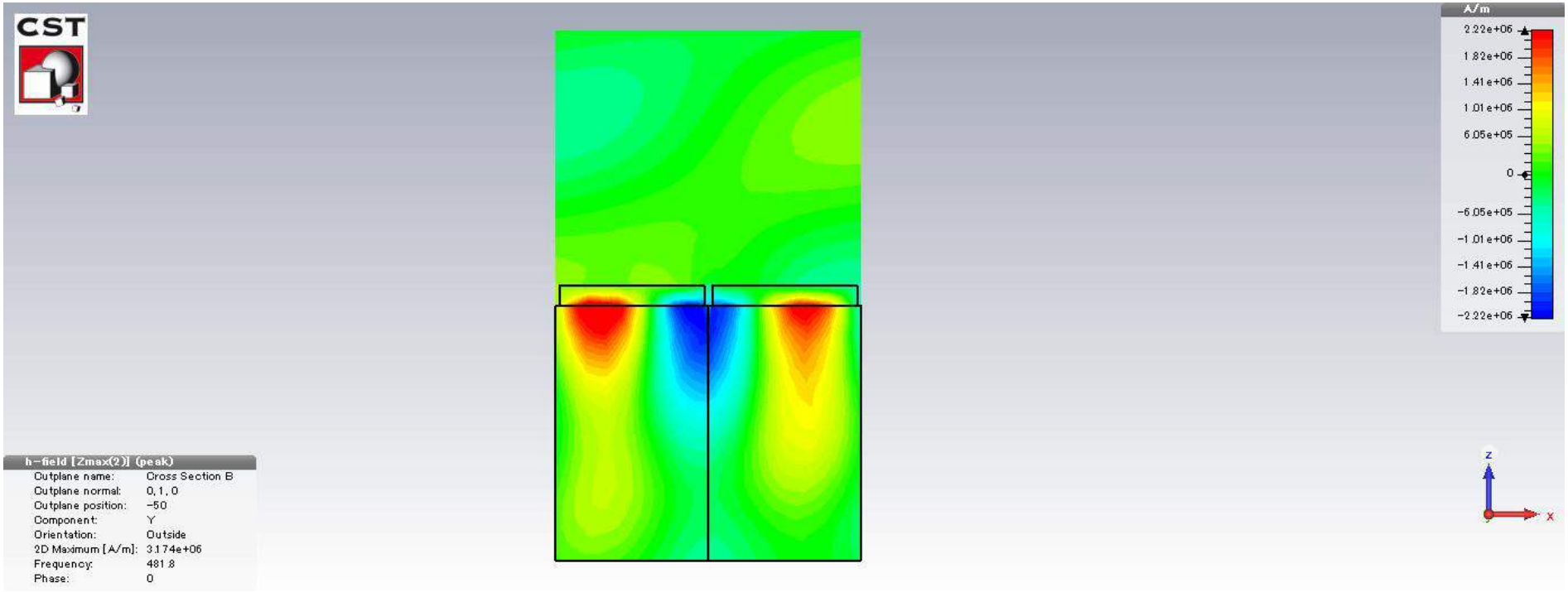

金属／誘電体界面に局在

Pendryの完全レンズ

Pendry, "Negative Refraction Makes a Perfect Lens," PRL (2000).

$$E(r,t) = \sum_{\sigma,k_x,k_y} E_\sigma(k_x,k_y)\exp\left(ik_z z + ik_x x + ik_y y - i\omega t\right)$$

$$k_z = +\sqrt{\omega^2/c^2 - k_x^2 - k_y^2}$$

$$\Delta \approx \frac{2\pi}{k_{\max}} = \frac{2\pi c}{\lambda}$$

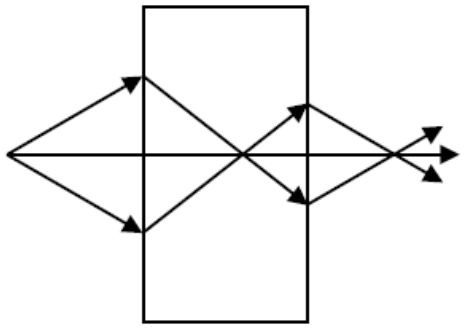

FIG. 1. A negative refractive index medium bends light to a negative angle with the surface normal. Light formerly diverging from a point source is set in reverse and converges back to a point. Released from the medium the light reaches a focus for a second time.

$\varepsilon = \mu = -1$ ならこの限界が破れる！

Pendryの完全レンズ

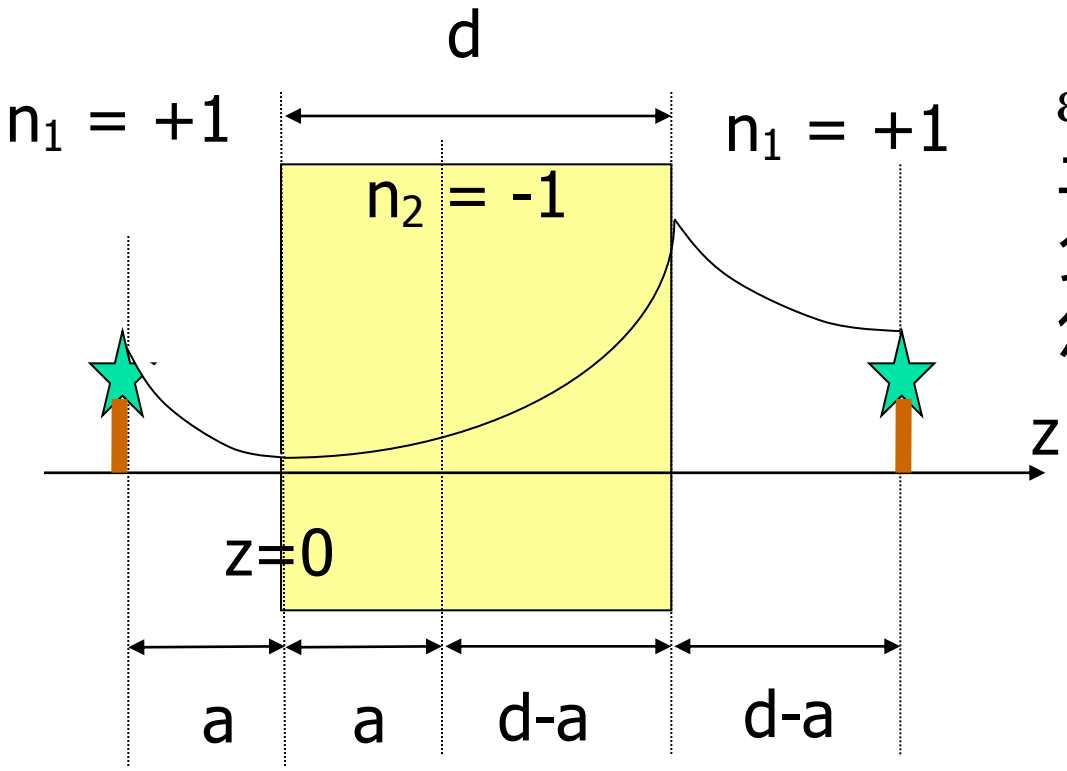

ε=μ=-1の時
エバネッセント波の振幅は
負屈折率媒質内で増大し、
焦点の位置で回復する。

$$E = E_0 e^{i(k_x x + k_y y) - \kappa z}; \quad z < 0$$

$$E = E_0{}' e^{i(k_x x + k_y y) - \kappa (d - z)}; \quad 0 < z < d$$

$$E = E_0{}' e^{i(k_x x + k_y y) - \kappa (z - d)}; \quad d < z$$

- ε=μ=-1; n = -1 の薄板は近接場まで含めてすべてをイメージングする。⇒ 完全レンズ
- 光に関する「反物質」

electrostatic limit

medium *does* amplify evanescent waves. Hence we conclude that with this new lens *both propagating and evanescent waves contribute to the resolution of the image*. Therefore there is no physical obstacle to perfect reconstruction of the image beyond practical limitations of apertures and perfection of the lens surface. This is the principal conclusion of this Letter.

No scheme can be of much interest if the means of realizing it are not available. Fortunately several recent developments make such a lens a practical possibility, at least in some regions of the spectrum. Some time ago it was shown that wire structures with lattice spacings of the order of a few millimeters behave like a plasma with a resonant frequency, ω_{ep}, in the GHz region [2]. The ideal dielectric response of a plasma is given by

$$\varepsilon = 1 - \frac{\omega_{ep}^2}{\omega^2} \tag{24}$$

and takes negative values for $\omega < \omega_{ep}$. More recently we have also shown [3] that a structure containing loops of conducting wire has properties mimicking a magnetic plasma,

$$\mu \approx 1 - \frac{\omega_{mp}^2}{\omega^2}, \tag{25}$$

and, although the analogy is less perfect, it has been shown that $-ve\,\mu$ has been attained in these structures [4]. Thus

$$\lim_{\varepsilon\to -1}\lim_{k_x^2+k_z^2\to\infty} T_P = \lim_{\varepsilon\to -1}\frac{4\varepsilon\exp(ik_z d)}{(\varepsilon+1)^2-(\varepsilon-1)^2\exp(2ik_z d)} = \exp(-ik_z d) = \exp(+\sqrt{k_x^2+k_x^2}\,d) \tag{31}$$

to obtain focusing of a quasielectrostatic field, without placing any conditions on μ. It is interesting to note that

and the magnetostatics claim the S-polarized fields.

In the electrostatic limit,

$$\omega \ll c_0\sqrt{k_x^2+k_y^2}\,. \tag{27}$$

It follows from (14) that

$$\lim_{k_x^2+k_z^2\to\infty} k_z = \lim_{k_x^2+k_z^2\to\infty} i\sqrt{k_x^2+k_y^2-\omega^2 c_0^{-2}} = i\sqrt{k_x^2+k_x^2} \tag{28}$$

and, from (17)

$$\lim_{k_x^2+k_z^2\to\infty} k_z' = \lim_{k_x^2+k_z^2\to\infty} i\sqrt{k_x^2+k_y^2-\varepsilon\mu\omega^2 c_0^{-2}} = i\sqrt{k_x^2+k_x^2} = k_z\,. \tag{29}$$

Hence in this limit we see that, for the P-polarized fields, dependence on μ is eliminated and only the dielectric function is relevant. The transmission coefficient of the slab becomes

$$\lim_{k_x^2+k_z^2\to\infty} T_P = \lim_{k_x^2+k_z^2\to\infty}\frac{2\varepsilon k_z}{\varepsilon k_z + k_z'}\frac{2k_z'}{k_z'+\varepsilon k_z} \times \frac{\exp(ik_z' d)}{1-(\frac{k_z'-\varepsilon k_z}{k_z'+\varepsilon k_z})^2\exp(2ik_z' d)} = \frac{4\varepsilon\exp(ik_z d)}{(\varepsilon+1)^2-(\varepsilon-1)^2\exp(2ik_z d)}, \tag{30}$$

and hence, in this limit, we need only assume

the higher order Fourier components of the potential are

準定常極限

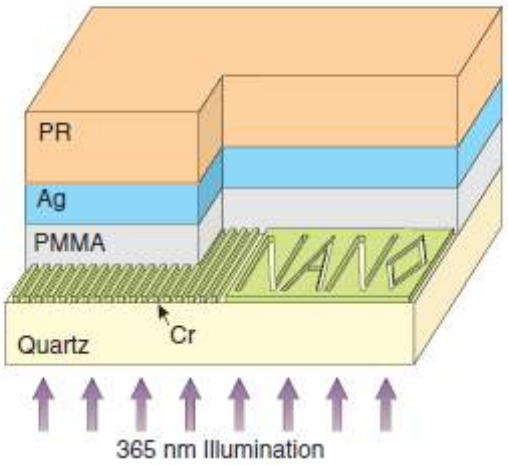

Fig. 1. Optical superlensing experiment. The embedded objects are inscribed onto the 50-nm-thick chrome (Cr); at left is an array of 60-nm-wide slots of 120 nm pitch, separated from the 35-nm-thick silver film by a 40-nm PMMA spacer layer. The image of the object is recorded by the photoresist on the other side of the silver superlens.

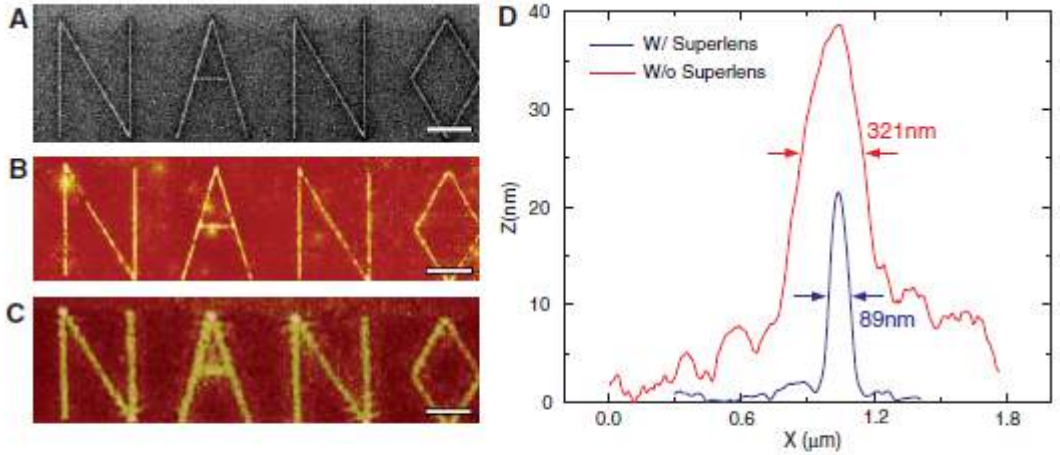

Fig. 4. An arbitrary object "NANO" was imaged by silver superlens. (A) FIB image of the object. The linewidth of the "NANO" object was 40 nm. Scale bar in (A) to (C), 2 μm. (B) AFM of the developed image on photoresist with a silver superlens. (C) AFM of the developed image on photoresist when the 35-nm-thick layer of silver was replaced by PMMA spacer as a control experiment. (D) The averaged cross section of letter "A" shows an exposed line width of 89 nm (blue line), whereas in the control experiment, we measured a diffraction-limited full width at half-maximum line width of 321 ± 10 nm (red line).

Fang & Zhang, "Sub–Diffraction-Limited Optical Imaging with a Silver Superlens," Science 2005.

S偏光ブリュースター角

Brewster角は通常p偏光でしか存在しない。比透磁率が1からずれれば存在可能。

$$r_s = \frac{\sqrt{\mu_1/\varepsilon_1}\cos\theta_1 - \sqrt{\mu_2/\varepsilon_2}\cos\theta_2}{\sqrt{\mu_1/\varepsilon_1}\cos\theta_1 + \sqrt{\mu_2/\varepsilon_2}\cos\theta_2}$$

$$\frac{\sin\theta_1}{\sin\theta_2} = \frac{\sqrt{\varepsilon_2\mu_2}}{\sqrt{\varepsilon_1\mu_1}}$$

$$\sin^2\theta_1 = \frac{\mu_2(\mu_2\varepsilon_1 - \mu_1\varepsilon_2)}{\varepsilon_1(\mu_2^2 - \mu_1^2)} \Rightarrow \frac{\mu_2(\mu_2 - \varepsilon_2)}{\mu_2^2 - 1}$$

$$0 < \frac{\mu_2(\mu_2 - \varepsilon_2)}{\mu_2^2 - 1} < 1$$

光線伝搬と等角写像

Controlling Electromagnetic Fields
J. B. Pendry, *et al.*
Science **312**, 1780 (2006);

$$\varepsilon'_u = \varepsilon_u \frac{Q_u Q_v Q_w}{Q_u^2},$$

$$\mu'_u = \mu_u \frac{Q_u Q_v Q_w}{Q_u^2}, \text{ etc.}$$

$$E'_u = Q_u E_u,\ H'_u = Q_u H_u, \text{ etc.}$$

where,

$$Q_u^2 = \left(\frac{\partial x}{\partial u}\right)^2 + \left(\frac{\partial y}{\partial u}\right)^2 + \left(\frac{\partial z}{\partial u}\right)^2$$

$$Q_v^2 = \left(\frac{\partial x}{\partial v}\right)^2 + \left(\frac{\partial y}{\partial v}\right)^2 + \left(\frac{\partial z}{\partial v}\right)^2$$

$$Q_w^2 = \left(\frac{\partial x}{\partial w}\right)^2 + \left(\frac{\partial y}{\partial w}\right)^2 + \left(\frac{\partial z}{\partial w}\right)^2$$

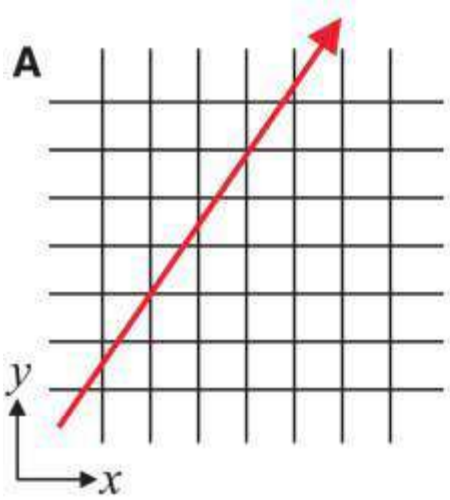

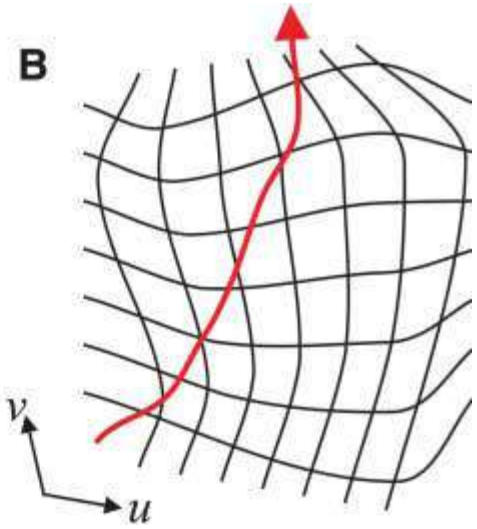

$R_1 < r < R_2$

$$r' = R_1 + r(R_2 - R_1)/R_2,$$

$$\theta' = \theta,$$

$$\phi' = \phi$$

$$\varepsilon'_{r'} = \mu'_{r'} = \frac{R_2}{R_2 - R_1}\frac{(r' - R_1)^2}{r'},$$

$$\varepsilon'_{\theta'} = \mu'_{\theta'} = \frac{R_2}{R_2 - R_1},$$

$$\varepsilon'_{\phi'} = \mu'_{\phi'} = \frac{R_2}{R_2 - R_1}$$

クローキング技術

Wave impedance

$$Z = \sqrt{|\mu|/|\varepsilon|}$$

Refractive index

$$n = \pm\sqrt{|\varepsilon||\mu|}$$

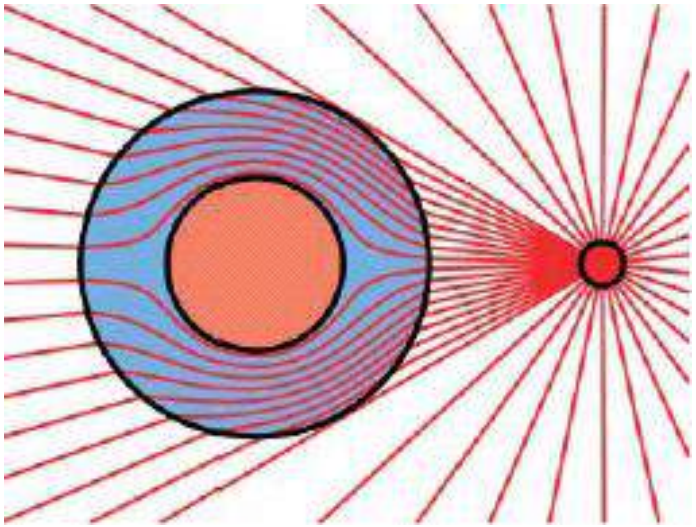

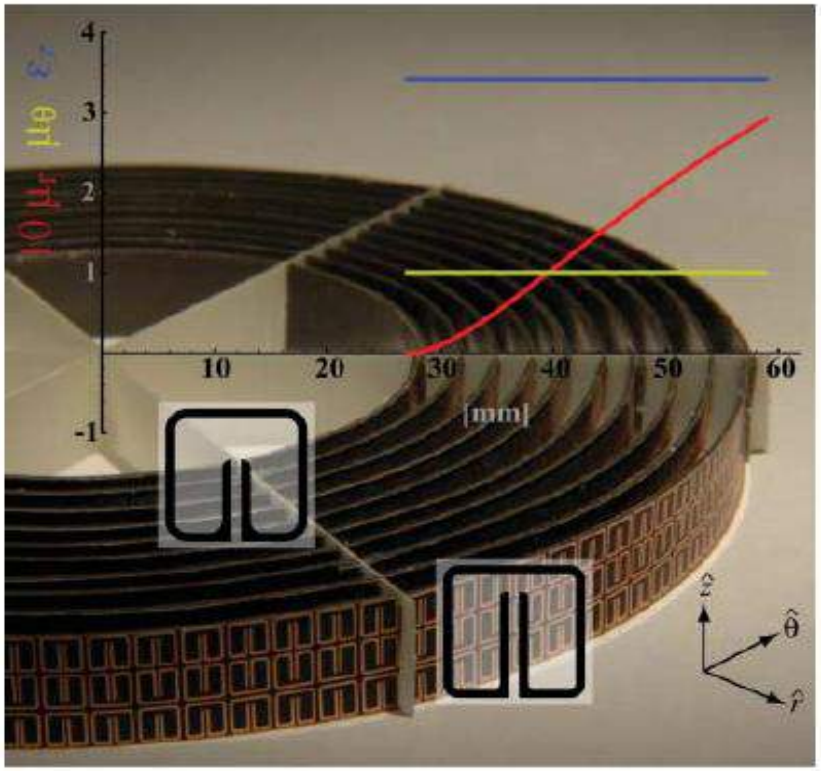

Metamaterial Electromagnetic Cloak at Microwave Frequencies
D. Schurig, *et al.*
Science **314**, 977 (2006);

透明マント：計算と実験

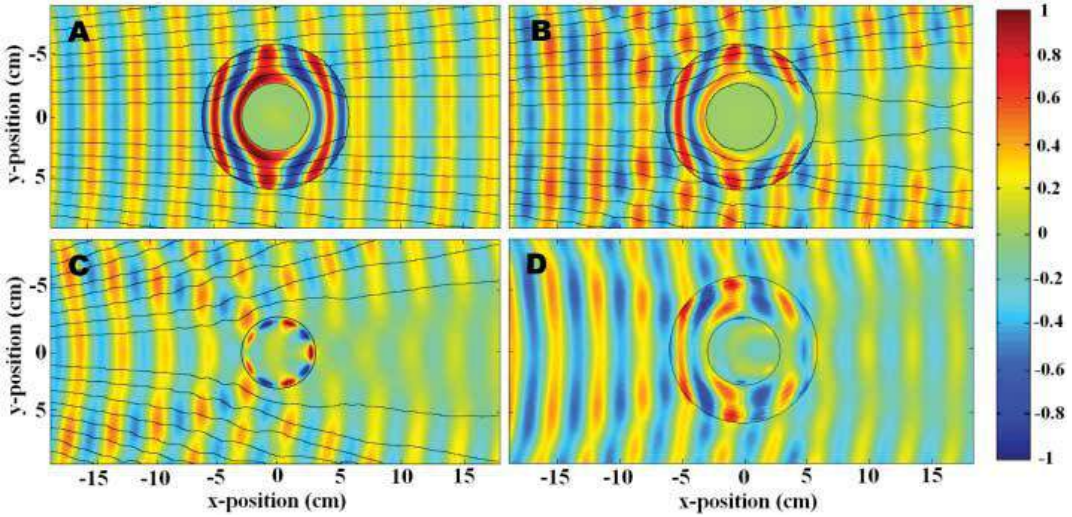

図14：クローキングの電場分布のシミュレーション(A),(B)
とクロークなしの実測値（C）およびクロークで囲んだ場合の実測値。
（A）は理想的な場合、（B）は損失を取り入れた現実的なパラメタによる計算。

See also Invisibility Cloak movie at Youtube
https://www.youtube.com/watch?v=qD37iLWRdD4

スーパーレンズから ハイパーレンズへ

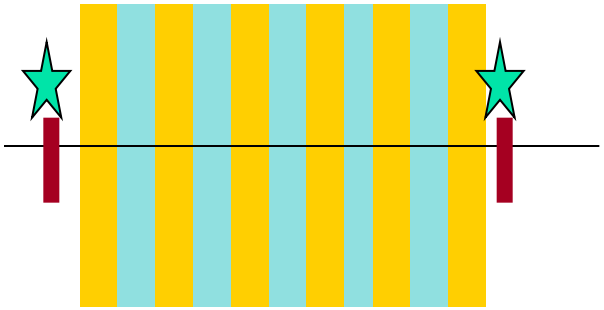

金属誘電体多層膜はp偏光に対して
完全レンズの代替品となる。

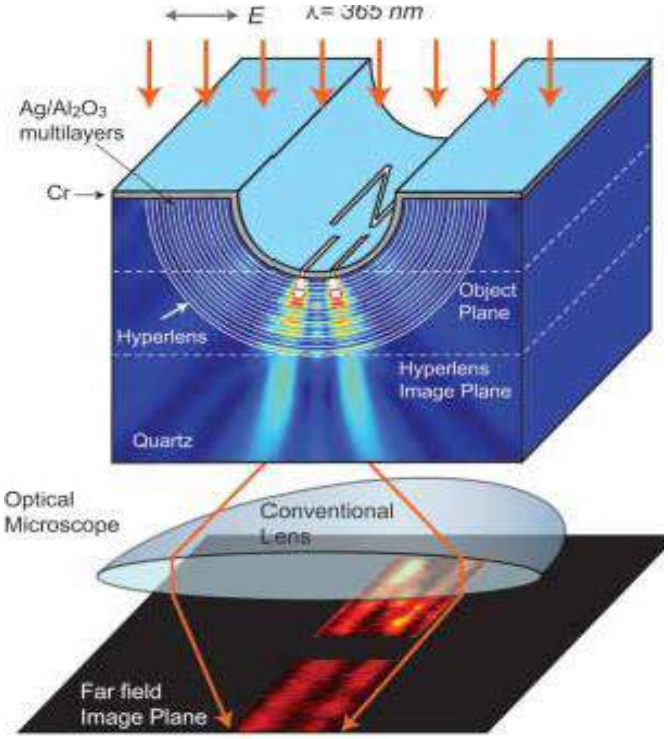

First step to real-time
super-resolution imaging
X. Zhang (2007) 張翔

Nature Materials 7 (2008)435.

ハイパボリック分散

$$\frac{1}{\varepsilon_{\parallel}}(k_x^2+k_y^2)+\frac{1}{\varepsilon_{\perp}}k_z^2=\left(\frac{\omega}{c}\right)^2=k_0^2$$

$\varepsilon_{\perp}\varepsilon_{\parallel}<0$

なら双曲線
kの値に上限はない

$$k_x>\sqrt{\varepsilon_{\parallel}}\frac{\omega}{c}$$

の高い空間周波数が伝搬

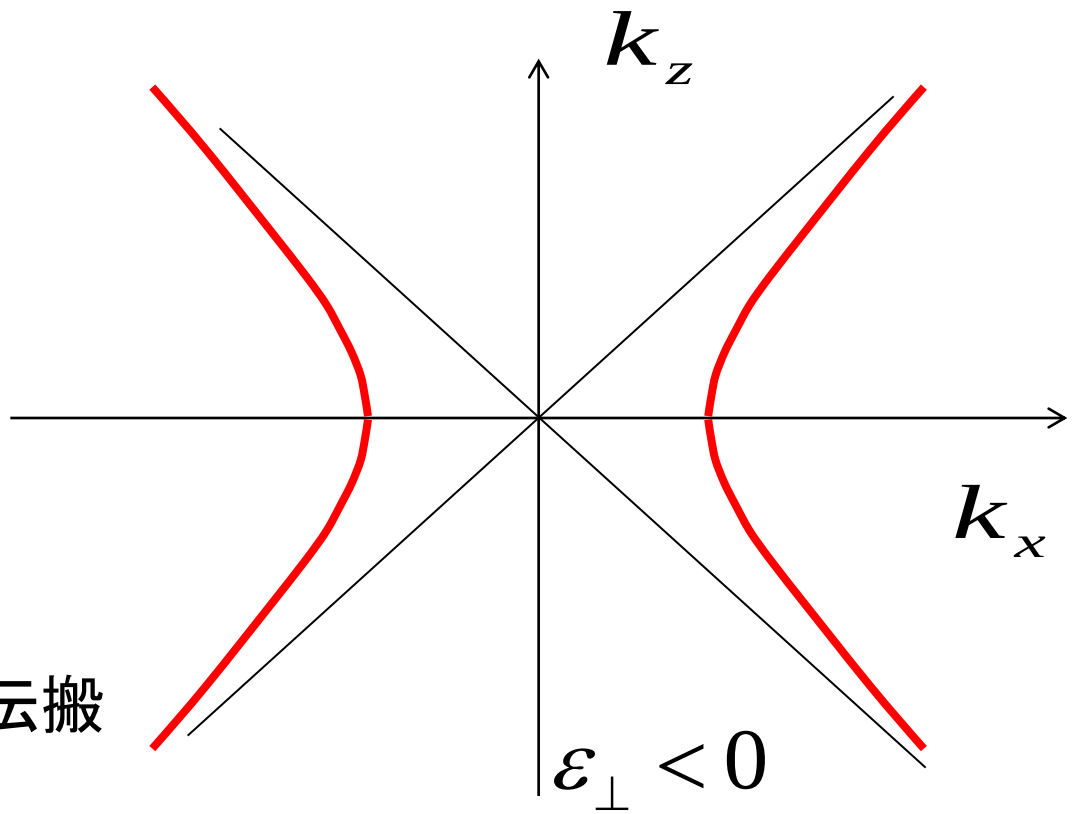

ハイパボリック媒質の電磁場伝搬:Hy

$(D10/M10/D10)_{50}$

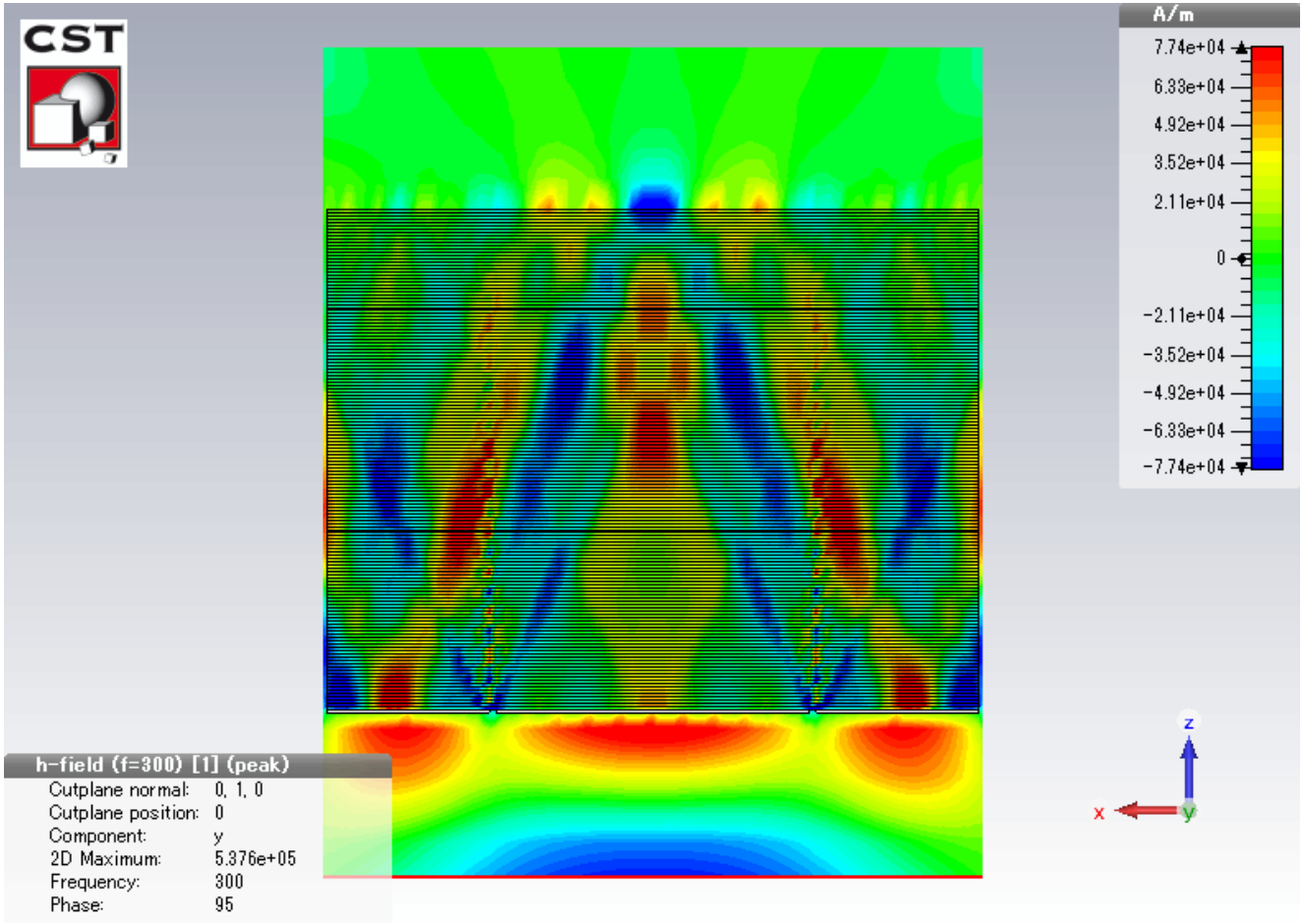

ナノ加工の方法

1) 電子線描画法
2) FIB (Focused Ion Beam)法
3) ナノインプリント法
4) レーザ直描法

電子線による微細加工

目的：　光（波長数百ナノメータ）領域のメタマテリアル作製

数10nmスケールの（2次元）金属周期的構造が作りたい

基板の上に金属薄膜を付ける（蒸着またはスパッタ）

その上にレジストと呼ばれる物質の薄膜を付ける

絞り込んだ電子ビームを移動して必要なパターンをレジストに照射

　　電子はレジストと相互作用して、

　　架橋したり（ネガのとき）、

　　結合を切ったり（ポジのとき）する。

適当な液体に浸して不要な部分を除去する。（現像）

レジストをマスクとして、ドライエッチングを行い、金属を削る。

レジストを除去して完成。

試料作製： 新しい物理の舞台を準備

スパッタ製膜装置

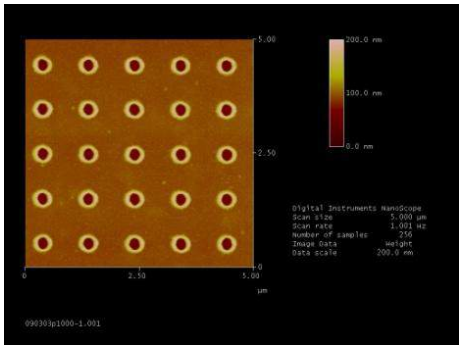

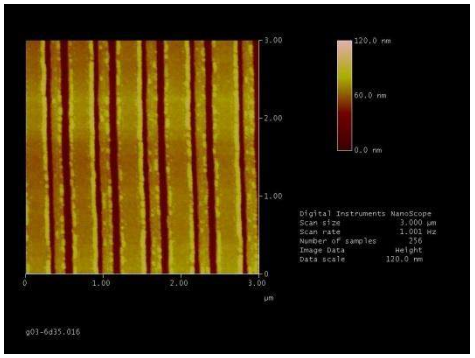

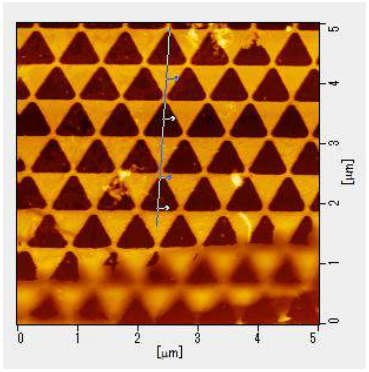

電子線描画装置

世界のどこにもない物理系を
自分の手でデザイン、作製し、測定する！

ELS G125S

エリオニクス社製　電子線描画装置@東北大西澤センター

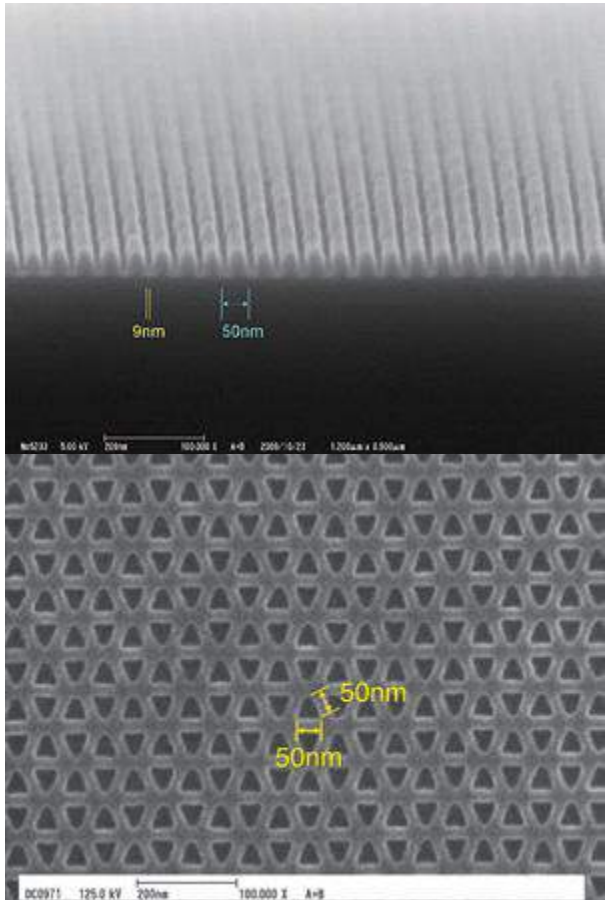

電子銃	ZrO/W熱電界放射型
加速電圧	125kV, 75kV, 25kV
最小電子ビーム径	φ1.7nm (於125kV)
描画最小線幅	5nm (於125kV)
ビーム電流強度	5×10-12～1×10-7A
描画フィールドサイズ	最大3,000μm x 3,000μm 最小100μm x 100μm
ビームポジション	最大1,000,000 x 1,000,000（20bit DAC)
ビーム位置決め分解能	0.01nm
最大試料サイズ	8インチφウェハー又は8インチ□マスク

微細加工プロセスの例

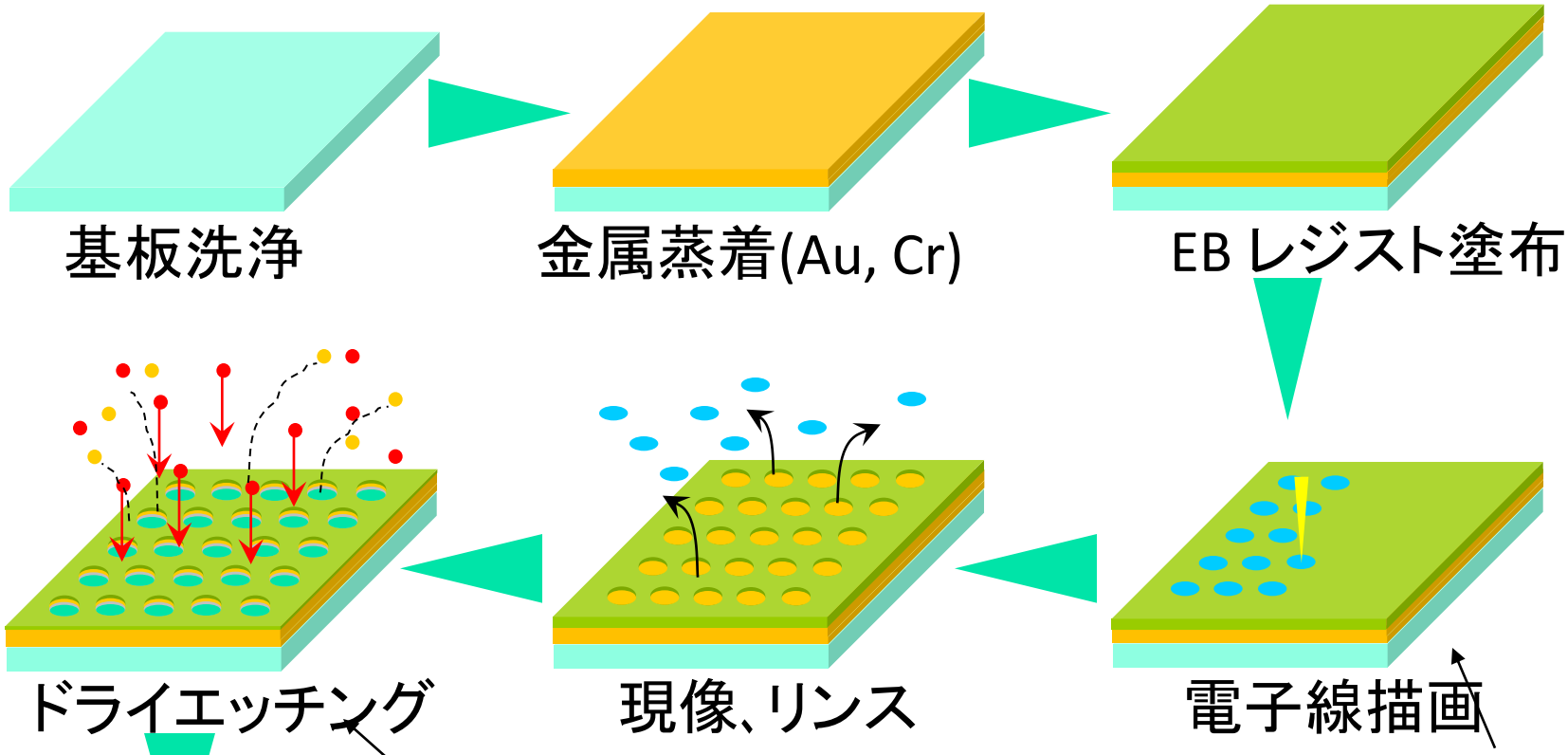

反応性イオンエッチング装置

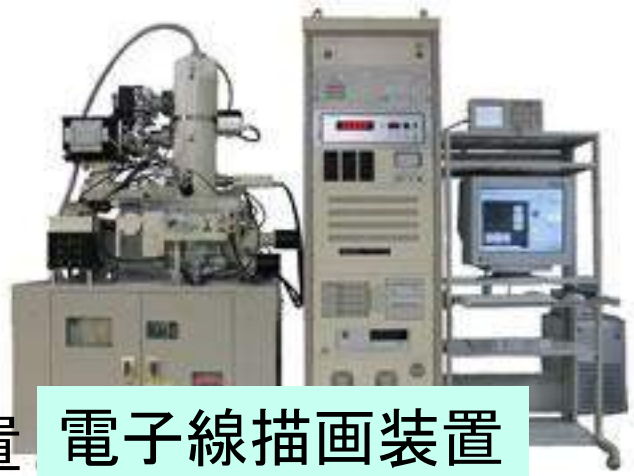

電子線描画装置

試料のSEM画像

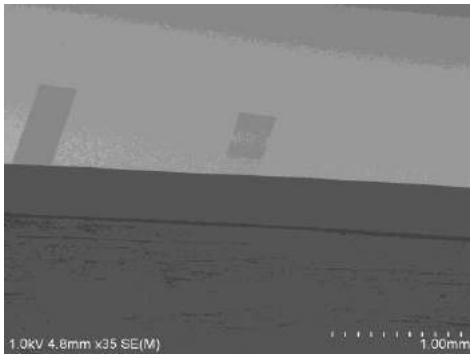

ELS7700（理化学研究所所蔵）

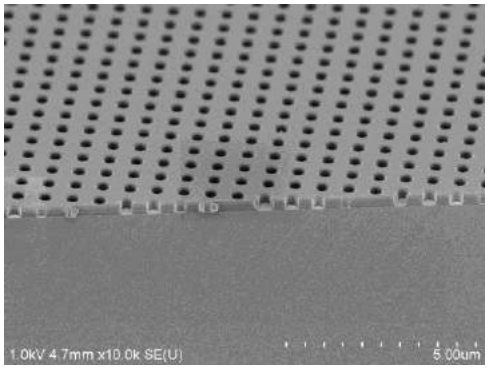

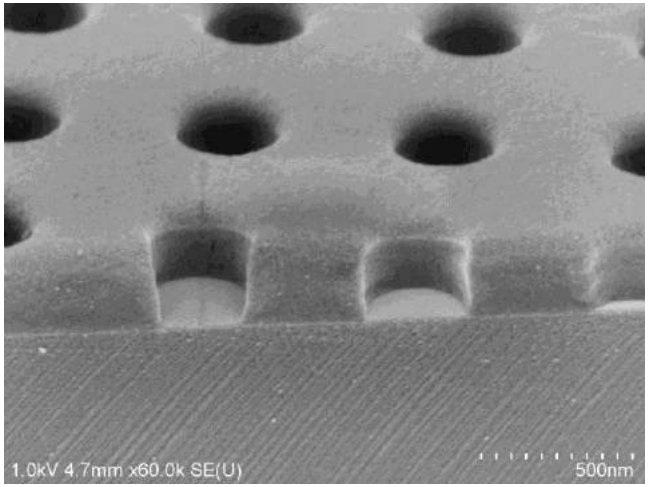

ナノインプリントリソグラフィー

Adhesive molecular monolayer for NIL

Dewetting suppression
and high resolution Au patterns
by wet etching

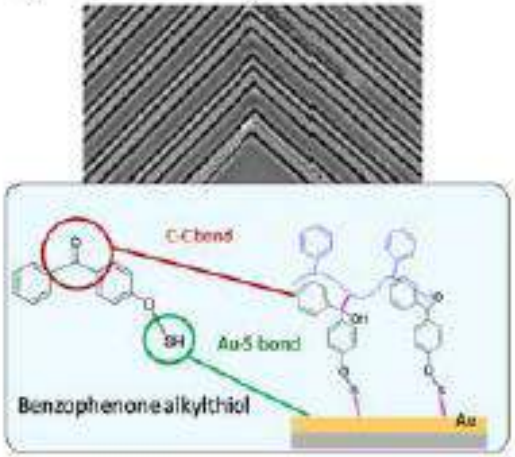

Langmuir **2009**, 25, 6604

Au line width perfectly
decreased by
wet side etching

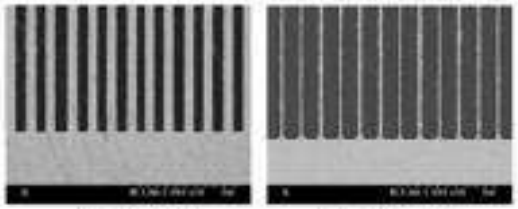

0.49 μm 0.35 μm

Chem. Lett. **2012**, *41*, 1291

Polystyrene grafted layer assisting
Au selective electrodeposition

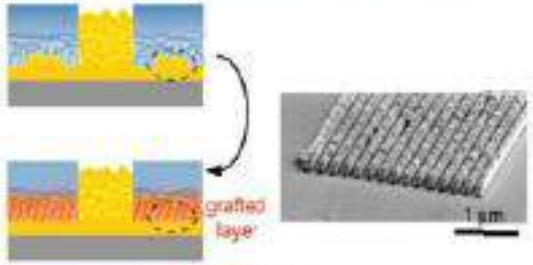

shield effect

Langmuir **2012**, *28*, 11646

Slit ring resonators for visible frequency metamaterials

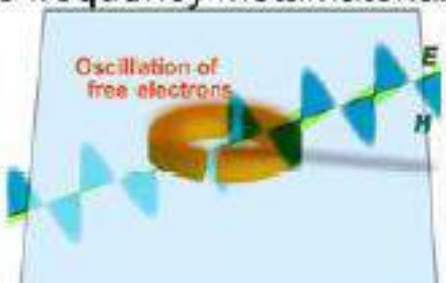

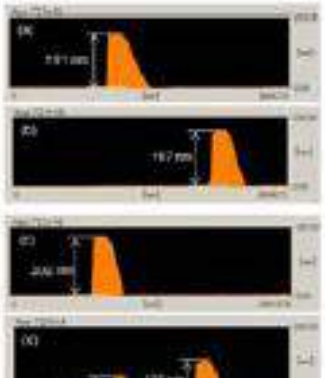

Covalent
anchoring
showing
mechanical
durability

ナノインプリントによるSRR

5-mm square array containing

360 million **Au** SRRs

line width: 47 ± 3 nm

gap width: 42 ± 3 nm

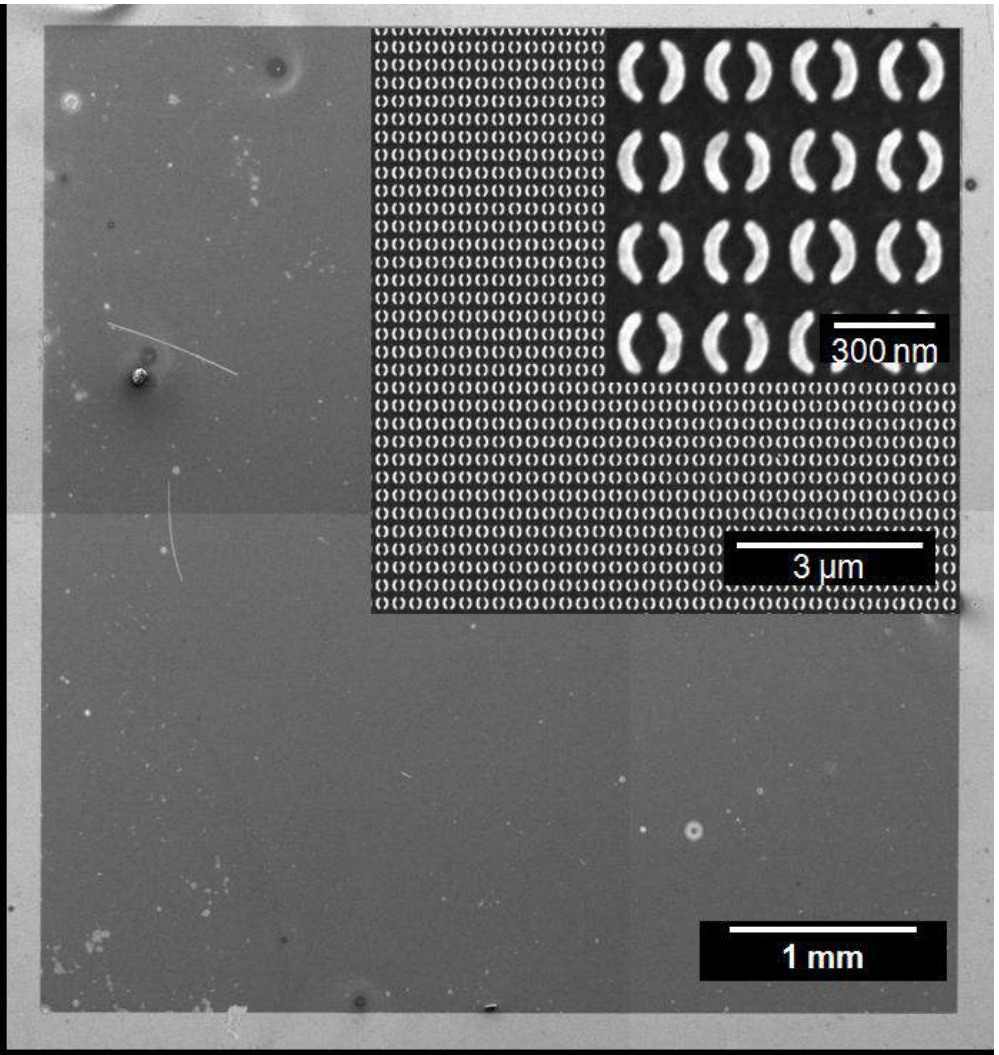

Tomioka, Kubo, Hoga, Nakagawa, Tanaka, *Appl. Phys. Lett.***2013**, *103*, 071104

Laser Direct Writing I

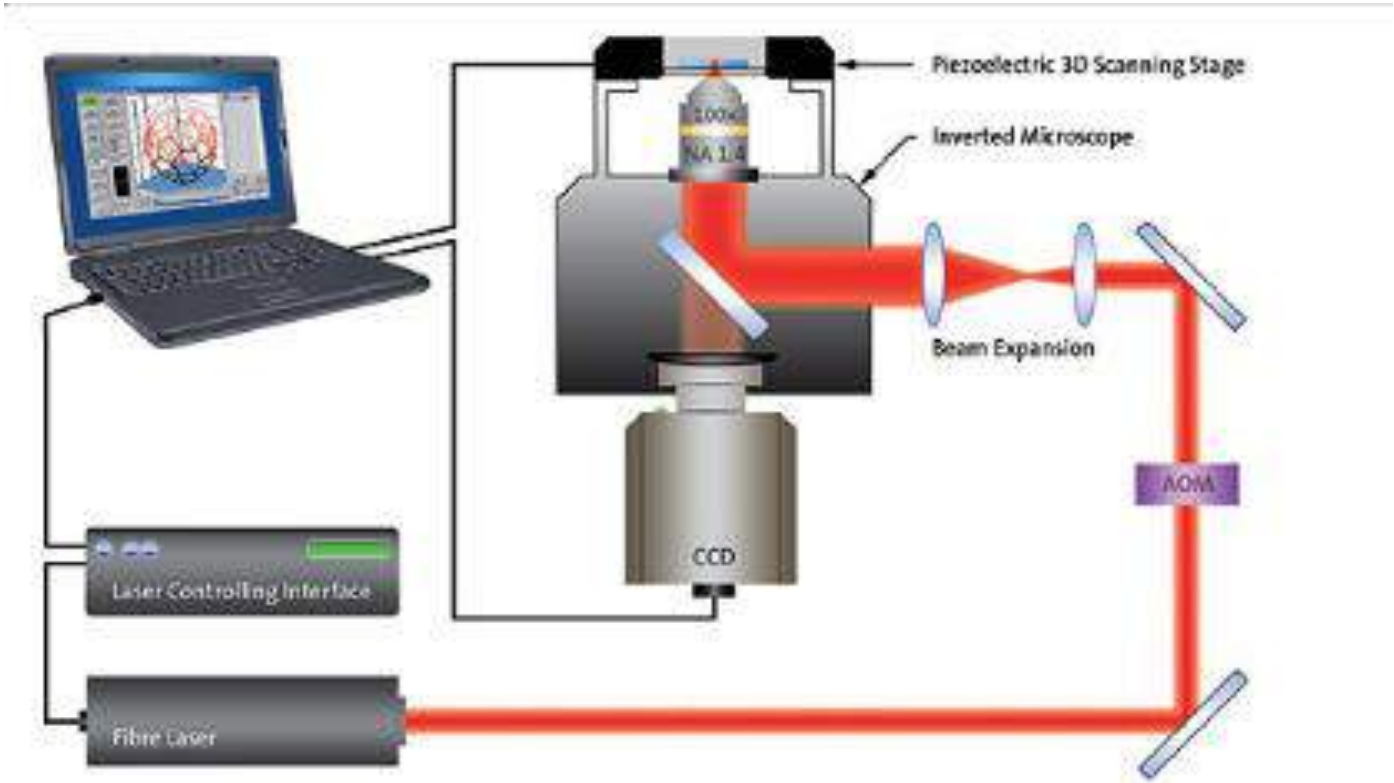

Laser Direct Writing II

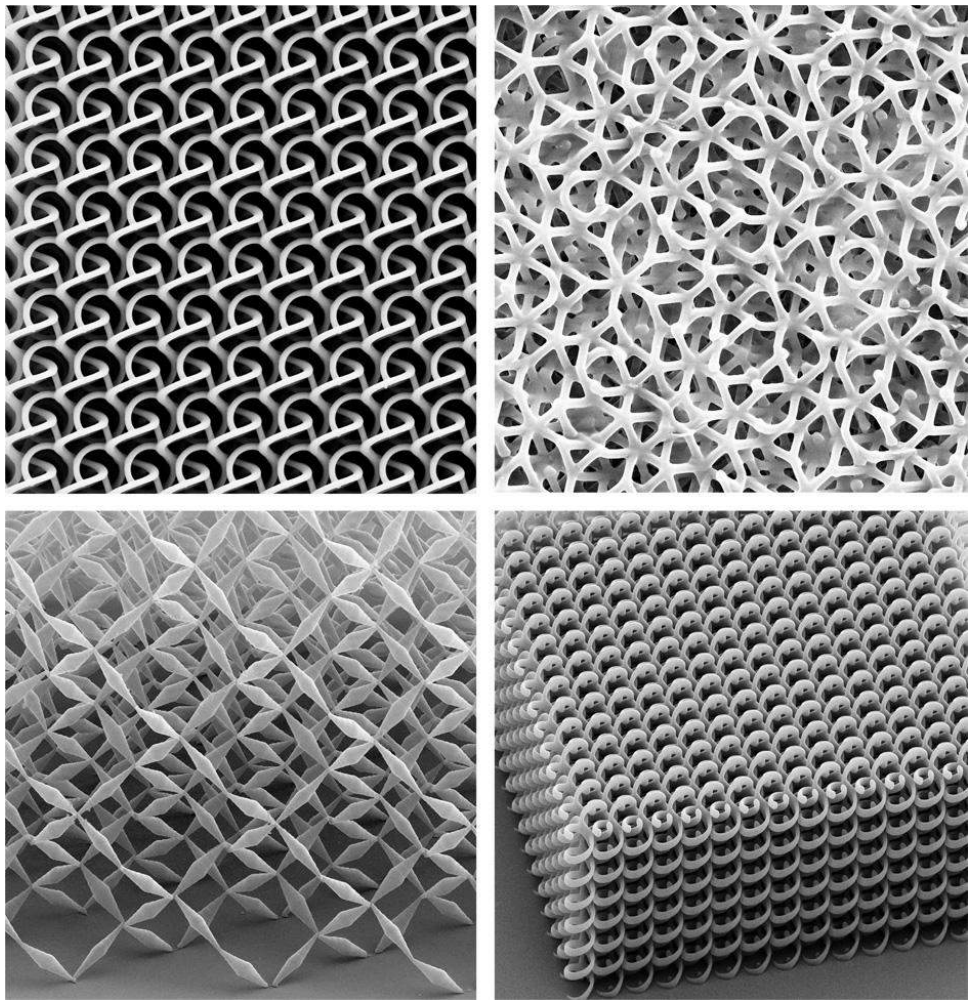

M. Wegener's group
IEEE Spectrum (2014).

Surface plasmon excitation

Surface Plasmons: coherent oscillations of electron density at metal/dielectric interface

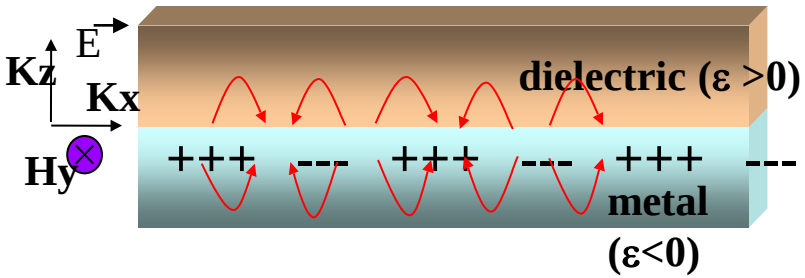

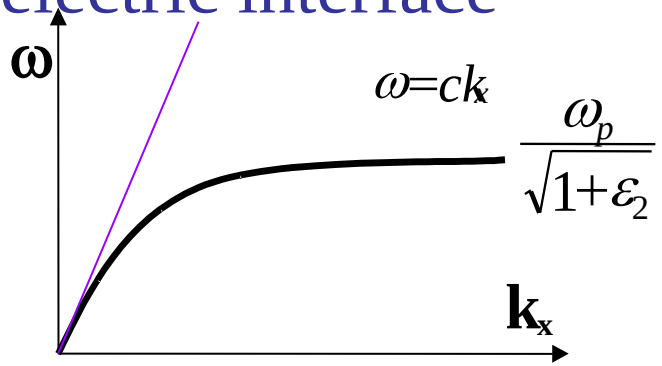

Dispersion relation

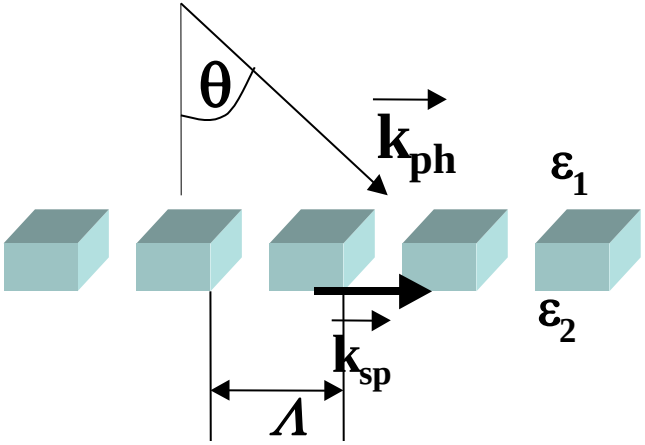

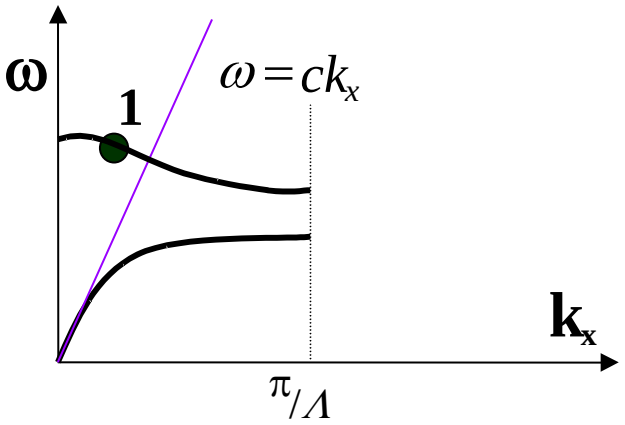

Surface Plasmon Lithography: The mechanism

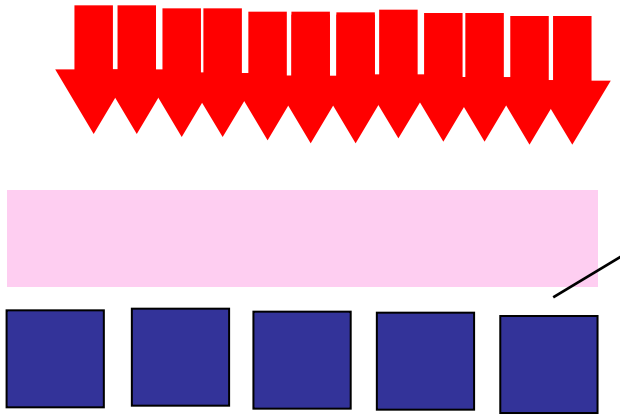

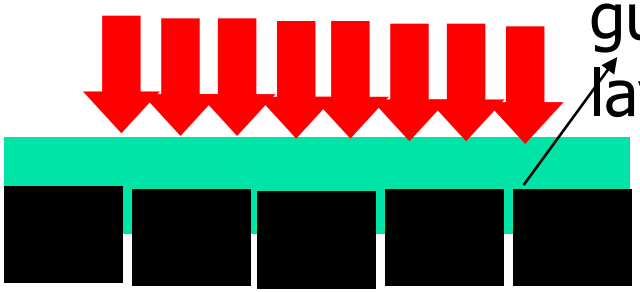

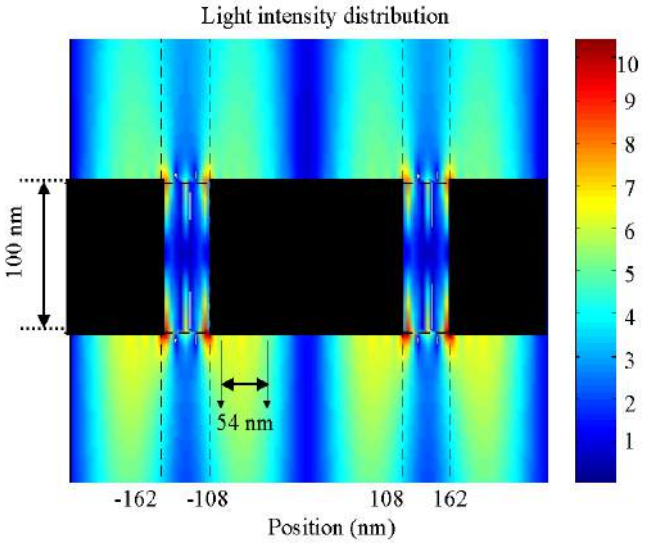

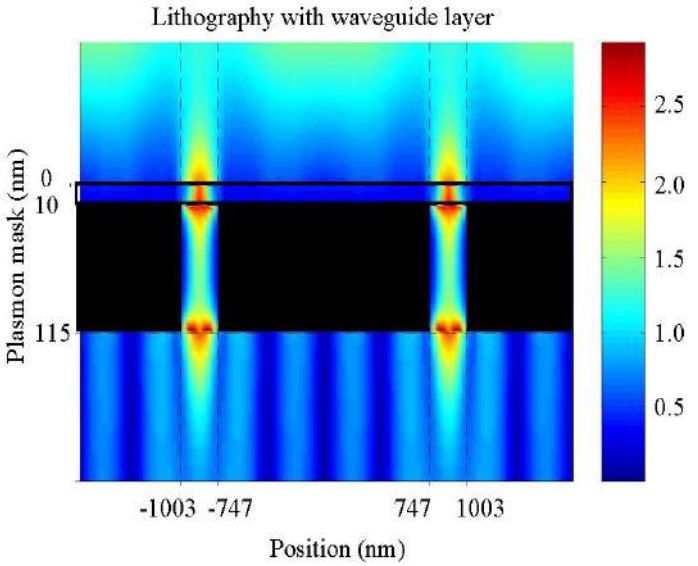

有効誘電率、有効透磁率の決定

$$Z^2 = \frac{(1+r)^2 - t^2}{(1-r)^2 - n_s{}^2 t^2} \qquad \therefore Z = \pm\sqrt{\frac{(1+r)^2 - t^2}{(1-r)^2 - n_s{}^2 t^2}}$$

$$n = \frac{c}{\omega d}\cos^{-1}\left(\frac{n_s t^2 - r^2 + 1}{(n_s - 1)r + n_s + 1}\frac{1}{t}\right)$$

$$n = \sqrt{\varepsilon\mu}\,; \quad \mathrm{Z} = \sqrt{\mu/\varepsilon}$$

$$\therefore \quad \mu = nZ; \quad \varepsilon = n/Z$$

MZ干渉計

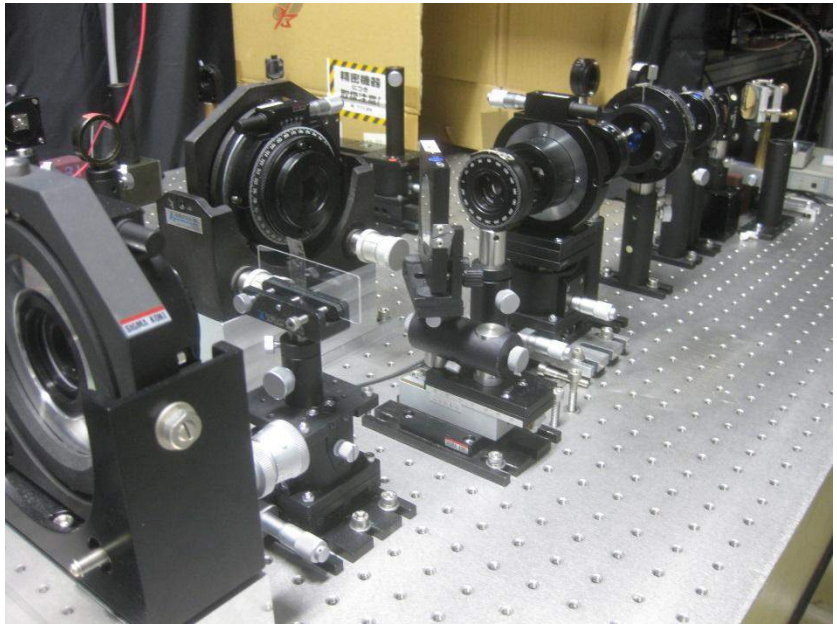

HL: Halogen Lamp
P1,P2: Polarizer
LCR: Liquid Crystal Retarder
W1,W2: Walk-off Prism
HP: Half-Wave Plate
SA: Sample
SU: Substrate
| • : Polarization direction

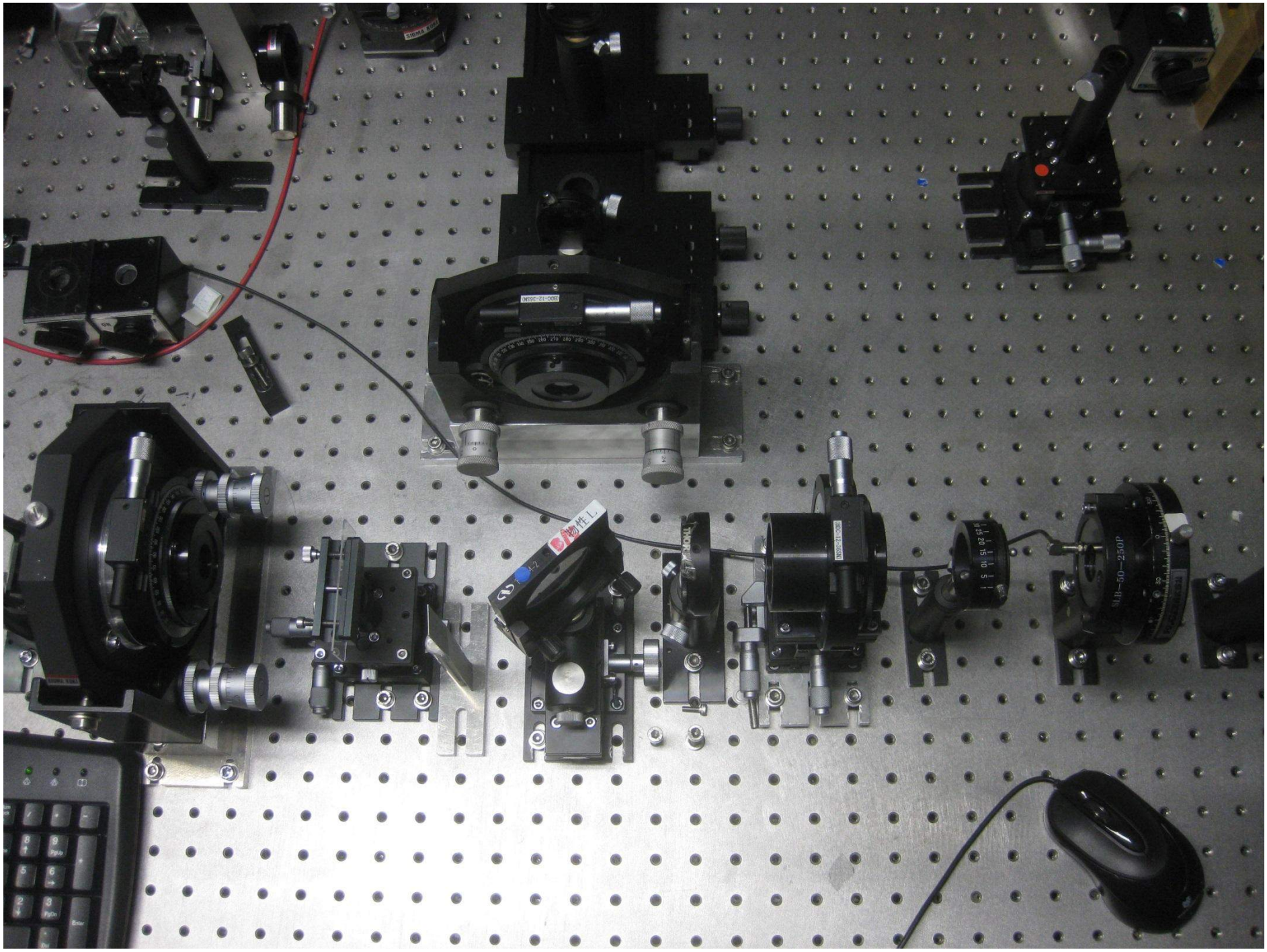

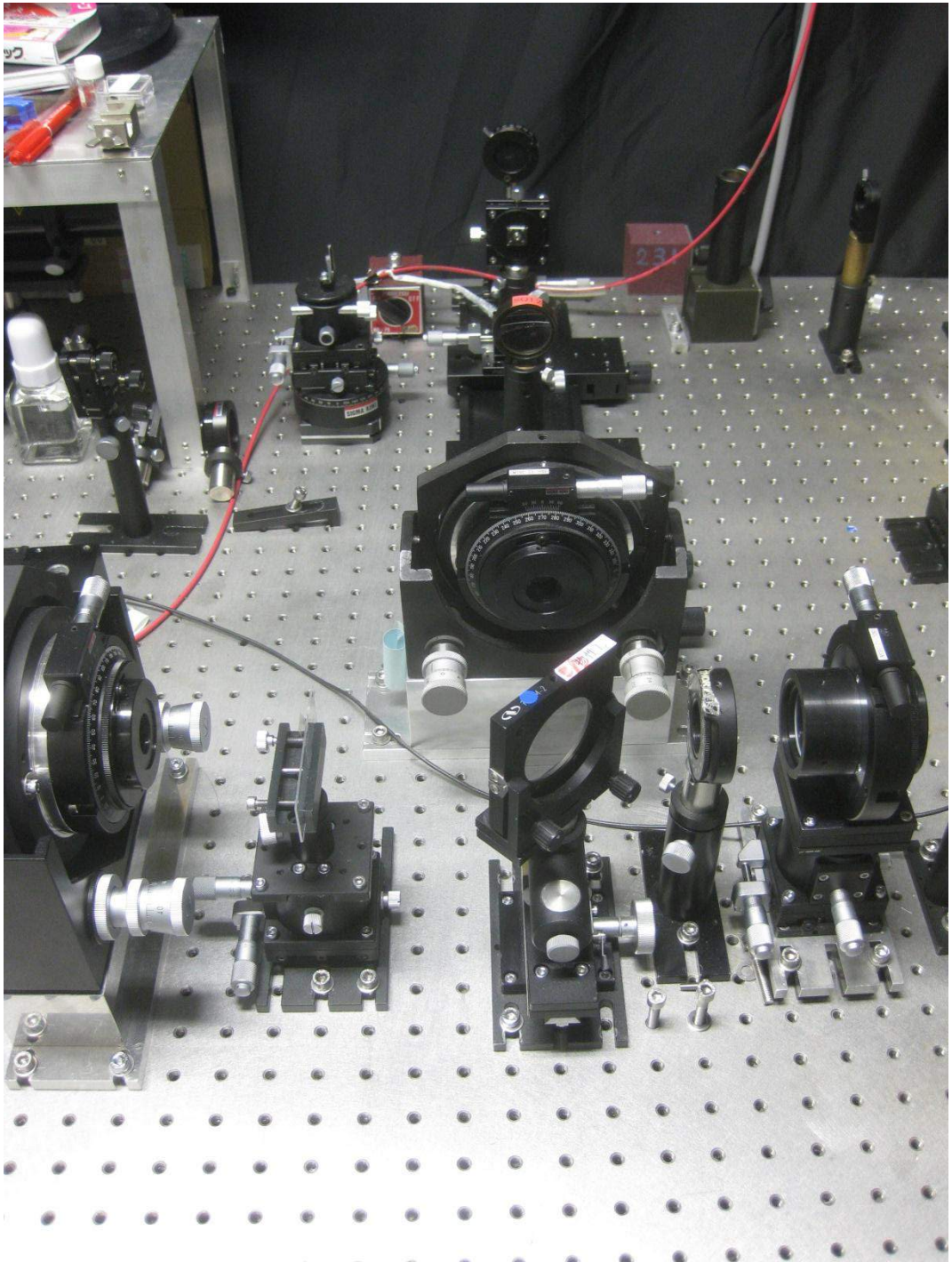

干涉計出力の位相依存性

$$I_{sample} = A\left|t_s E_1 + E_2 e^{i\phi}\right|^2 = AE^2\left|\sqrt{T_s}e^{i\phi_s} + e^{i\phi}\right|^2$$

$$= AE^2(\sqrt{T_s}e^{i\phi_s} + e^{i\phi})(\sqrt{T_s}e^{-i\phi_s} + e^{-i\phi}) = AE^2(T_s + 2\sqrt{T_s}\cos(\phi - \phi_s) + 1)$$

$$t_s = \sqrt{T_s}e^{i\phi_s} \ : \text{complex transmission};\ \phi : \text{retardar phase}$$

$$I_{sample,\max} = AE^2(\sqrt{T_s} + 1)^2,\quad I_{sample,\min} = AE^2(\sqrt{T_s} - 1)^2$$

$$I_{sample,\max} + I_{sample,\min} = 2AE^2(T_s + 1)$$

$$I_{sample,\max} - I_{sample,\min} = 4AE^2\sqrt{T_s}$$

$$I_{sample} = \frac{I_{sample,\max} + I_{sample,\min}}{2} + \frac{I_{sample,\max} - I_{sample,\min}}{2}\cos(\phi - \phi_s)$$

$$I_{reference} = A\left|E_1 + E_2 e^{i\phi}\right|^2$$

$$I_{reference} = \frac{I_{reference,\max} + I_{reference,\min}}{2} + \frac{I_{reference,\max} - I_{reference,\min}}{2}\cos(\phi)$$

強度から位相へ

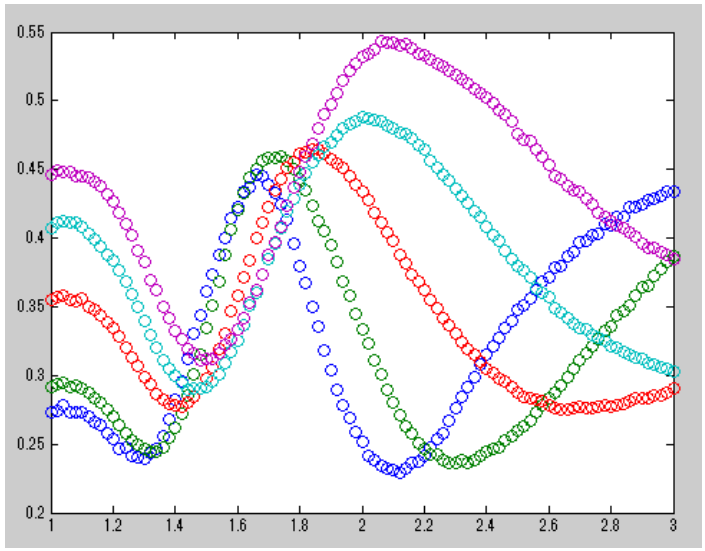

各波長における光強度の電圧依存性

$$I_{sample} = \frac{I_{sample,\max} + I_{sample,\min}}{2} + \frac{I_{sample,\max} - I_{sample,\min}}{2}\cos(\phi - \phi_s)$$

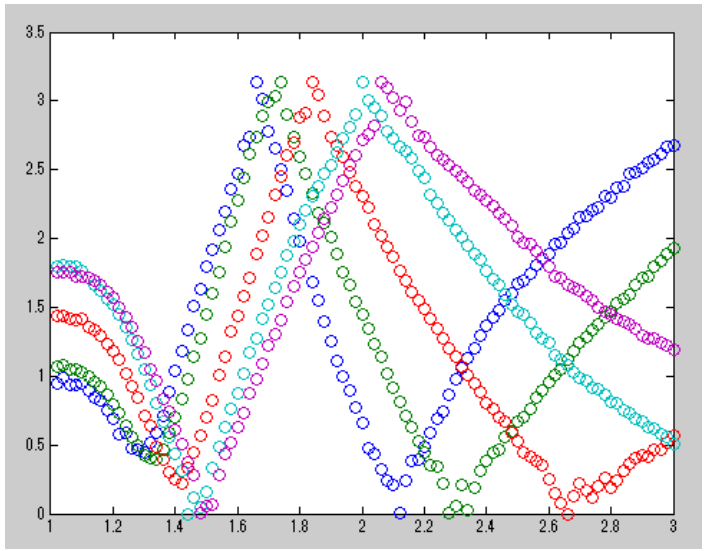

各波長における光強度の電圧依存性

unwrapping

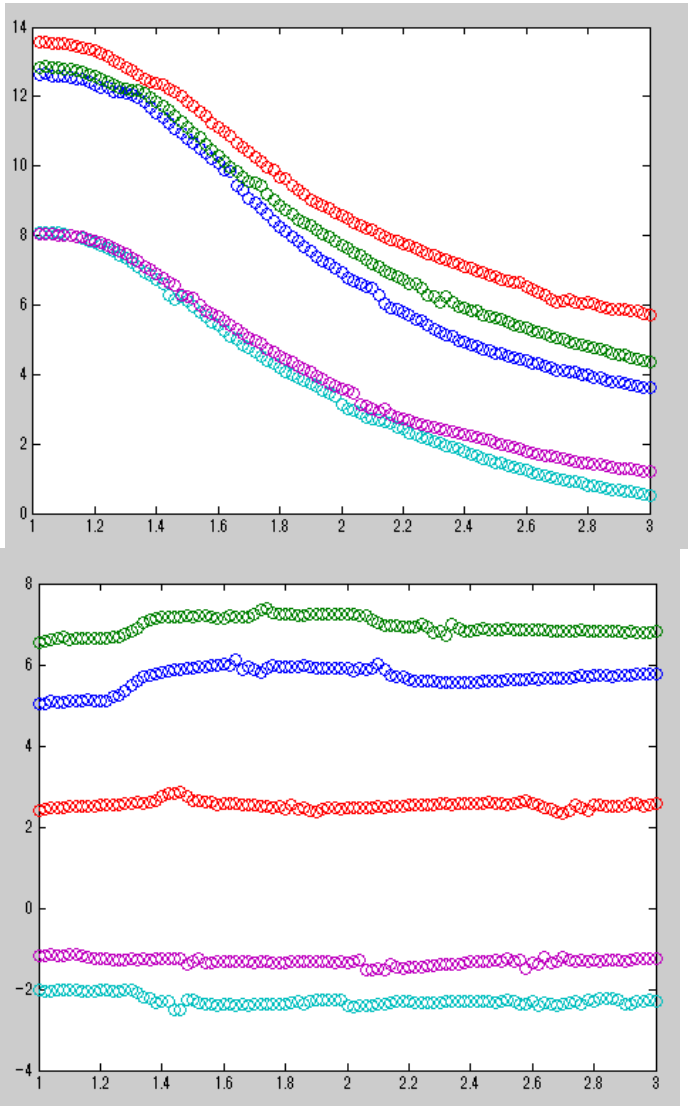

位相のunwrapping

λ= 493.4, 535.2, 577.70 618.47 659.9 nm

各波長における位相差の電圧依存性

干渉計による位相測定

transmission data for Uehara SRR

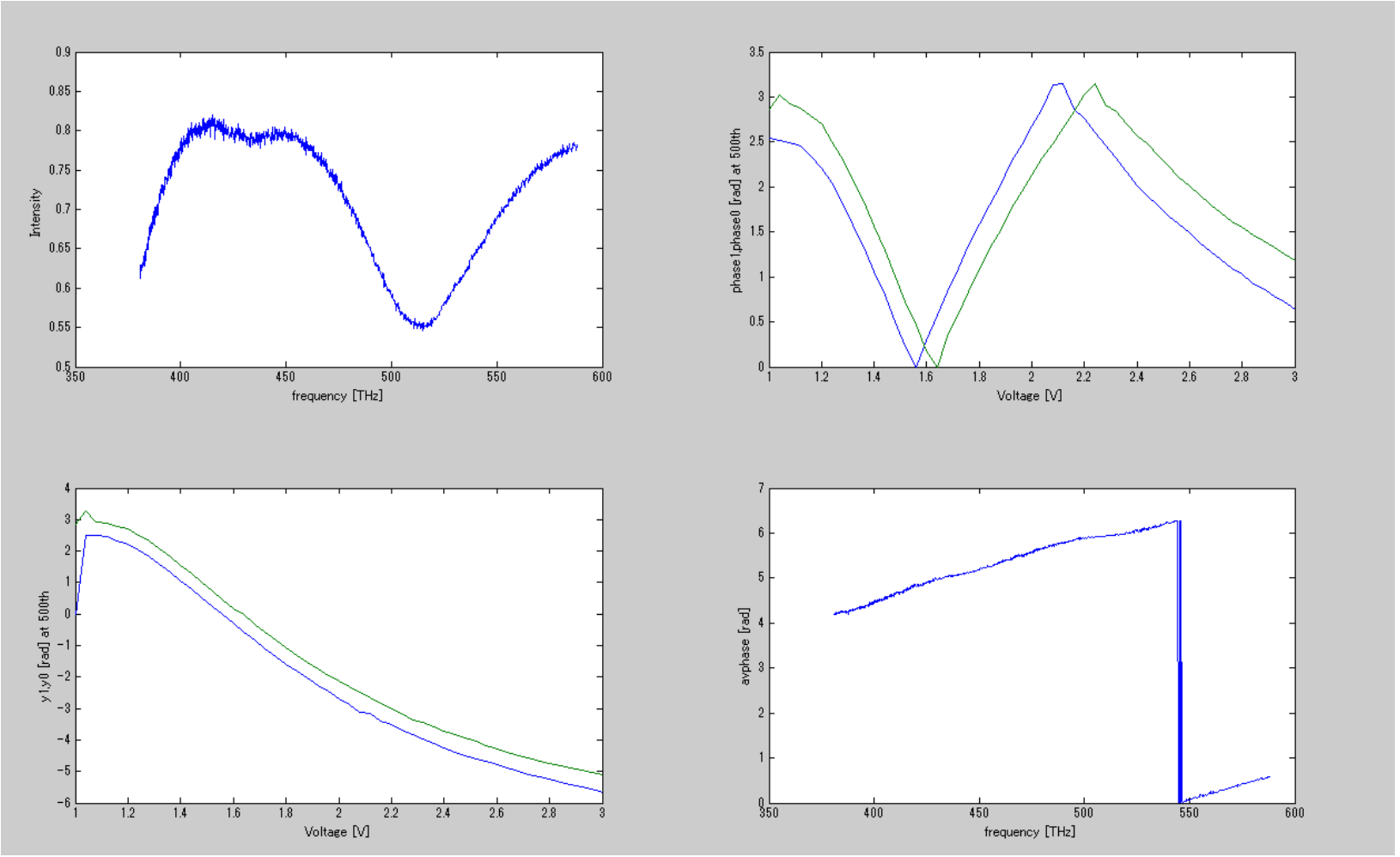

干渉計による位相測定

transmission data for Uehara SRR

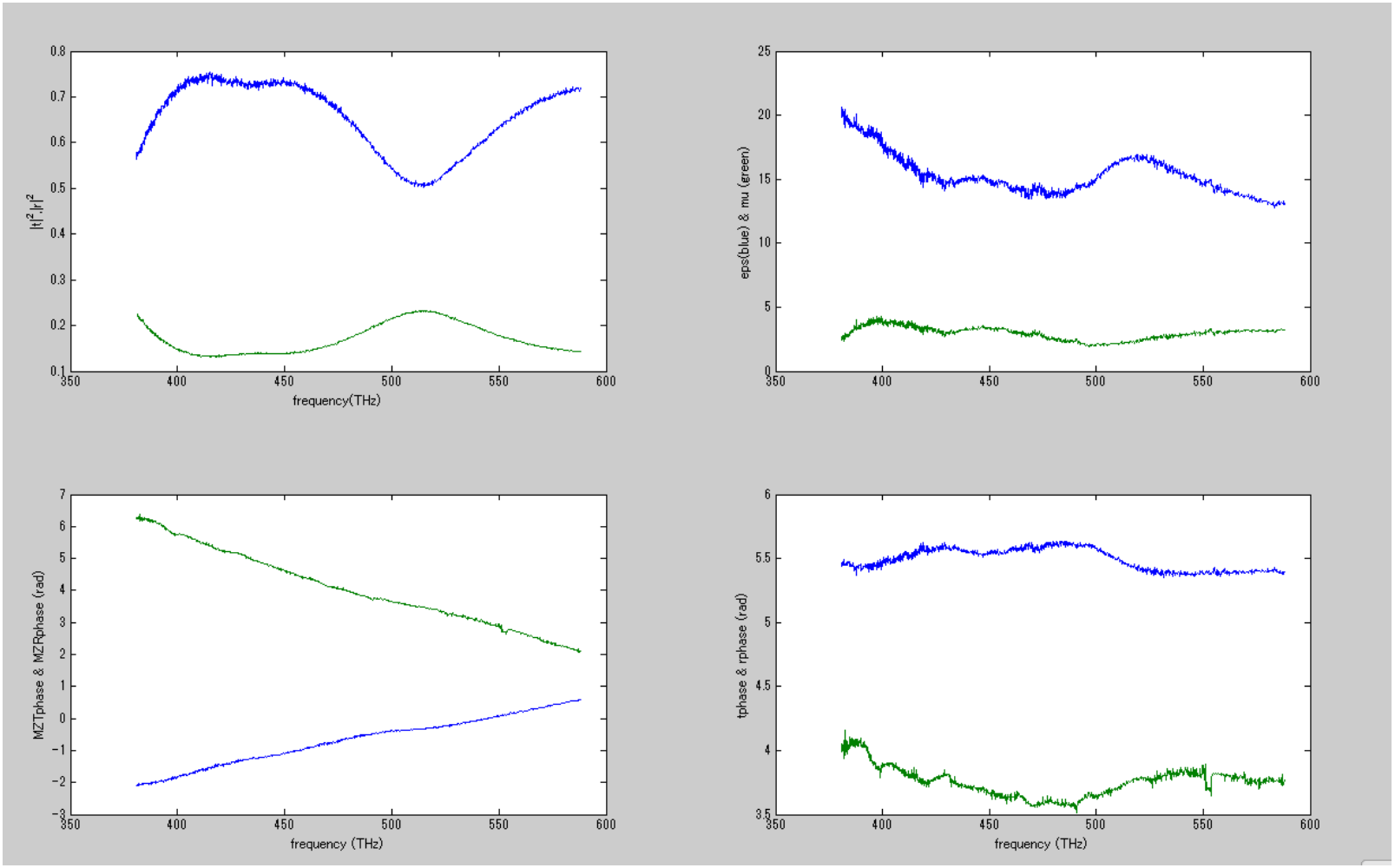

電磁場シミュレーション

FDTD（有限差分時間領域法）

FEM(有限要素法)

BEM(境界要素法)

2日目のまとめ

完全レンズの原理
ハイパボリック分散
クローキング
光領域メタマテリアルの作製方法
有効誘電率、有効透磁率の測定方法

訂正

p.20

押し付けることで形状を転写するナノプリント

押し付けることで形状を転写するナノインプリント

CST StudioSuite Student ed.

Metamaterials@YouTube

- Negarive Refraction
- Metamaterials and Science on Invisibility, Newton Lecture 2013 (J. Pendry)
- Smart Materials (5 of 5) Invisibility Cloak (D.Smith)

3） メタマテリアルにおける光物性

構造色

メタ表面

第二高調波生成

光整流

光スピンホール効果

将来の展望

Metamolecule design

Nanoantenna

Cut wire pairs

プラズモンによる構造色

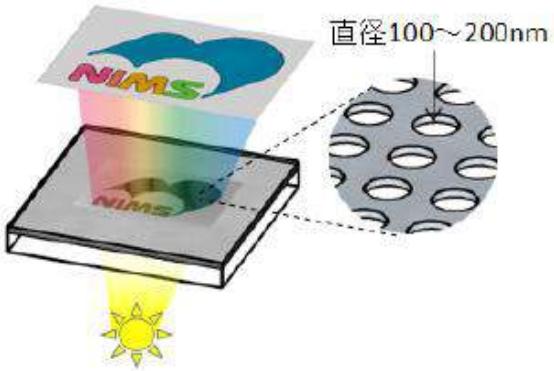

(a)　概略図

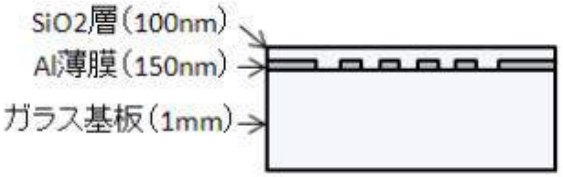

(b) 構造断面図

D. Inoue et al.,
Polarization independent visible color filter comprising an aluminum film with surface plasmon enhanced transmission through a subwavelength array of holes.
Appl Phys Lett 98(9):093113

円偏光に対する不可視物質

$$D = \varepsilon E - i\xi B; \quad \mathrm{H} = \mu^{-1} B - i\xi E$$

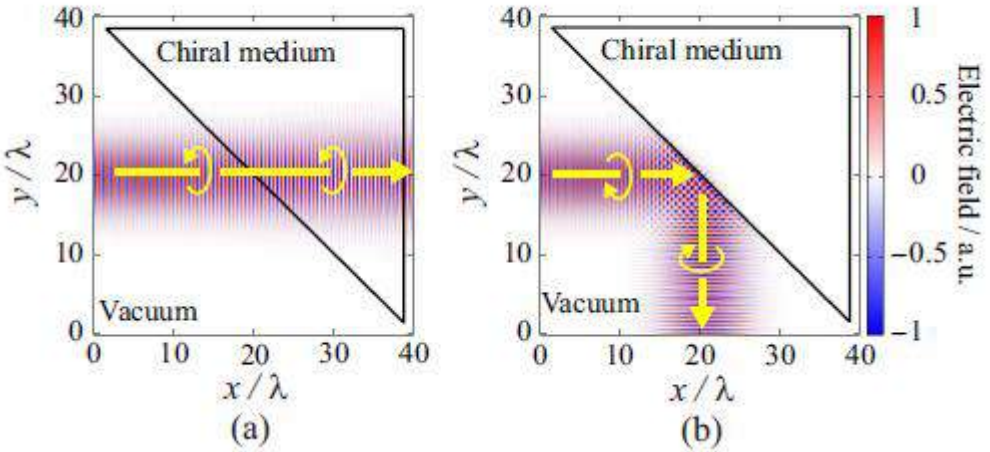

分極と磁化の効果を相殺することで不可視化を実現

Y. Tamayama, T. Nakanishi, K. Sugiyama and M. Kitano

OPTICS EXPRESS (2008) 20869.

メタ表面

Yu, …, Capasso,…(Harvard),
"Light Propagation with Phase Discontinuities: Generalized Laws of Reflection and Refraction," Science (2011).

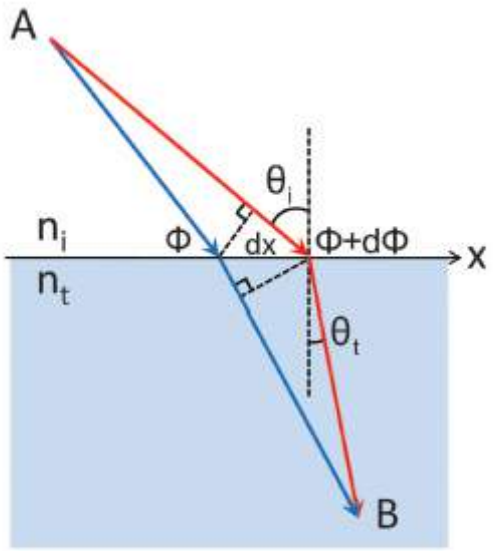

Fig. 1. Schematics used to derive the generalized Snell's law of refraction. The interface between the two media is artificially structured in order to introduce an abrupt phase shift in the light path, which is a function of the position along the interface. Φ and Φ + *d*Φ are the phase shifts where the two paths (blue and red) cross the boundary.

位相勾配があったとき、反射、屈折の法則はどのように変わるか？

$$[k_0 n_i \sin\theta_i dx + \Phi + \Delta\Phi] - [k_0 n_t \sin\theta_t dx + \Phi] = 0$$

$$n_i \sin\theta_i - n_t \sin\theta_t = \frac{1}{k_0}\frac{d\Phi}{dx}$$

V字アンテナによる位相シフト

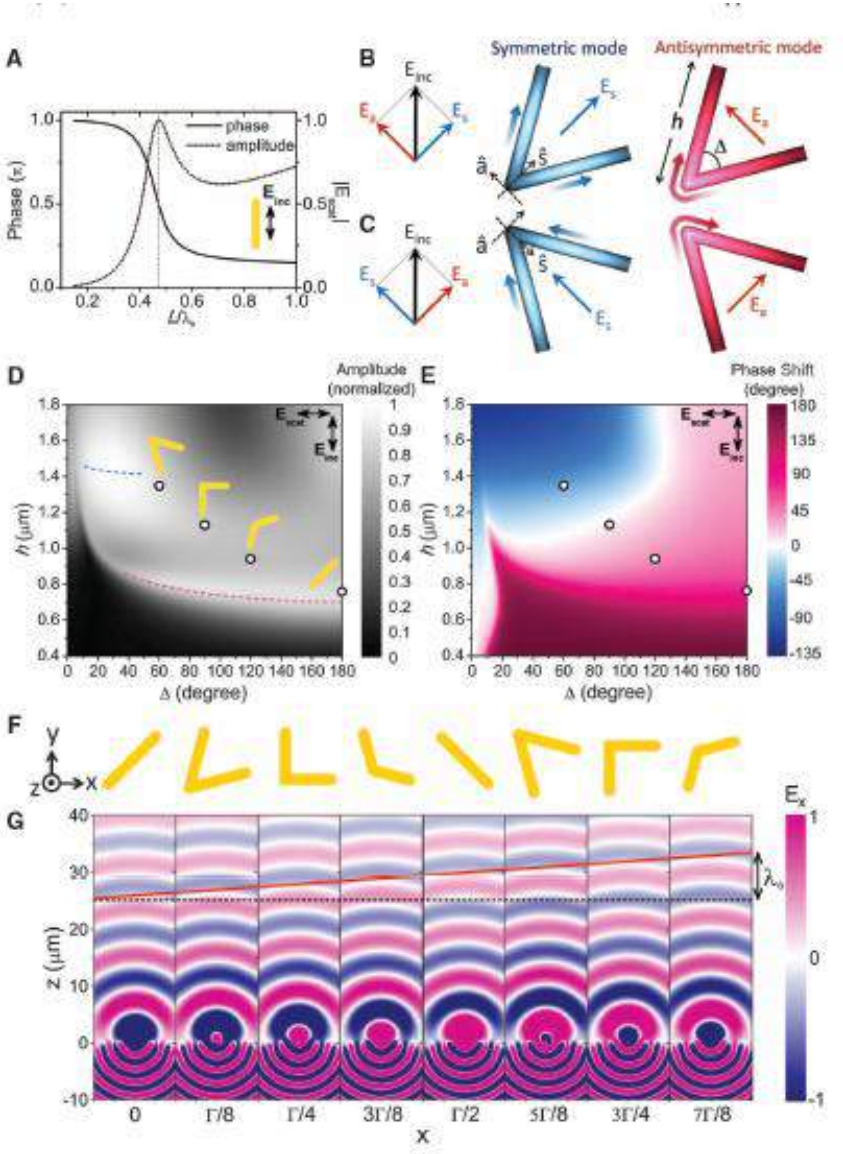

Yu, …, Capasso, Science (2011).

異常反射、異常屈折

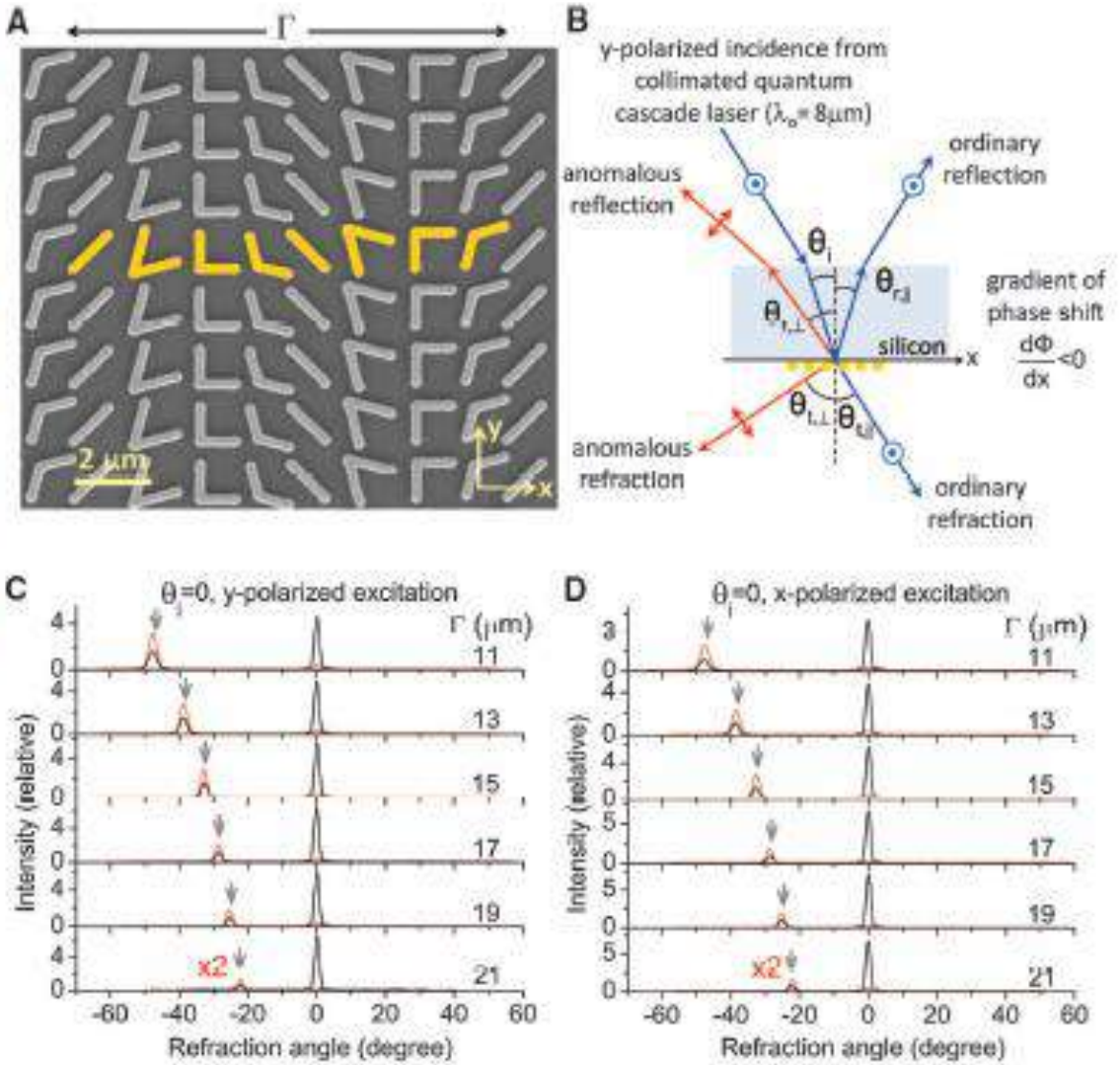
A
Γ
2 μm
y
x
B
y-polarized incidence from collimated quantum cascade laser (λ0= 8μm)
ordinary reflection
anomalous reflection
θi
θr,∥
θt,⊥
gradient of phase shift
dΦ/dx <0
silicon
x
θt,⊥
θt,∥
anomalous refraction
ordinary refraction
C
θi=0, y-polarized excitation
Γ (μm)
11
13
15
17
19
21
x2
Intensity (relative)
-60 -40 -20 0 20 40 60
Refraction angle (degree)
D
θi=0, x-polarized excitation
Γ (μm)
11
13
15
17
19
21
x2
Intensity (relative)
-60 -40 -20 0 20 40 60
Refraction angle (degree)

入射角度依存性

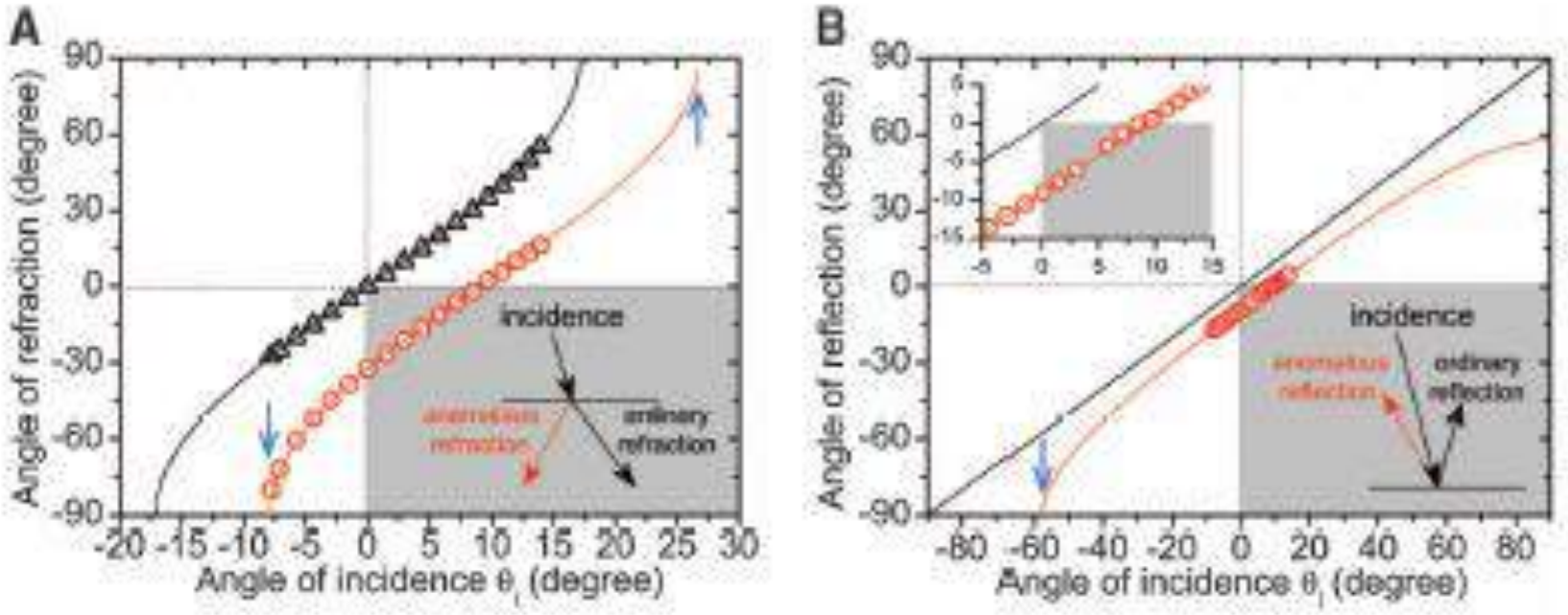
A
Angle of refraction (degree)
90
60
30
0
-30
-60
-90
-20 -15 -10 -5 0 5 10 15 20 25 30
Angle of incidence θi (degree)
incidence
ordinary refraction
B
Angle of reflection (degree)
-80 -60 -40 -20 0 20 40 60 80
Angle of incidence θi (degree)
incidence
ordinary reflection

メタ表面

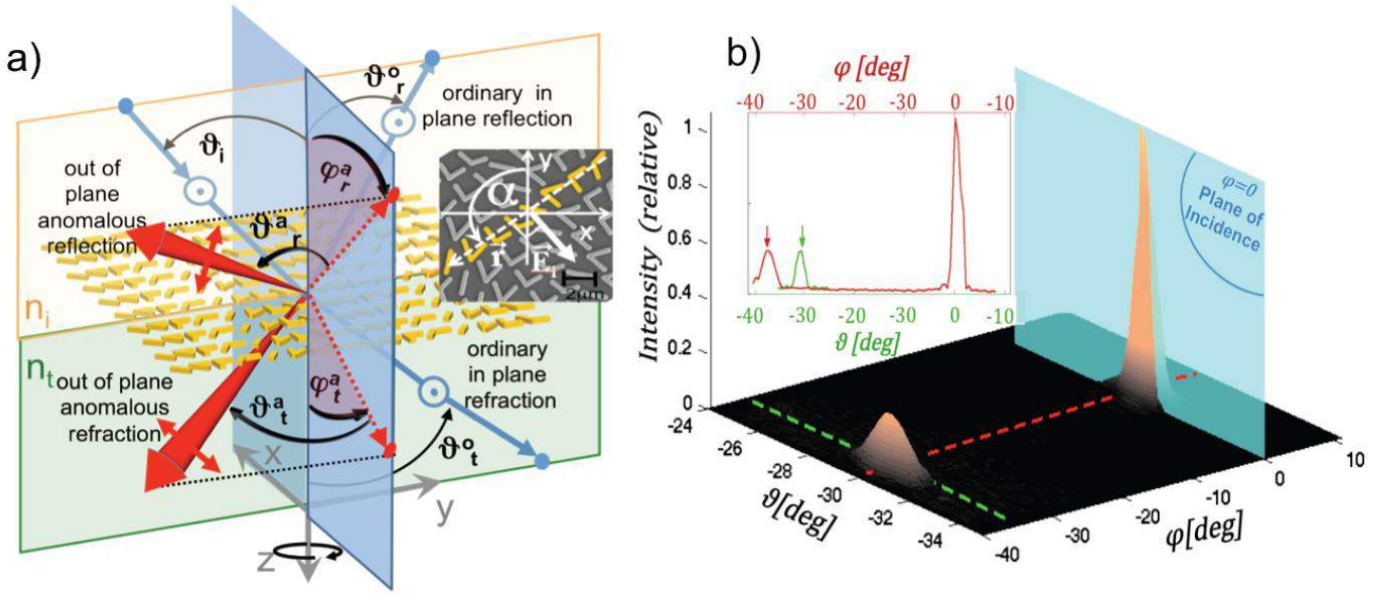

Fig. 1 – a) Schematic of the reflection and refraction in 3D: ϑ_i is the angle of incidence; ϑ_t^o is the angle of ordinary refraction; ϑ_t^a and φ_t^a are the angles of out-of-plane anomalous refraction. The subscript r refers to angles of reflection. Inset: scanning electron microscope image of the plasmonic antenna array used in the experiment. The angle α describes the direction of the gradient $\vec{r}$. The polarization of the incident field is indicated. b) Measured far-field intensity as a function of the angular position of the detector ϑ and φ for an incident angle $\vartheta_i = -8.45°$ and $\alpha = 90°$. The inset shows the angular distribution of the intensity at a fixed $\varphi = -38°$ (green curve) and at a fixed $\vartheta = -30°$ (red curve).

Capasso group (Harvard), Shalaev group (Purdue)

メタ表面を利用した広帯域λ/4板

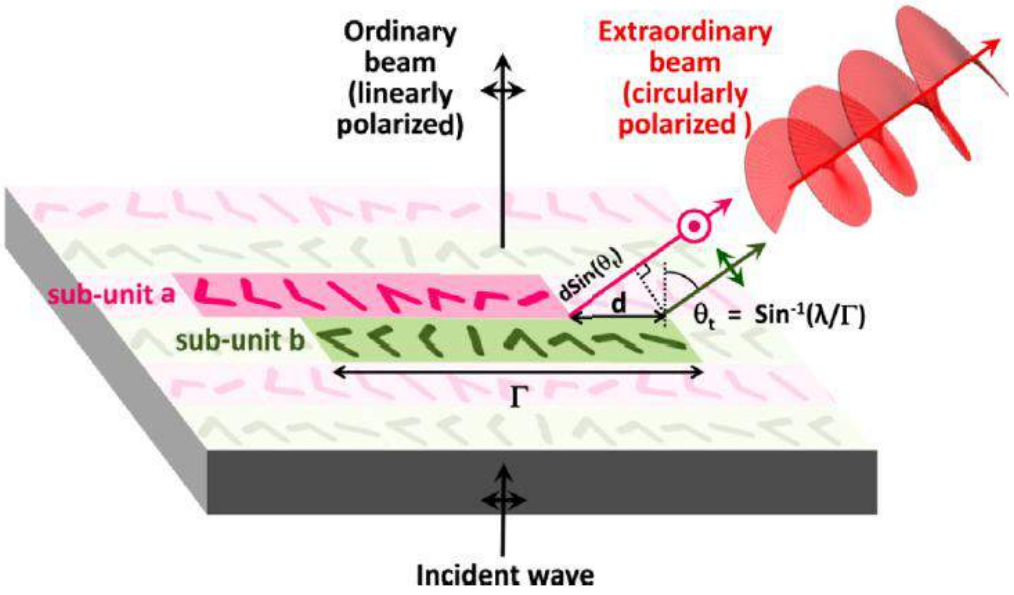

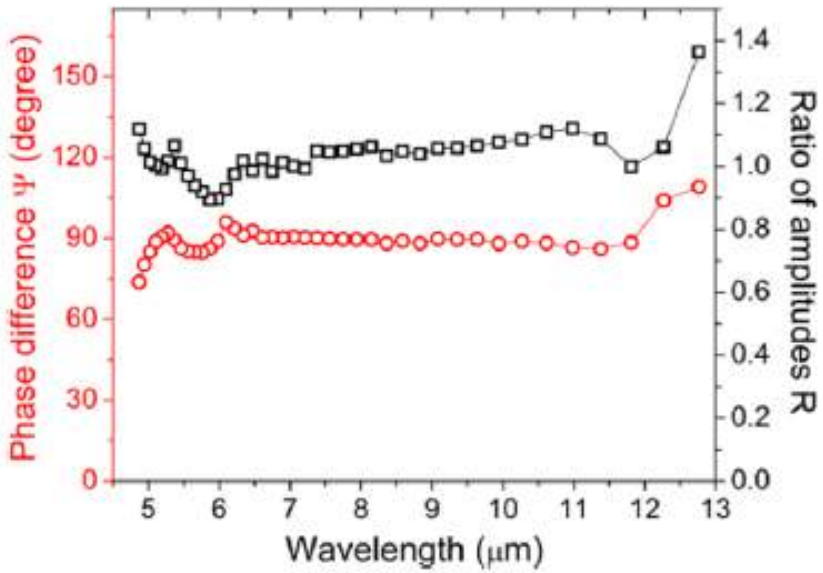

"A Broadband Background-free Quarter-Wave Plate Based on Plasmonic Metasurfaces"
Capasso's group, Nano Letters (2012).

非線形光学への応用

$$P = \chi^{(1)}E + \chi^{(2)}EE + \chi^{(3)}EEE + \cdots$$

$$P^{(2)} = \chi^{(2)}EE = \chi^{(2)}E_0^2 \cos^2 \omega t$$
$$= \tfrac{1}{2}\chi^{(2)}E_0^2\left(\cos 2\omega t + 1\right)$$

$$\chi^{(2)}(2\omega) = \Delta_{SHG}\chi^{(1)}(2\omega)\left(\chi^{(1)}(\omega)\right)^2$$
$$\chi^{(2)}(0) = \Delta_{PR}\chi^{(1)}(0)\left(\chi^{(1)}(\omega)\right)^2$$

$\Delta_{SHG}, \Delta_{PR}$ は物質によらず一定 (Miller則)

非線形感受率の予測

nature materials

LETTERS

PUBLISHED ONLINE: 9 FEBRUARY 2015 | DOI: 10.1038/NMAT4214

Predicting nonlinear properties of metamaterials from the linear response

Kevin O'Brien[1†], Haim Suchowski[1,2†], Junsuk Rho[1,2], Alessandro Salandrino[1], Boubacar Kante[1], Xiaobo Yin[1,2] and Xiang Zhang[1,2,3*]

The discovery of optical second harmonic generation in 1961 started modern nonlinear optics[1–3]. Soon after, R. C. Miller found empirically that the nonlinear susceptibility could be predicted from the linear susceptibilities. This important relation, known as Miller's Rule[4,5], allows a rapid determination of nonlinear susceptibilities from linear properties. In recent years, metamaterials, artificial materials that exhibit intriguing linear optical properties not found in natural materials[6], have shown novel nonlinear properties such as phase-mismatch-free nonlinear generation[7], new quasi-phase matching capabilities[8,9] and large nonlinear susceptibilities[8–10]. However, the understanding of nonlinear metamaterials is still in its infancy, with no general conclusion on the relationship between linear and nonlinear properties. The key question is then whether one can determine the nonlinear behaviour of these artificial materials from their exotic linear behaviour. Here, we show that the nonlinear oscillator model does not apply in general materials at optical[18–23] and microwave[24] frequencies. Researchers have found that in some cases, such as the third harmonic emission from bow-tie and double-bar nanostructures[18,19], Miller's rule or its equivalent nonlinear oscillator model[25] fairly accurately predicts the nonlinear susceptibilities. However, the general validity of Miller's rule in optical metamaterials for arbitrary nonlinear processes, and specifically for second-order susceptibilities, is not known. Here we show experimentally that Miller's rule fails to describe the second-order susceptibility of metamaterials and predicts an incorrect optimum geometry for generating the highest second-order nonlinearity. We however demonstrate the optimal geometry can be correctly predicted with a more general nonlinear scattering theory. This general principle describes not only second-order but also higher-order nonlinear optical responses of plasmonic nanostructures over a broad wavelength range. The predictive capability of nonlinear scattering theory enables rapid design of optimal nonlinear nanostructures for sensing and integrated photonics.

構造パラメタ依存性の測定

LETTERS NATURE MATERIALS DOI: 10.1038/NMAT4214

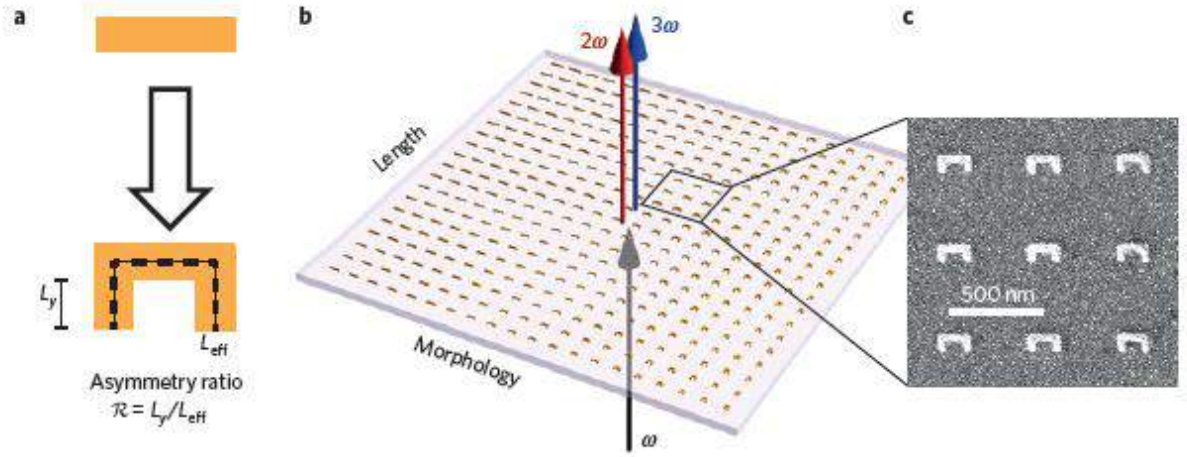

Figure 1 | Schematic of the metamaterial array. Nonlinear light generation from metamaterial arrays in which the geometry of the nanostructures varies gradually from a symmetric bar to an asymmetric U-shape. The second-order susceptibility is expected to be extremely sensitive to the symmetry of the metamaterial. **a**, Definition of the parameter space: the total length and asymmetry ratio of the nanostructures is changed throughout the array. Further details on the sample design are given in Supplementary Fig. 4. **b**, Schematic of the second and third harmonic generation as a function of the nanostructure length and morphology. A confocal microscope is used to excite the nanostructures with infrared laser pulses (1,305 nm). The nonlinear

構造パラメタ依存性

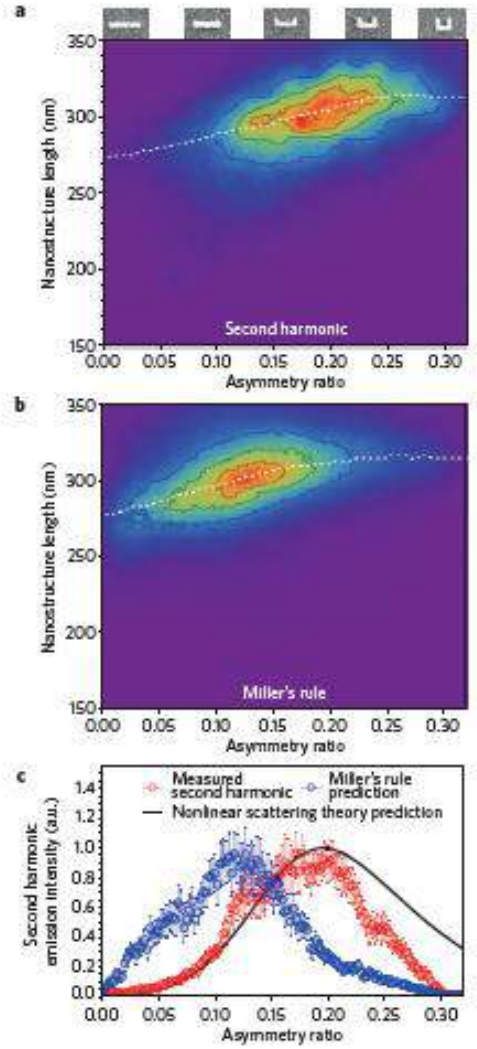

$$E_{SHG}(2\omega) \propto \int_{surface} \chi_{nnn} \mathbf{E}(2\omega)\left(\mathbf{E}(\omega)\right)^2 dS$$

外部電圧による制御

nature COMMUNICATIONS

ARTICLE

Received 10 May 2014 | Accepted 14 Jul 2014 | Published 11 Aug 2014

DOI: 10.1038/ncomms5680

Electrifying photonic metamaterials for tunable nonlinear optics

Lei Kang[1,*], Yonghao Cui[1,*], Shoufeng Lan[2,*], Sean P. Rodrigues[1,2], Mark L. Brongersma[3] & Wenshan Cai[1,2]

Metamaterials have not only enabled unprecedented flexibility in producing unconventional optical properties that are not found in nature, they have also provided exciting potential to create customized nonlinear media with high-order properties correlated to linear behaviour. Two particularly compelling directions are active metamaterials, whose optical properties can be purposely tailored by external stimuli in a reversible manner, and nonlinear metamaterials,

Authors

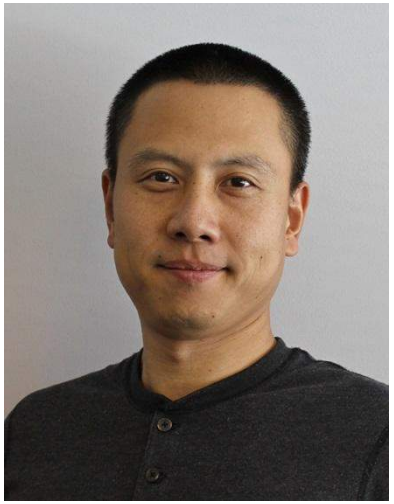

Lei Kang

Mark Brongersma

Wenshen Cai

Fig.1 Electrically controlled SHG and OR in a metamaterial absorber

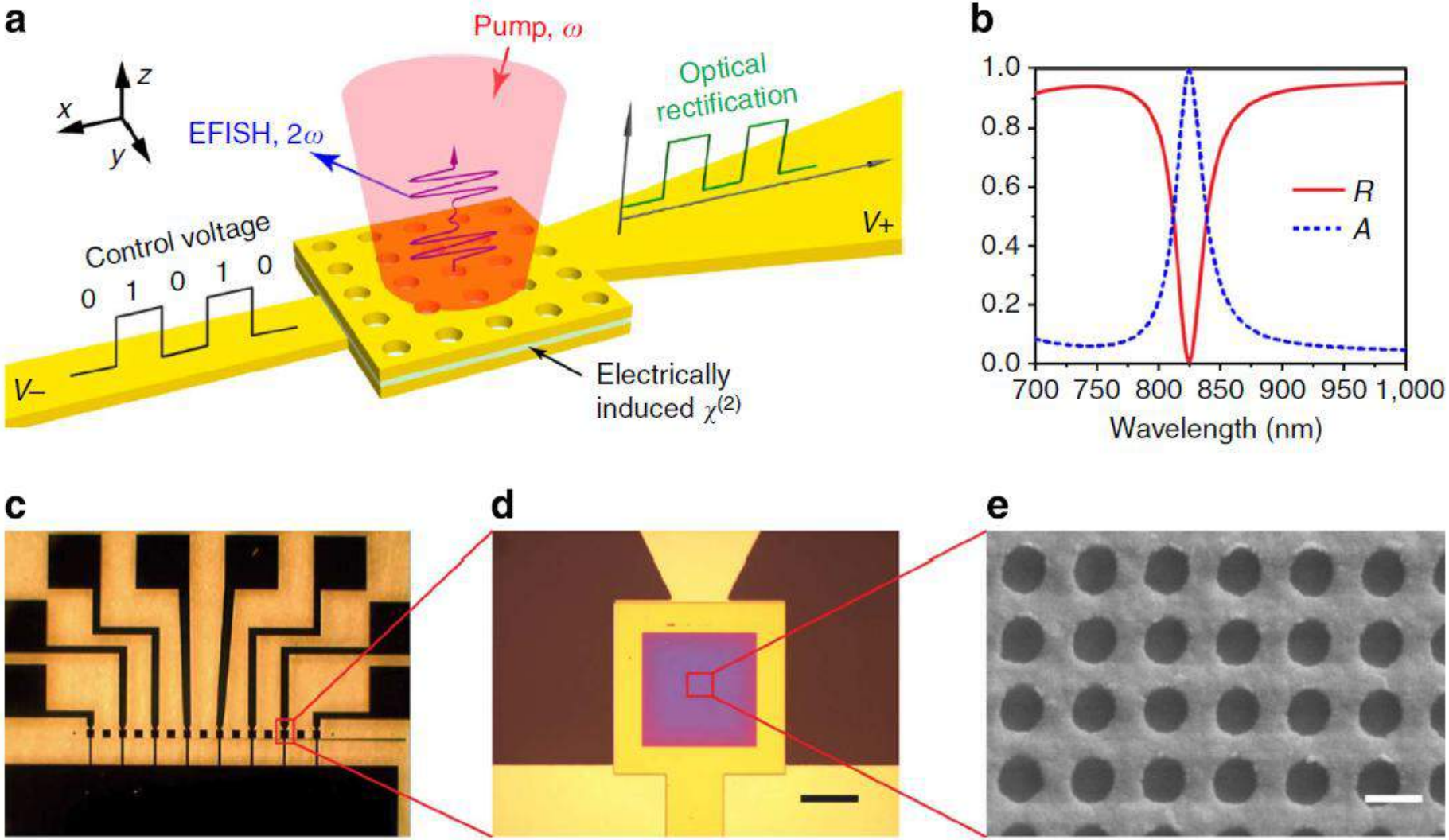

A1: Modelling with CST MicroWaveStudio

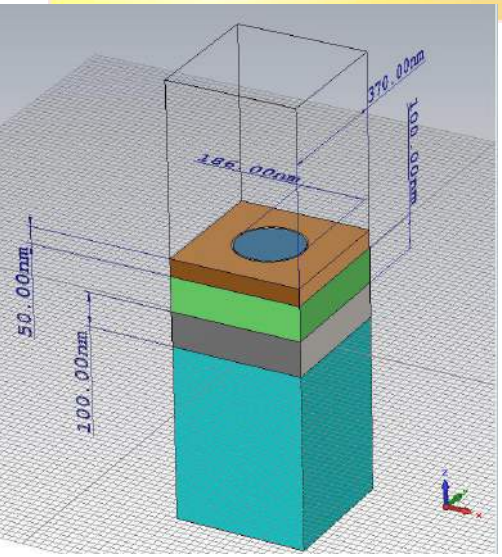

$Au/Al_2O_3/Ag/glass$
Al_2O_3 n=1.63
Au,Ag: Johnson-Christy
Glass n=1.5

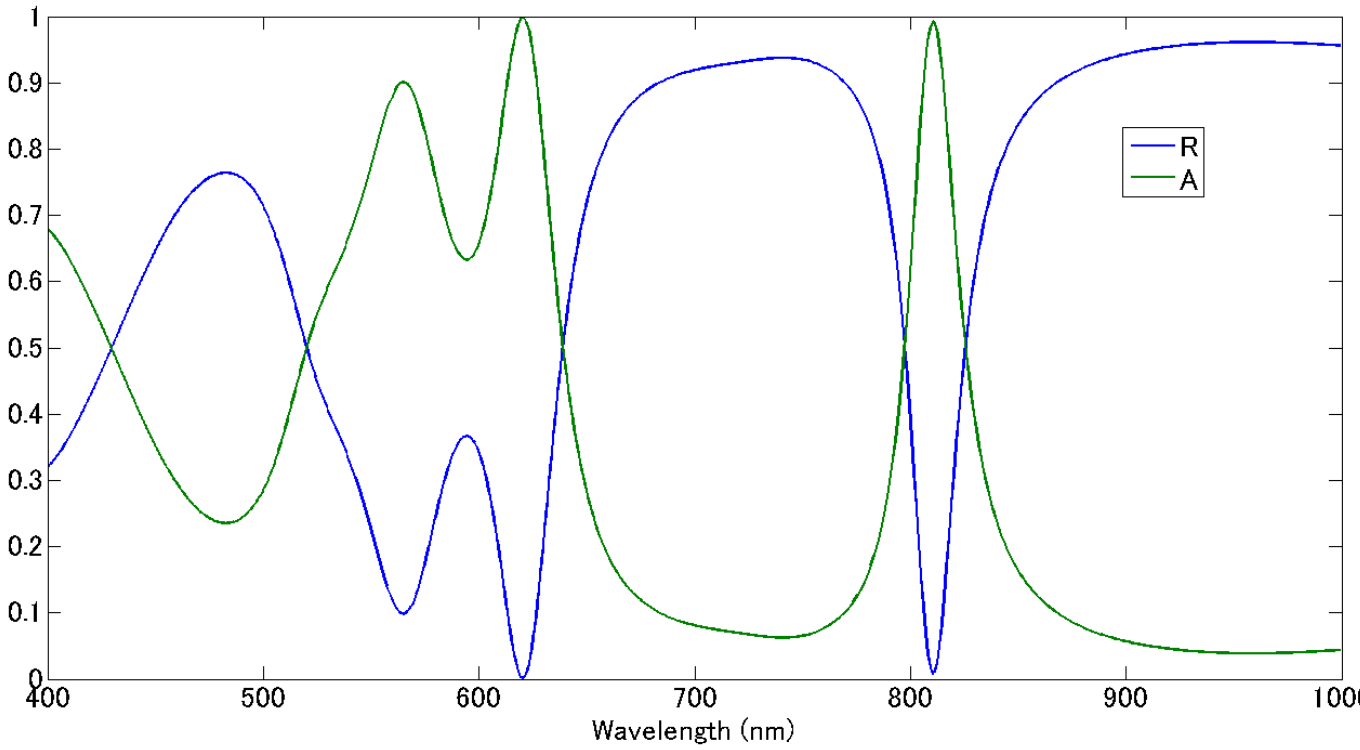

A2: Reproduced Calculation with CST

Electric field @324.5THz（805nm）

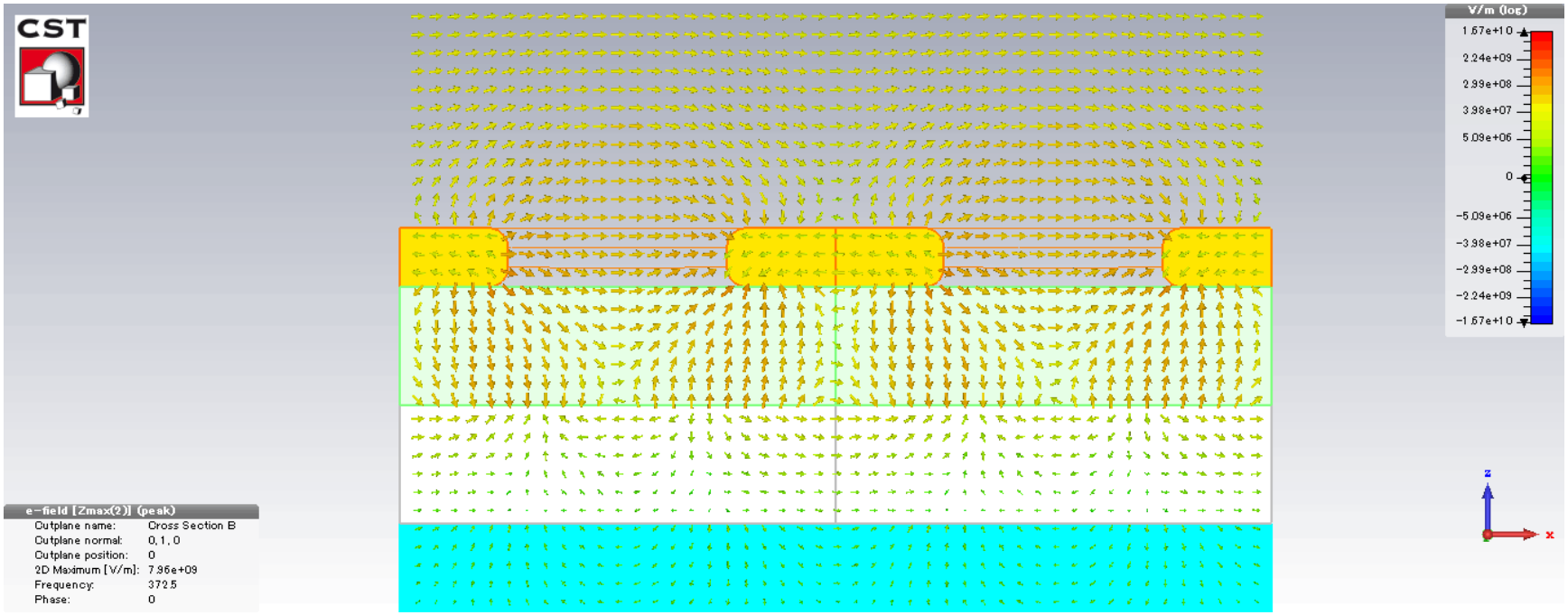

Fig.S1: Fabrication flowchart of the metamaterial absorber with electric contacts

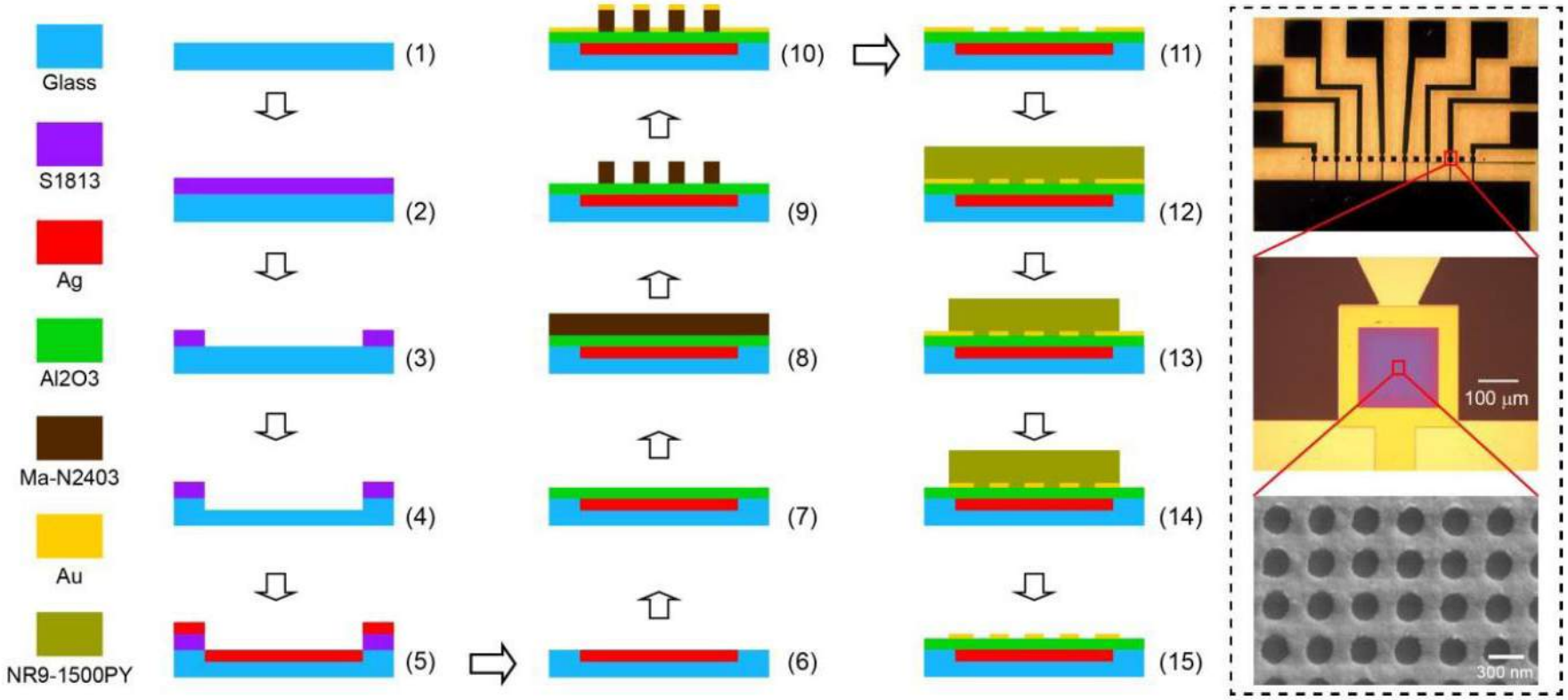

Fig.S2: Experimental setup for characterizing nonlinear effects in a metamaterial device

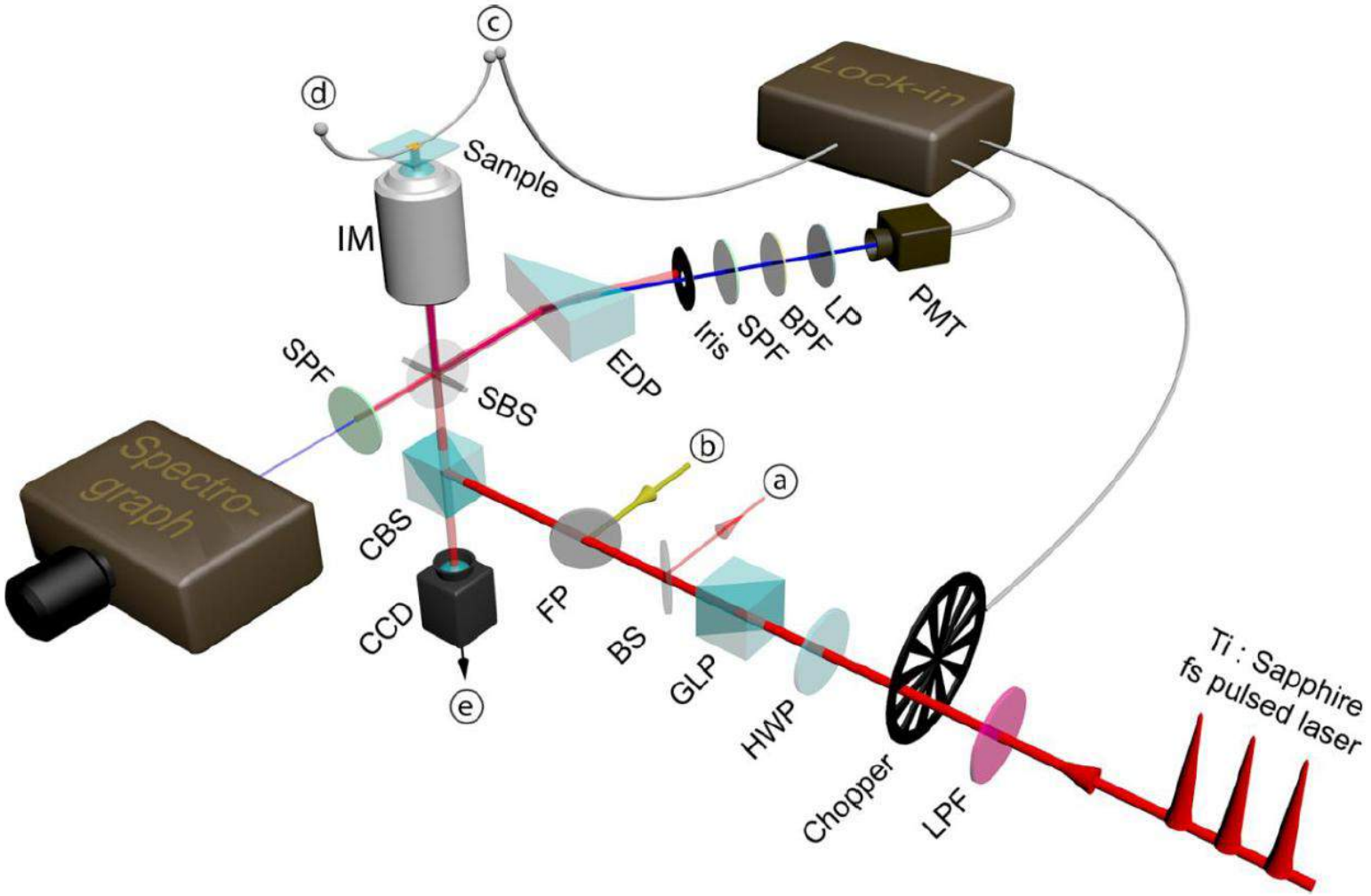

Fig.2 Nonlinear optical signals from the metamaterial absorber without the application of electrical control

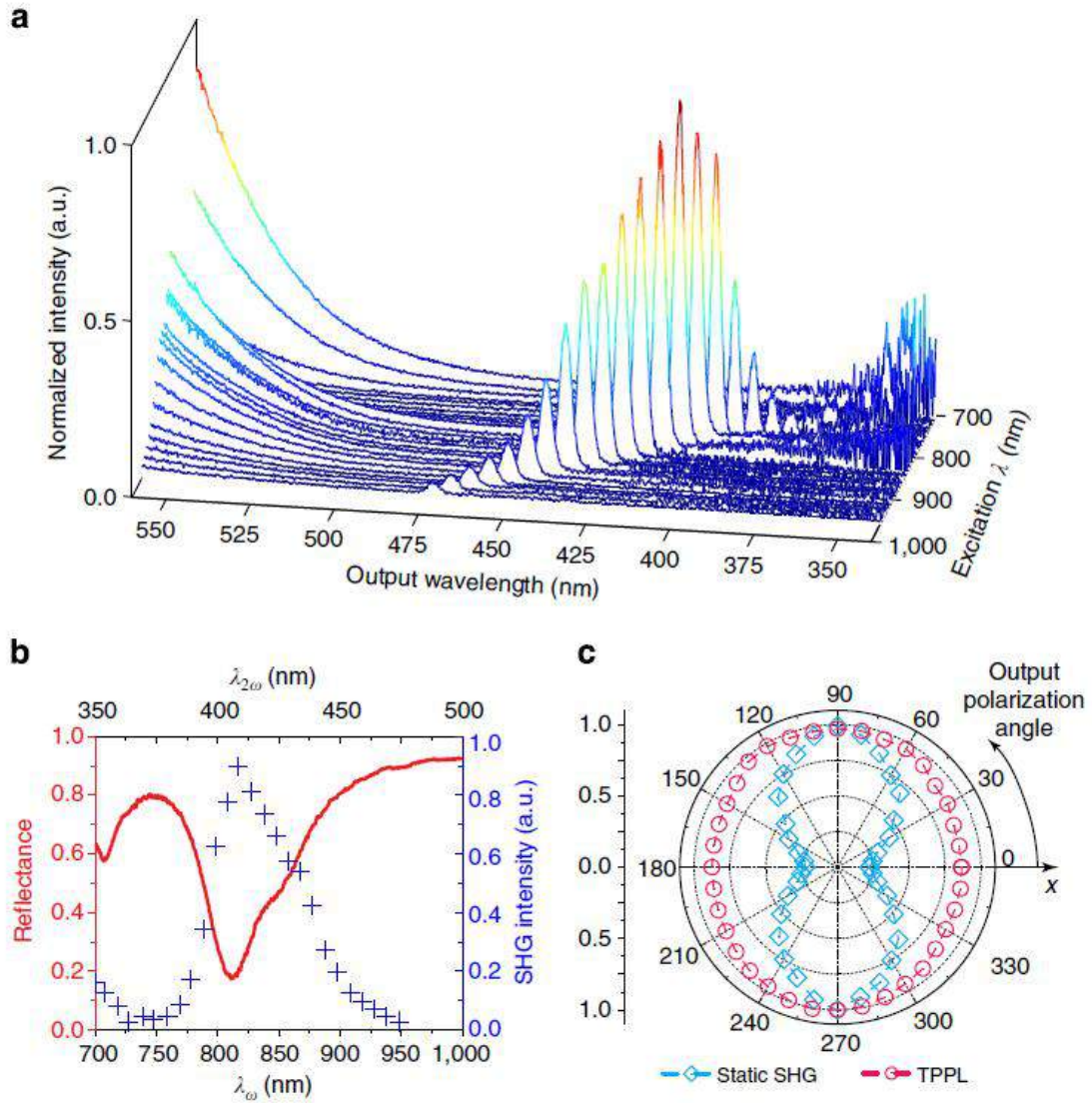

Fig.S3: Simulation results for the linear spectrum of the metamaterial

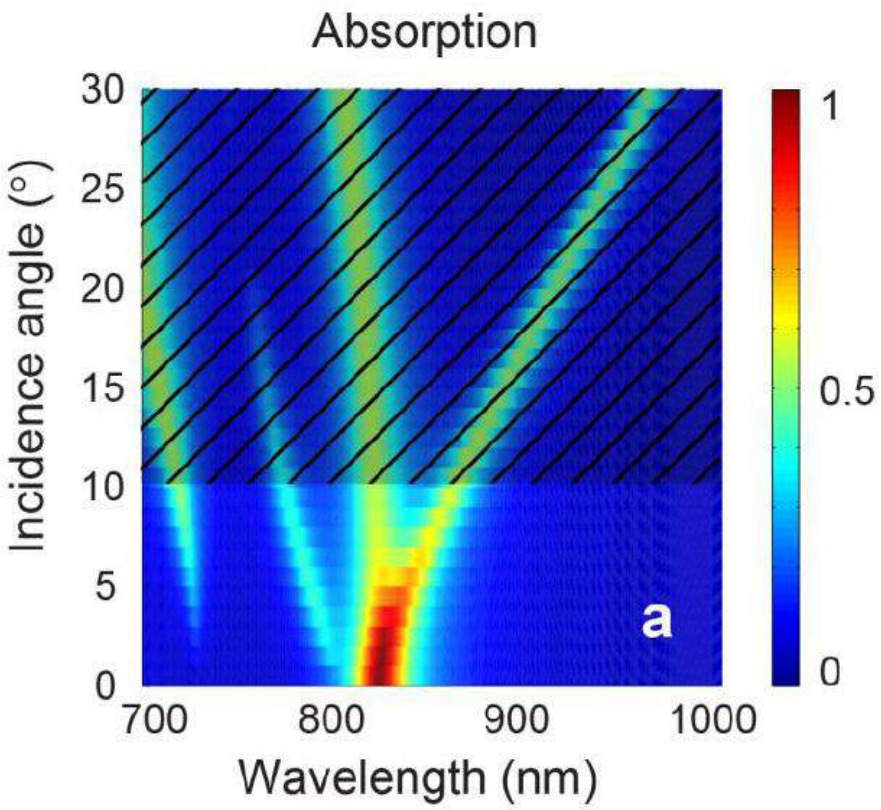

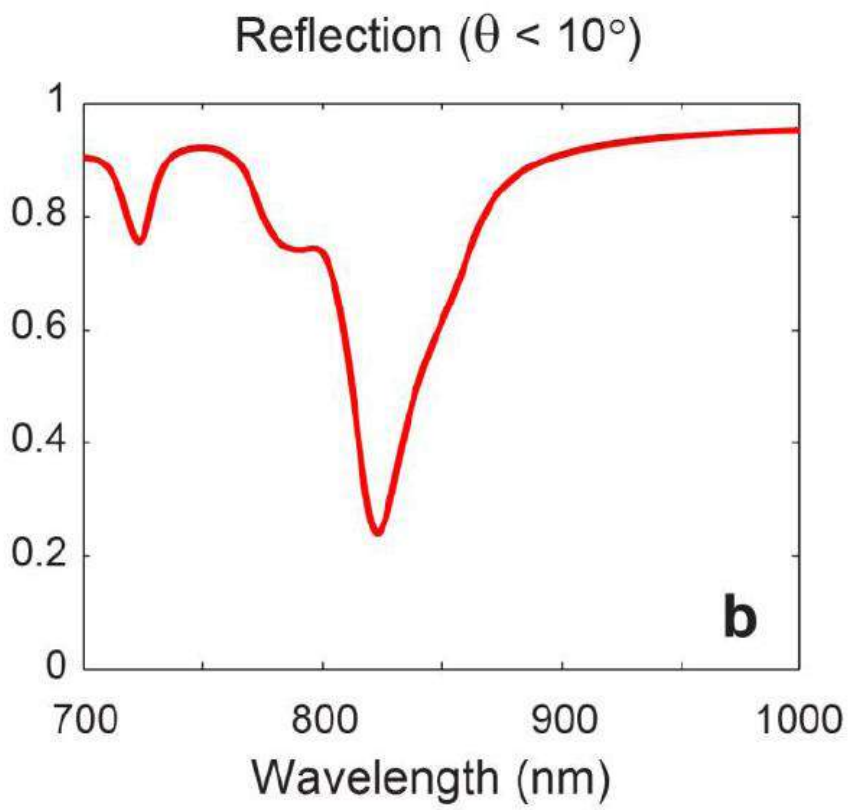

Fig.3 Electrically tunable SHG in the metamaterial absorber

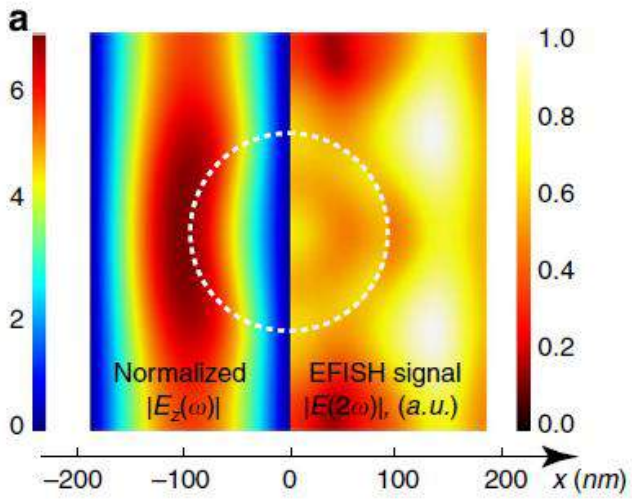

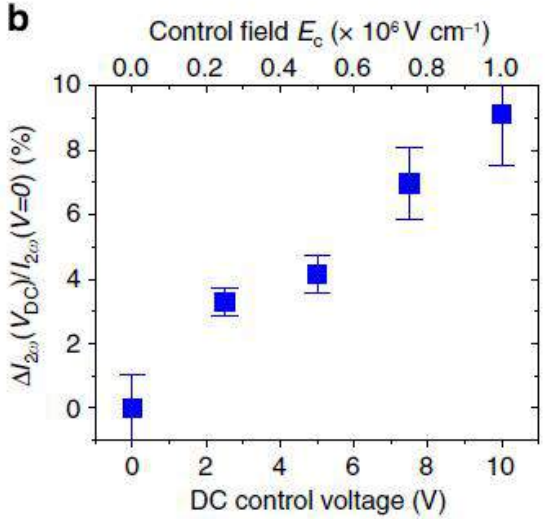

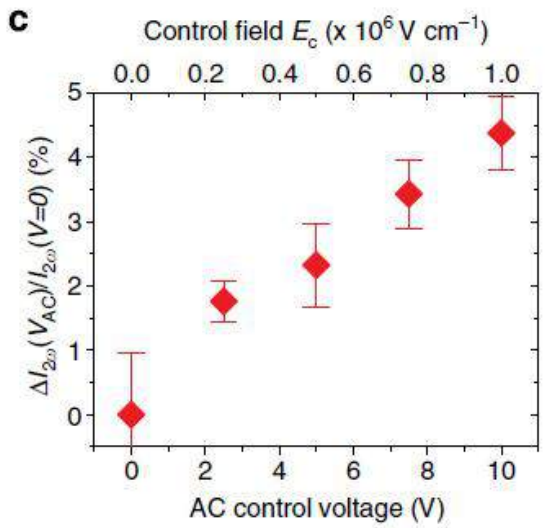

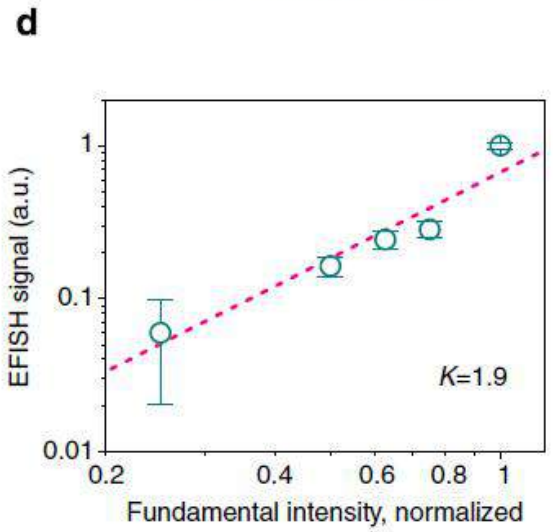

A3: Ez distribution at the spacer

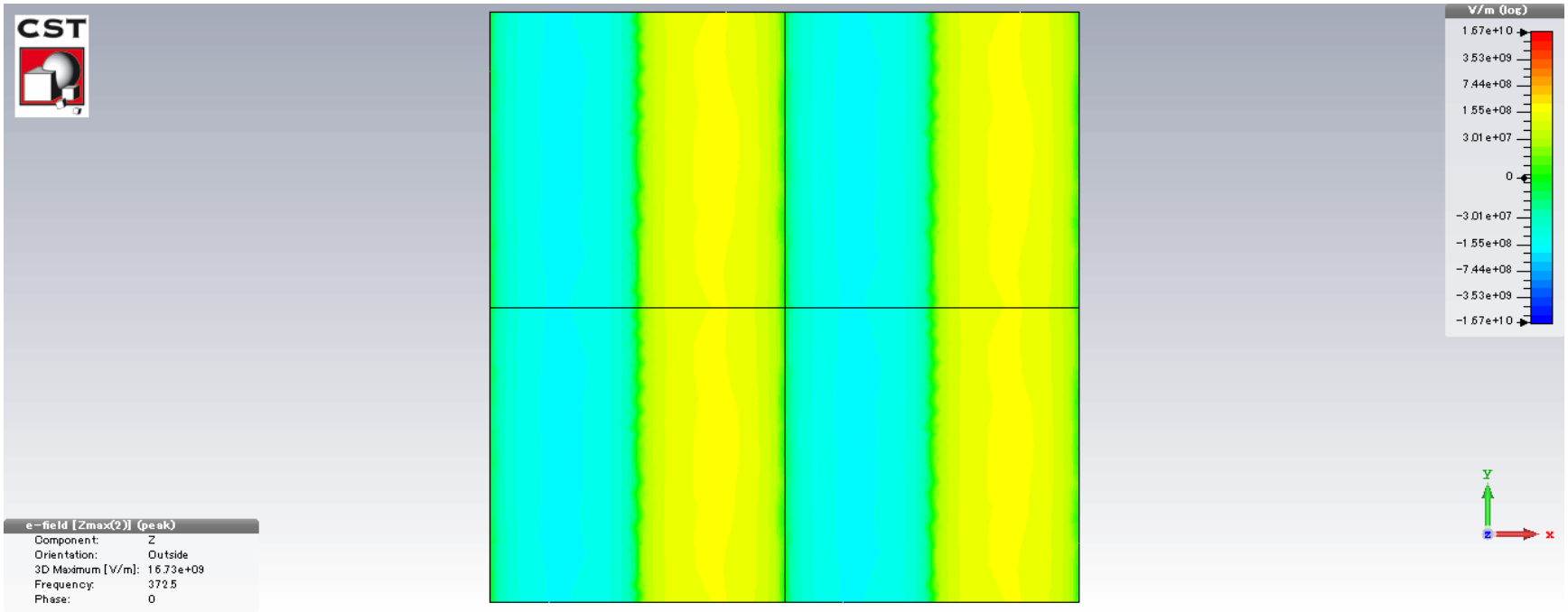

A4: DC field distribution

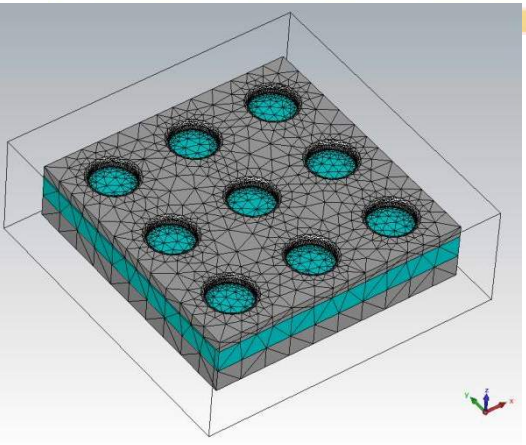

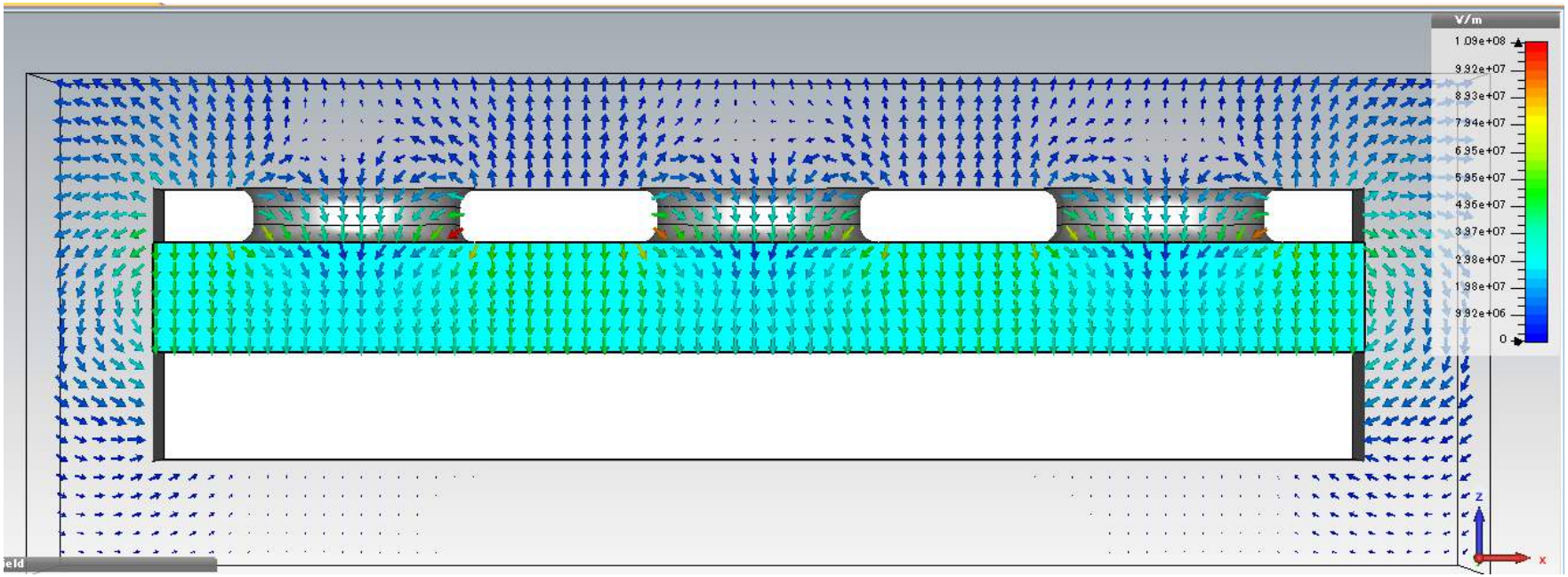

Fig.S4: Correlation between the linear resonance behavior and the EFISH generation efficiency of the metamaterial absorber

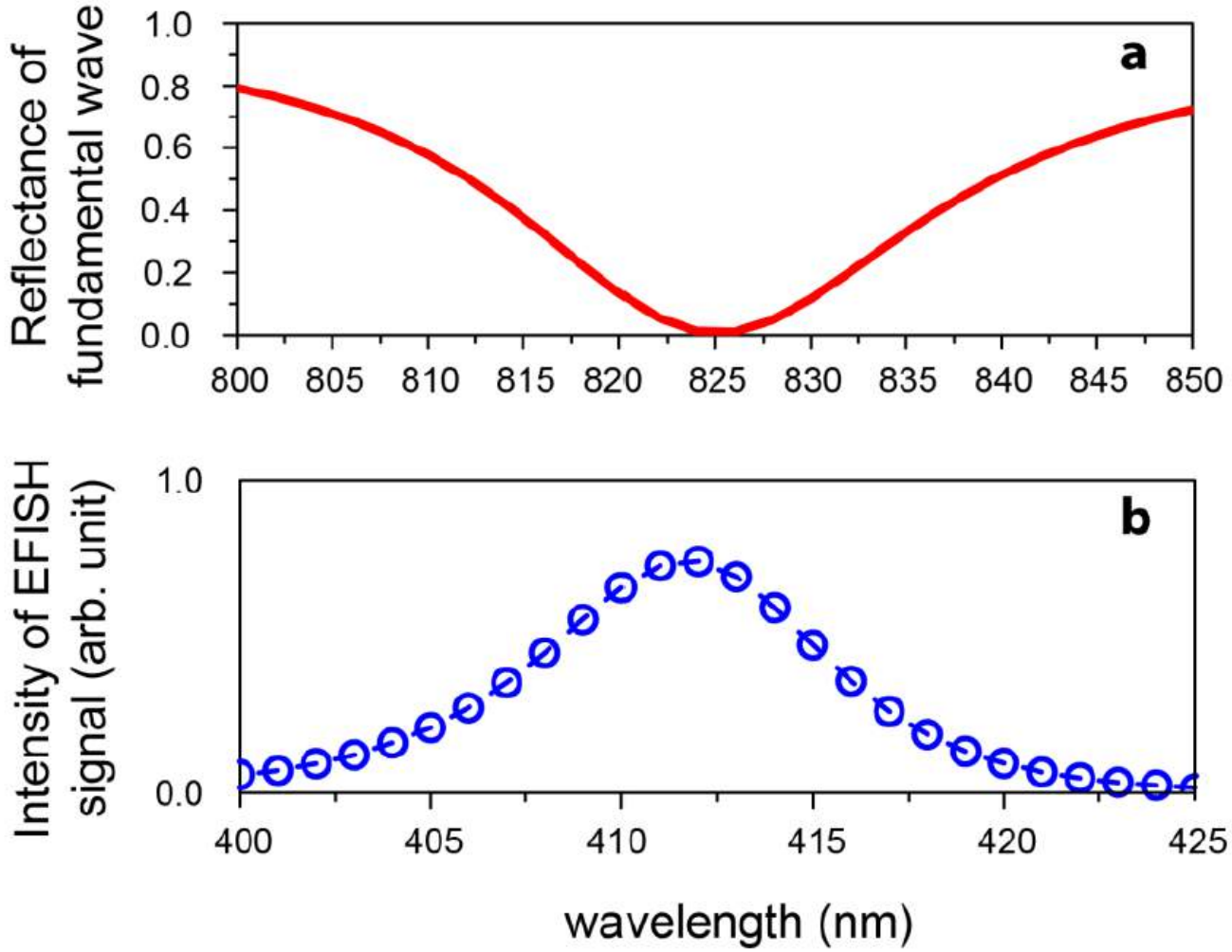

Fig.S5: Simulation results for the distribution of the EFISH signals in both the near- and far-fields.

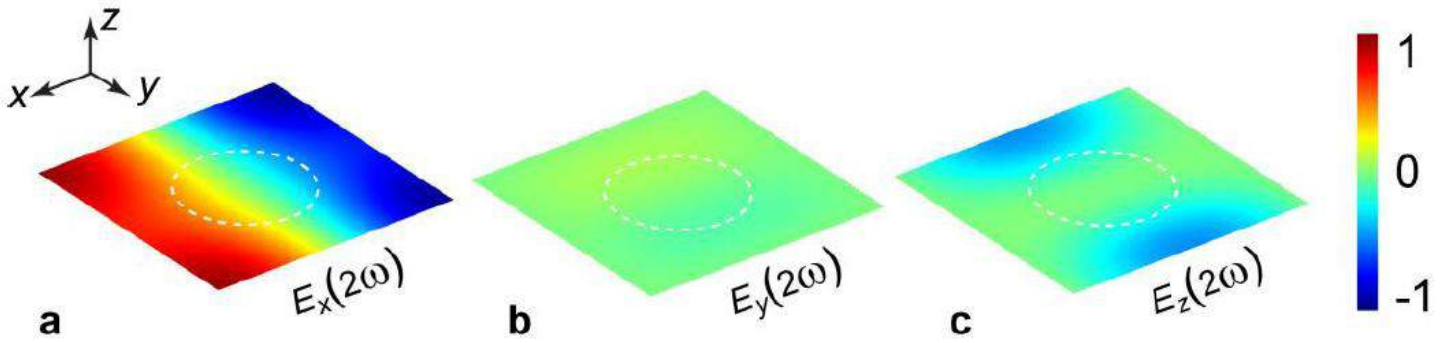

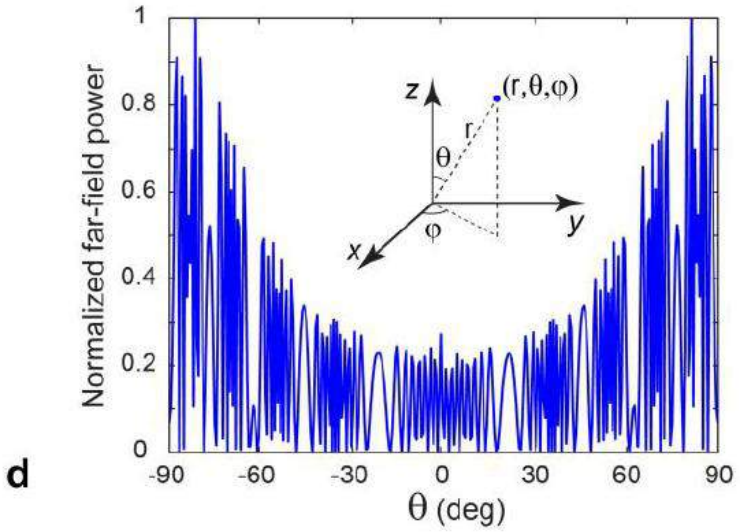

Fig.4 Electrically tunable OR in the metamaterial absorber

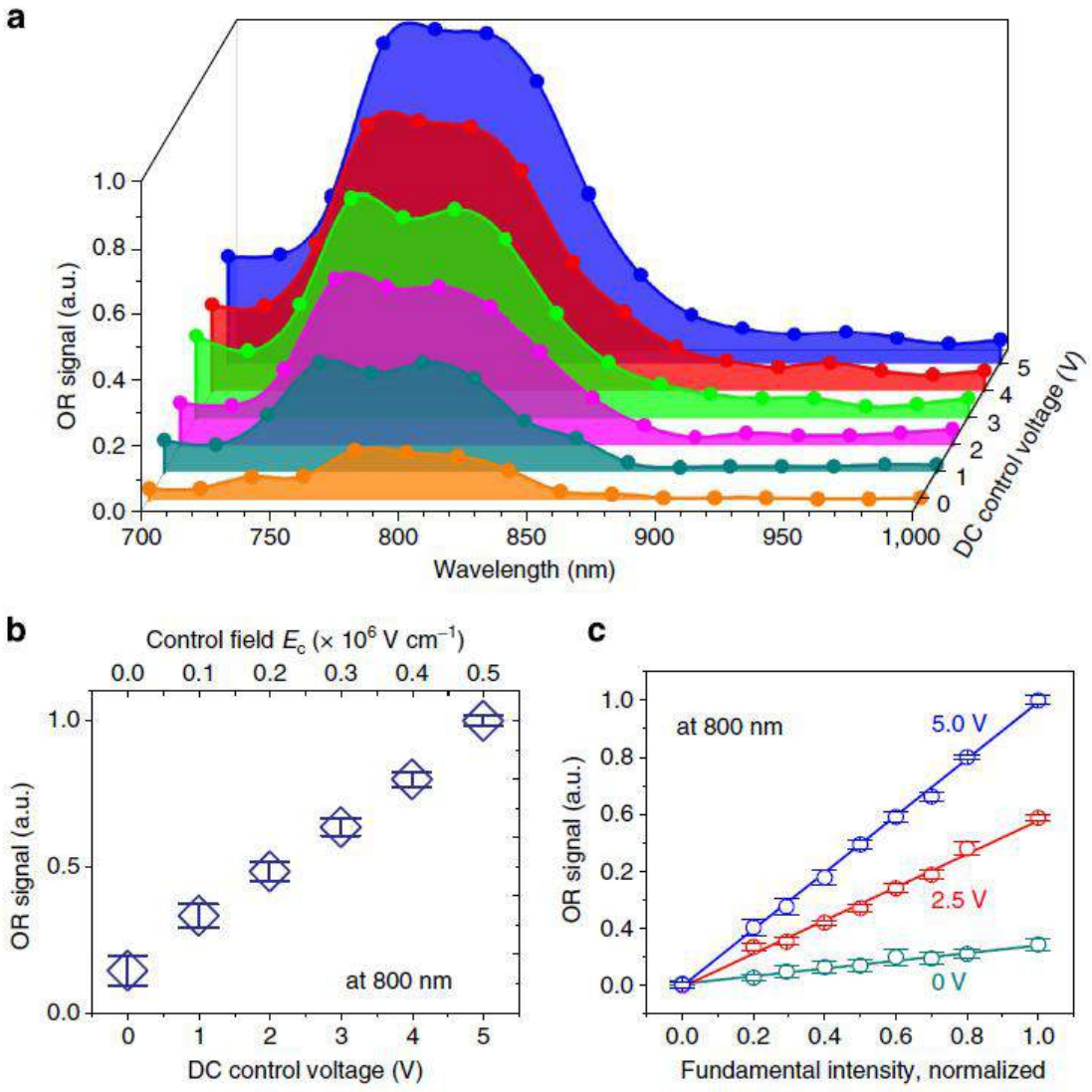

Discussion

Efficiency 2×10^{-11}

$$I_{2\omega} \propto I_{\omega}^{2}\left|\chi^{(2)} + \chi^{(3)}E_{c}\right|^{2}$$

$$\Delta I_{2\omega}(E_{c}) \propto I_{\omega}^{2}\left(\left[\chi^{(3)}E_{c}\right]^{2} + 2\chi^{(2)}\chi^{(3)}E_{c}\right)$$

二等辺三角形の非線形光学効果

Monoclinic:
xxx,xyy,xzz,xzx,xxz,yyz,yzy,yxy,yyx,zxx,zyy,zzz,zzx,zxz

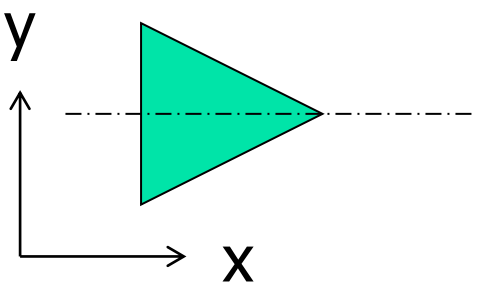

For normal incidence

$$\begin{pmatrix} P_x^{(2)} \\ P_y^{(2)} \end{pmatrix} = \begin{pmatrix} \chi_{xxx}^{(2)}\tilde{V}_x & \chi_{xyy}^{(2)}\tilde{V}_y \\ \chi_{yyx}^{(2)}\tilde{V}_y & \chi_{yxy}^{(2)}\tilde{V}_x \end{pmatrix} \begin{pmatrix} E_x \\ E_y \end{pmatrix}$$

$$\tilde{V}_x = V_x / a, \tilde{V}_y = V_y / b; \quad \text{normalized voltage}$$

$$\mathbf{D} = \varepsilon_0 \mathbf{E} + \mathbf{P}^{(1)} + \mathbf{P}^{(2)}$$

$$= (\varepsilon + \chi_{eff}(\tilde{V}_x, \tilde{V}_y))\mathbf{E}$$

多孔金属薄膜における光整流

PHYSICAL REVIEW LETTERS

Transverse Photovoltage Induced by Circularly Polarized Light

Takafumi Hatano (畑野敬史),[1,2] Teruya Ishihara (石原照也),[1,2,*] Sergei G. Tikhodeev,[3] and Nikolay A. Gippius[3,4]

[1]*Department of Physics, Tohoku University, Sendai, Japan*
[2]*Frontier Research System, RIKEN, Wako, Japan*
[3]*A. M. Prokhorov General Physics Institute, RAS, Moscow, Russia*
[4]*LASMEA, UMR 6602, Université Blaise Pascal, Aubierè, France*

(Received 29 April 2009; revised manuscript received 8 August 2009)

Longitudinal PIV

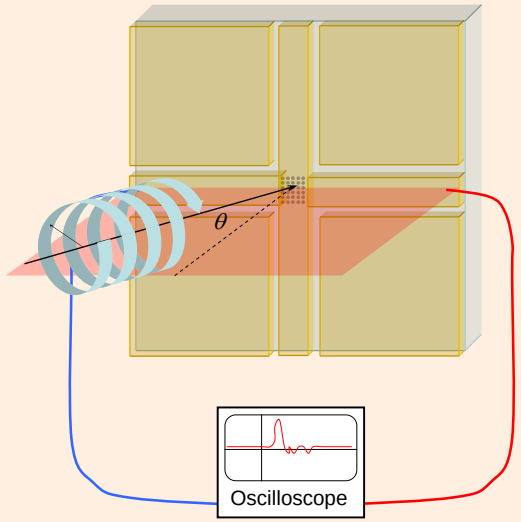

Transverse PIV

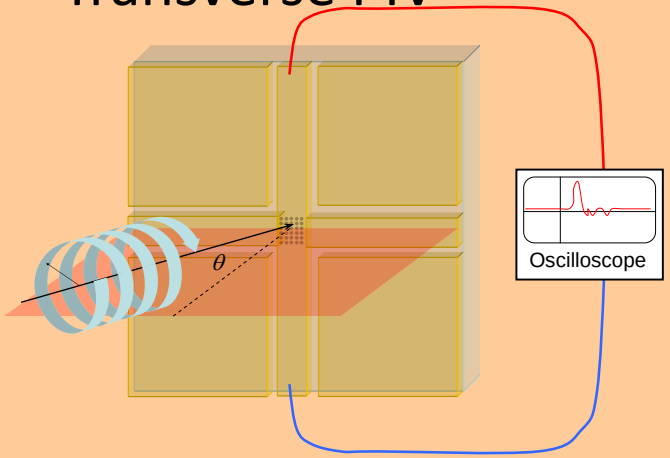

角度分解透過スペクトル

AFM image

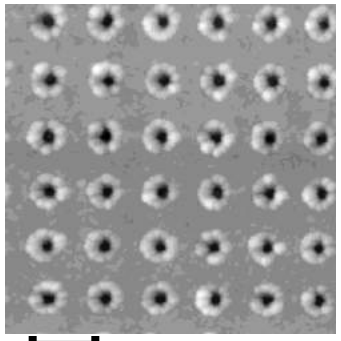

Pitch : 500 nm
Hole diameter : 120 nm
Au thickness : 40 nm
Sample size 0.6X0.6 mm^2

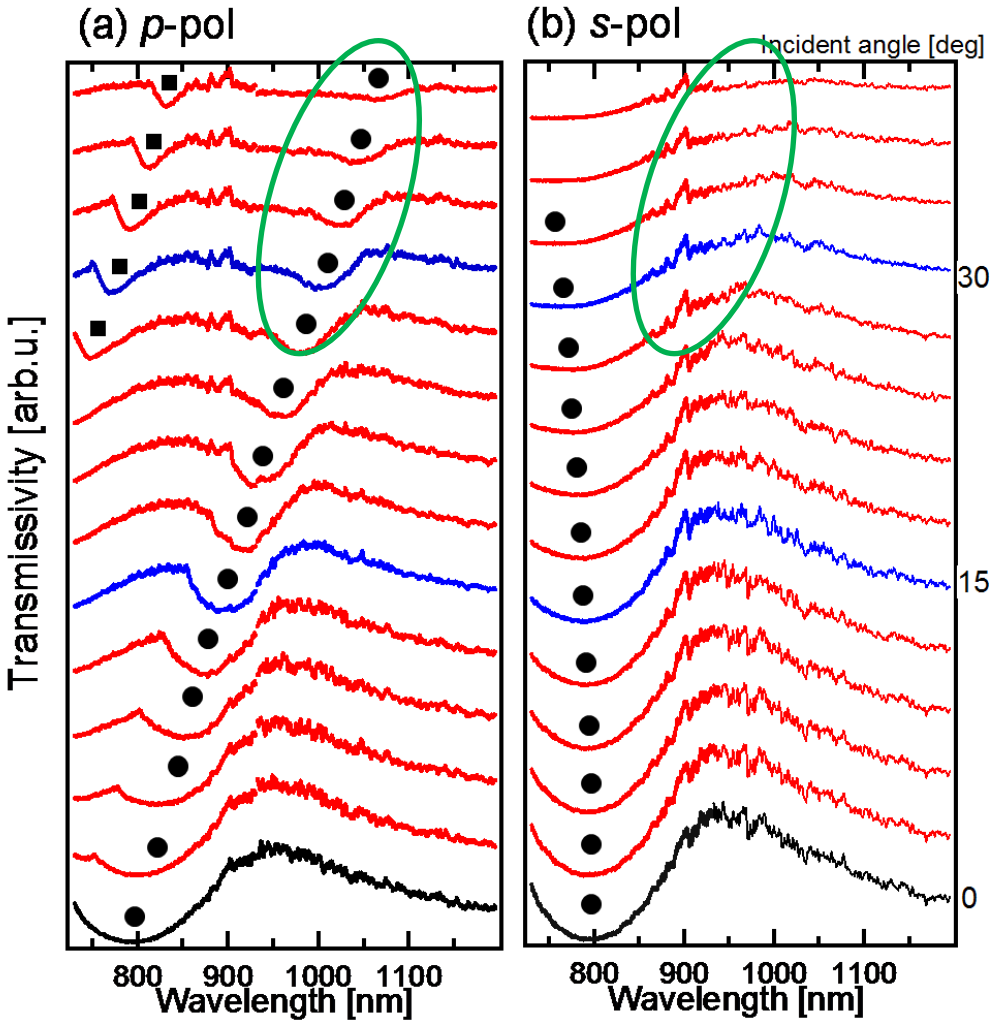

光整流スペクトル

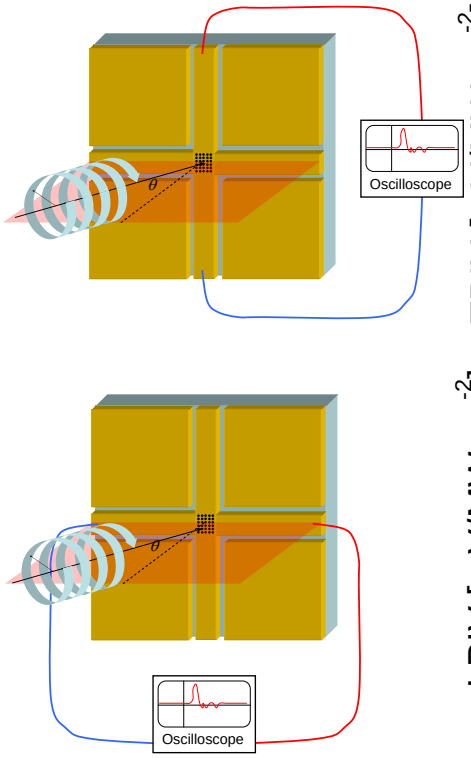
θ
Oscilloscope
θ
Oscilloscope

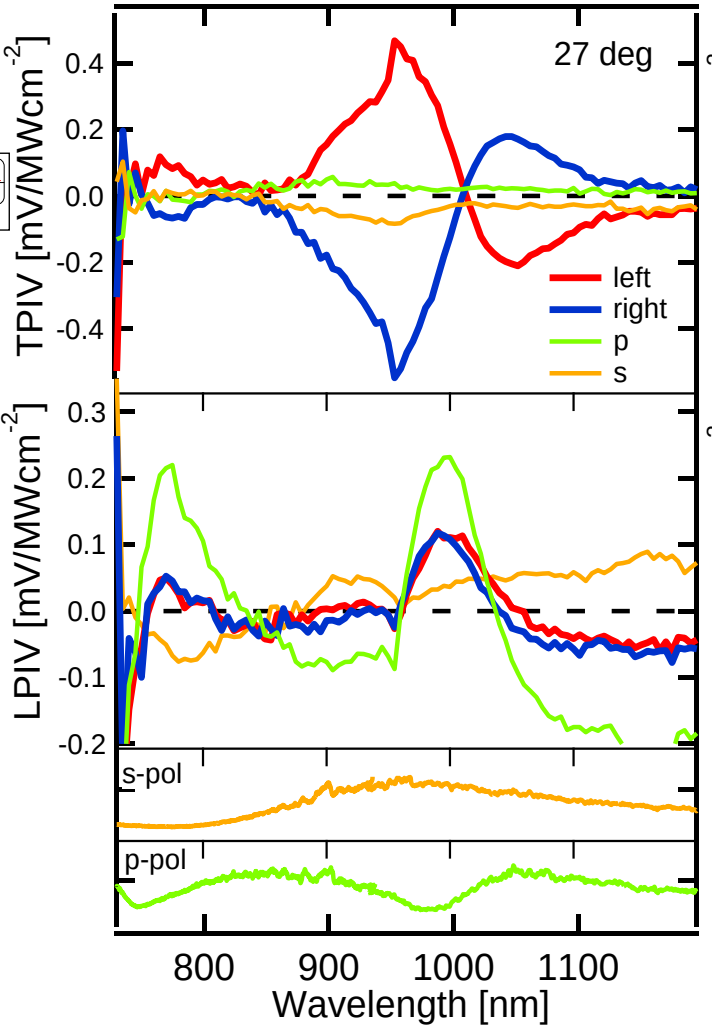
27 deg
TPIV [mV/MWcm-2]
0.4
0.2
0.0
-0.2
-0.4
left
right
p
s
LPIV [mV/MWcm-2]
0.3
0.2
0.1
0.0
-0.1
-0.2
s-pol
p-pol
800
900
1000
1100
Wavelength [nm]

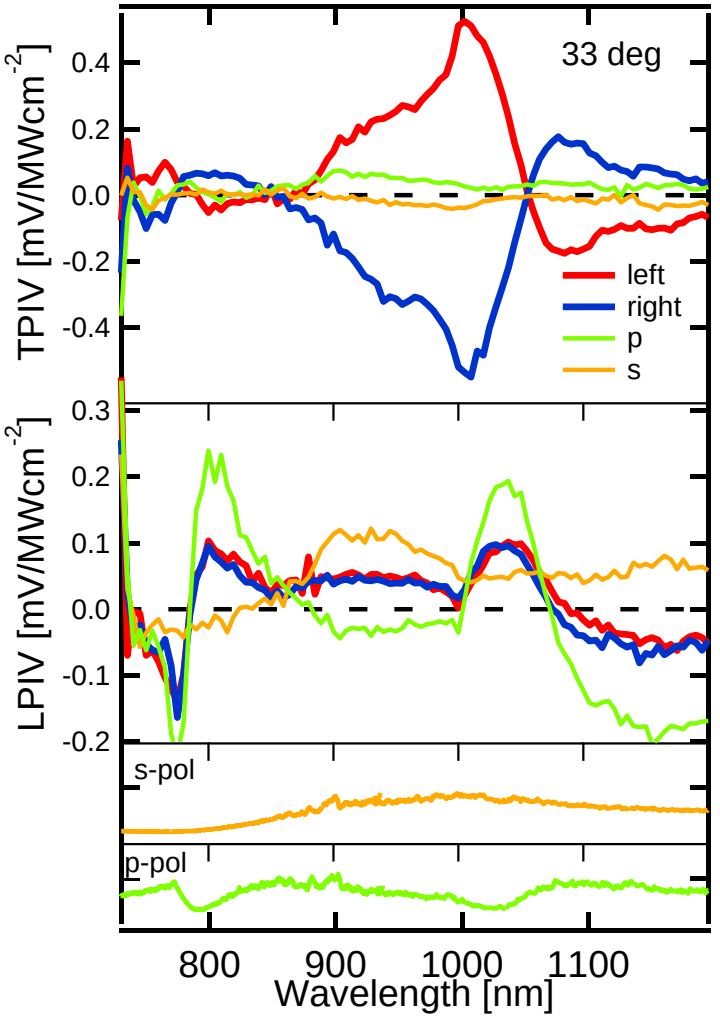
33 deg
TPIV [mV/MWcm-2]
0.4
0.2
0.0
-0.2
-0.4
left
right
p
s
LPIV [mV/MWcm-2]
0.3
0.2
0.1
0.0
-0.1
-0.2
s-pol
p-pol
800
900
1000
1100
Wavelength [nm]

直線偏光励起の電場強度分布

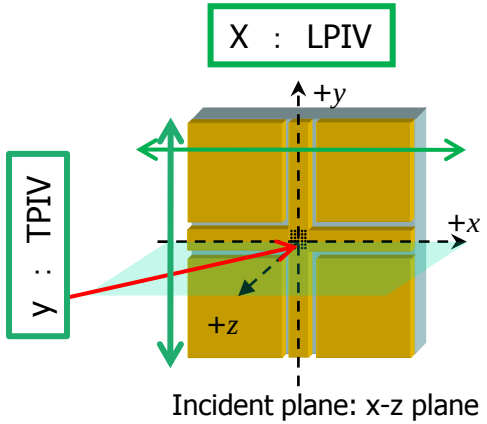

$$\mathbf{F}_{DC}^{(2)}(r) = -\frac{e^2}{4m(\omega^2+\gamma^2)}\nabla|\mathbf{E}|^2$$

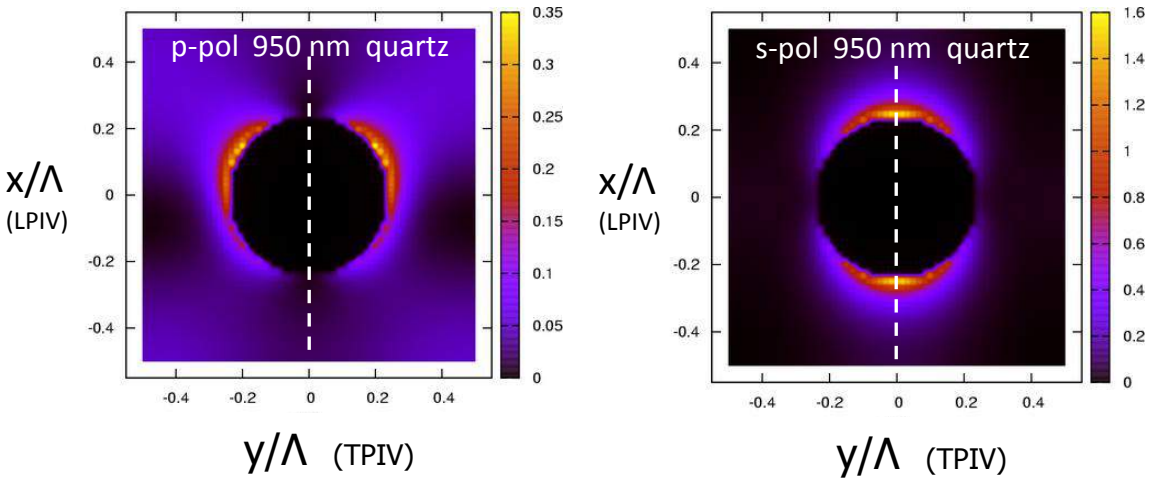

q=27° light intensity @ 8 nm above substrate

$|\mathbf{E}_p|^2$、$|\mathbf{E}_s|^2$ are even function in respect to xz-plane

円偏光励起の光強度分布

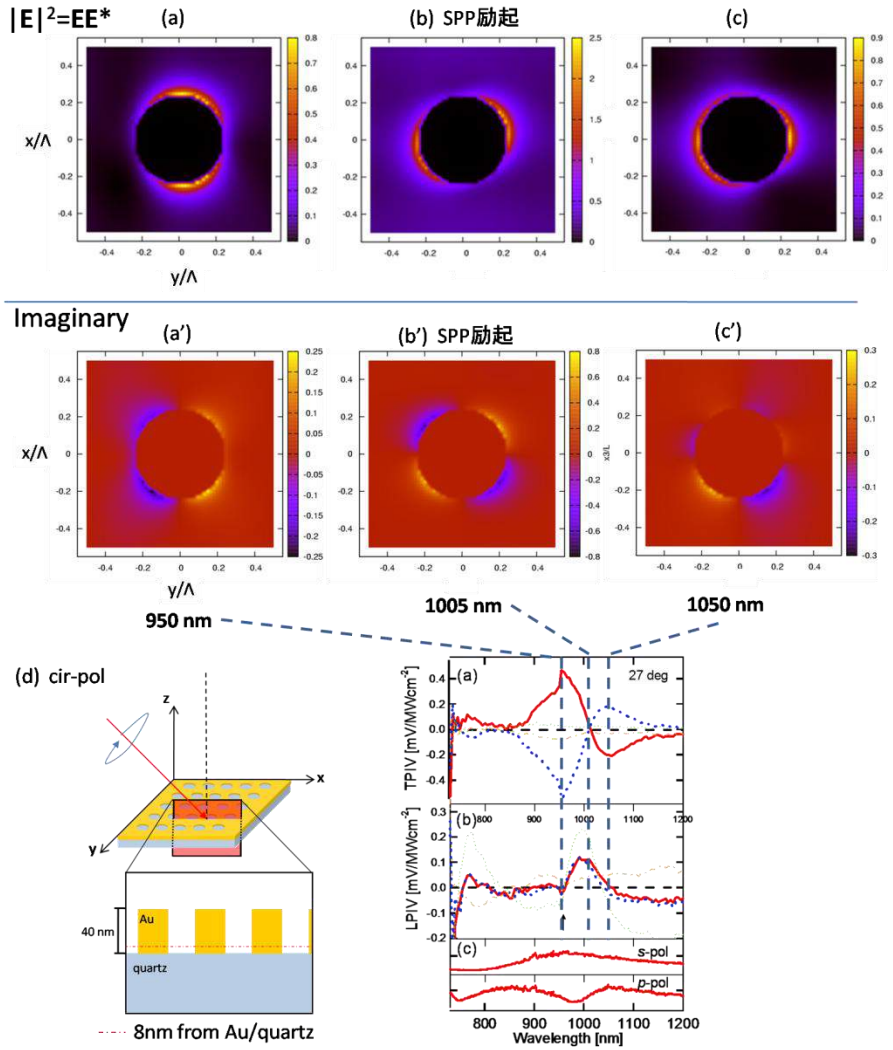

Light field distribution
is not symmetric
along y-direction
for circular polarization.

$$F \sim -\nabla\left|\mathbf{E}_{cir}^{\pm}(\mathbf{r})\right|^2$$

$$= -\frac{1}{2}\nabla(\mathbf{E}_p \pm i\mathbf{E}_s)(\mathbf{E}^*_p \mp i\mathbf{E}^*_s)$$

$$= -\frac{1}{2}\nabla\left(\left|\mathbf{E}_p\right|^2 + \left|\mathbf{E}_s\right|^2 \pm 2\,\mathrm{Im}[\mathbf{E}_p\mathbf{E}^*_s]\right)$$

数値計算との比較

LPIV

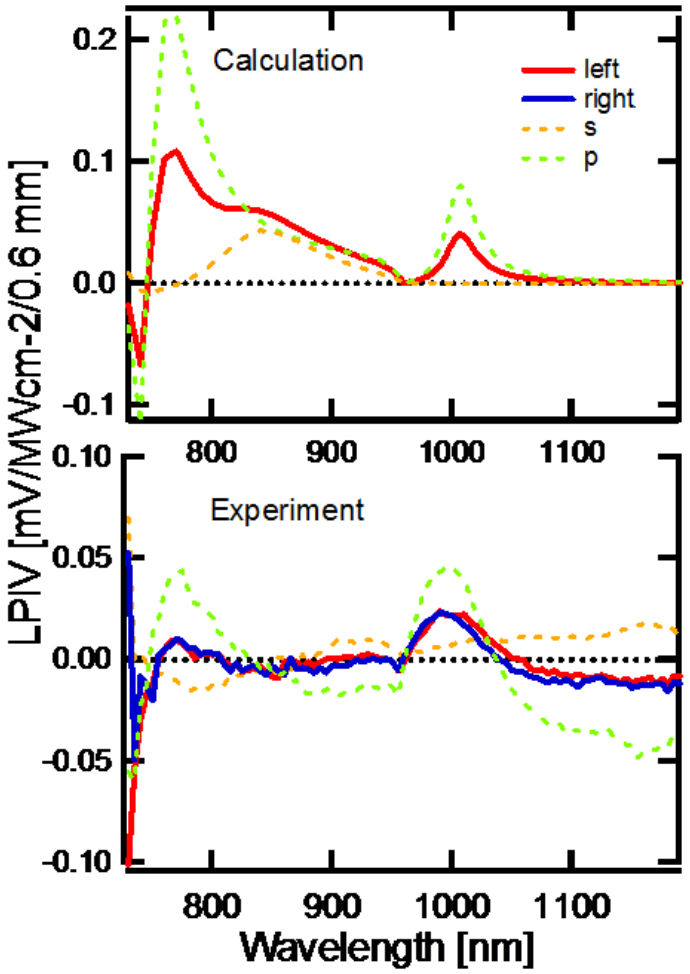

TPIV

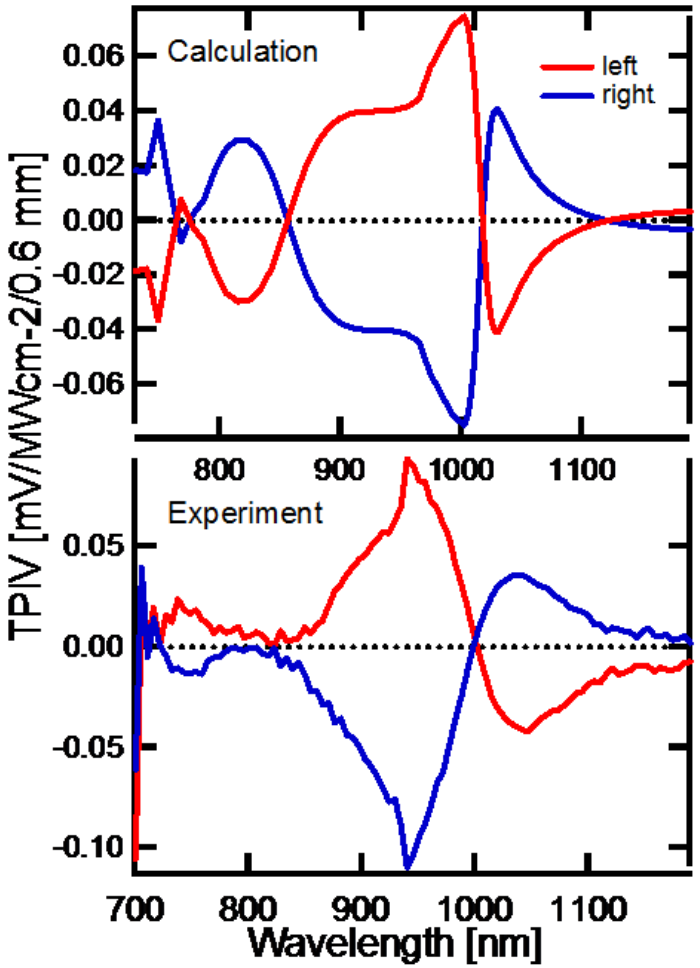

Surface plasmon drag effect in a dielectrically modulated metallic thin film

Kurosawa&Ishihara, OptExp(2012)

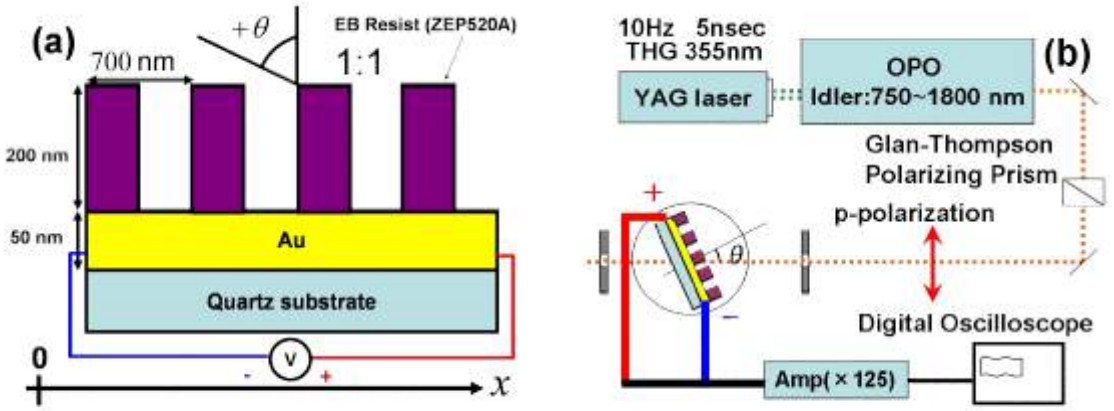

Fig. 1. (a): Schematic of the structure. (b): Experimental setup.

角度分解反射

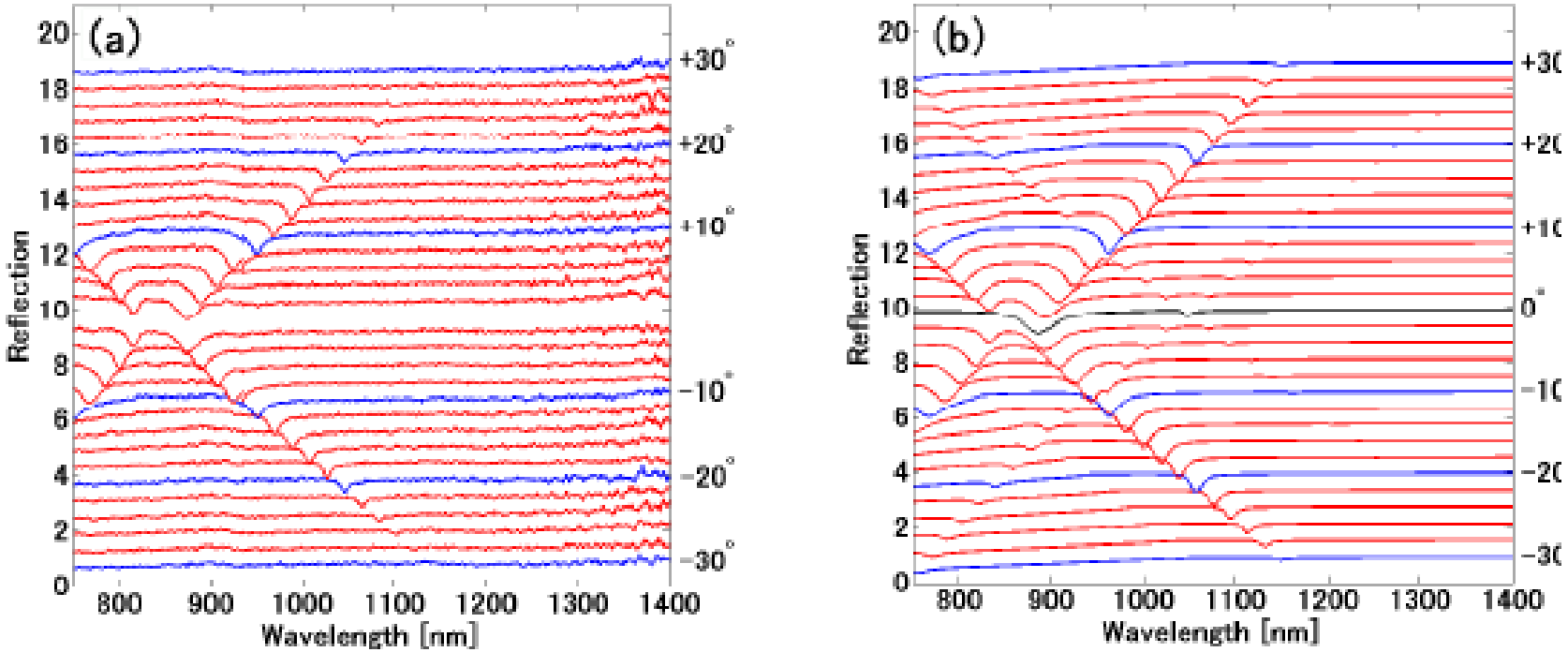

Fig. 2. (a): Experimental result of reflection spectra. (b): Numerical calculation of reflection spectra.

光起電力

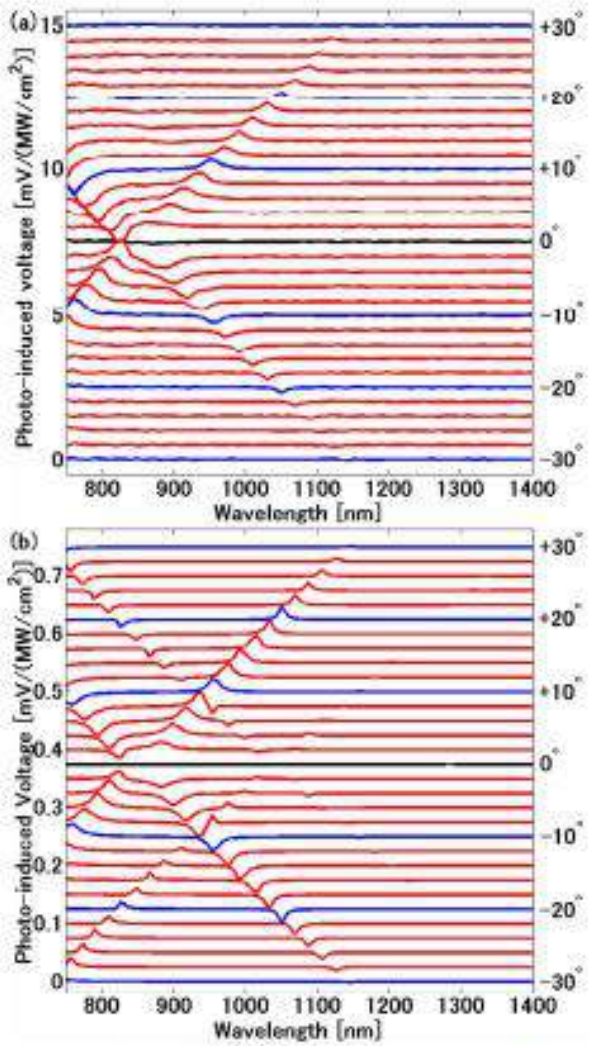

Fig. 4. (a): Experimental result of PIV measurement. (b): Calculation result of PIV evaluated by the microscopic model.

Photo-induced voltage in nano-porous gold thin film

Marjan Akbari,1 Masaru Onoda2 and Teruya Ishihara 1;

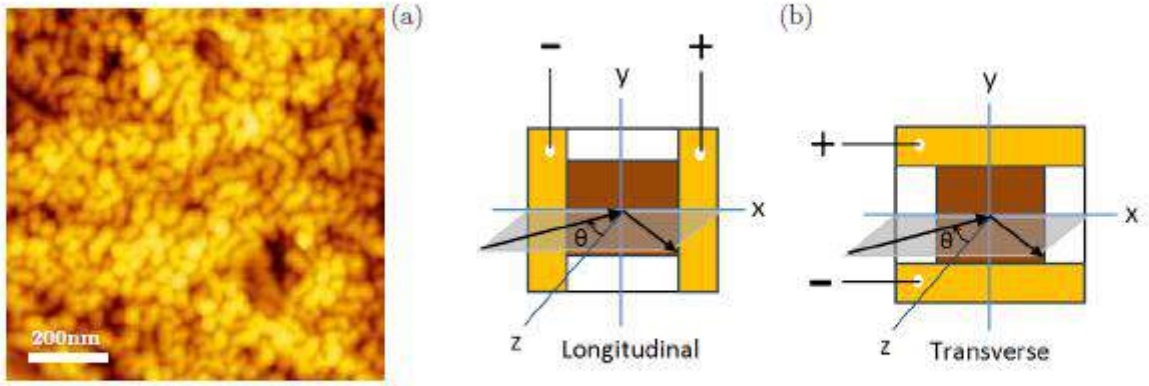

Fig. 1. (a) AFM image of NPG film shows that it is a network of pores and gold. (b) Two configurations for measuring PIV in NPG. The arrow shows definition of the positive incident angle (θ) in the configurations.

横起電力

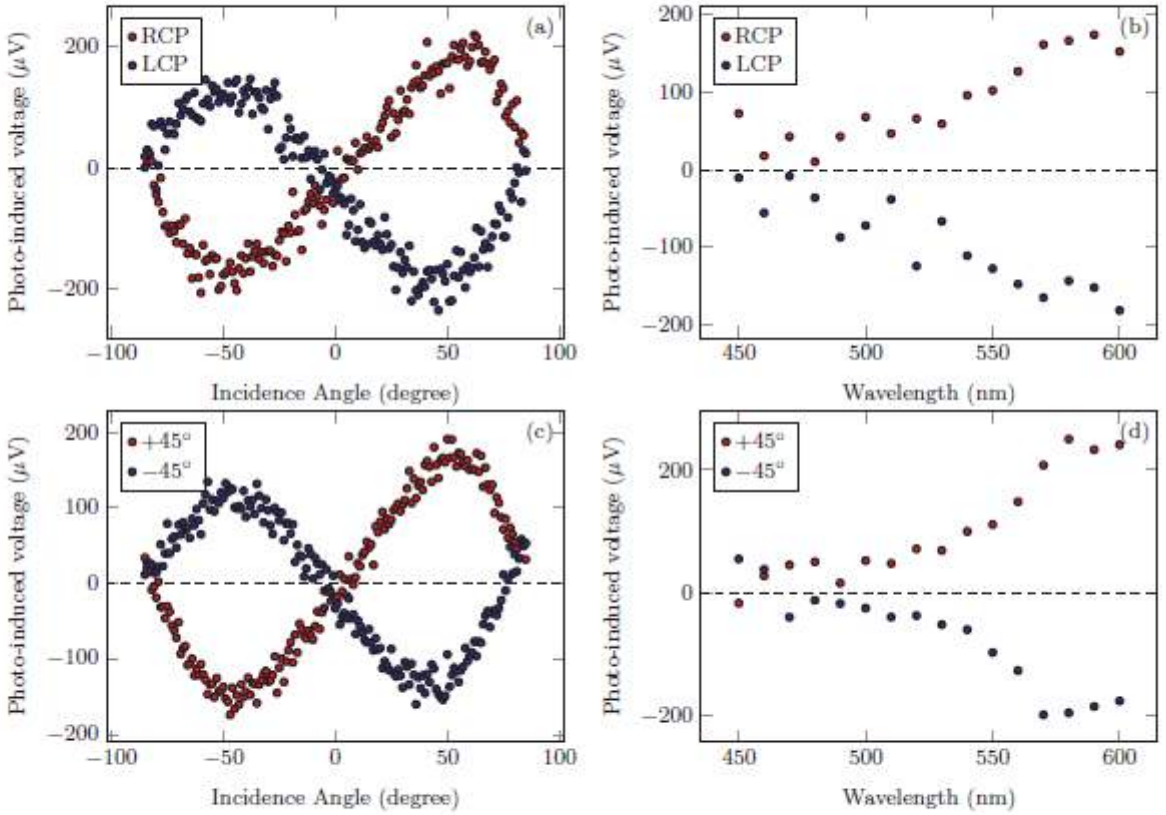

Fig. 4. (a) Angle resolved TPIV for 550 nm, circular polarized light. (b) Wavelength resolved TPIV for +50° incidence angle, circular polarized light. (c) Angle resolved TPIV for 550 nm, ±45° linear polarized light. (d) Wavelength resolved TPIV for +50° incidence angle, ±45° linear polarized light.

縦起電力

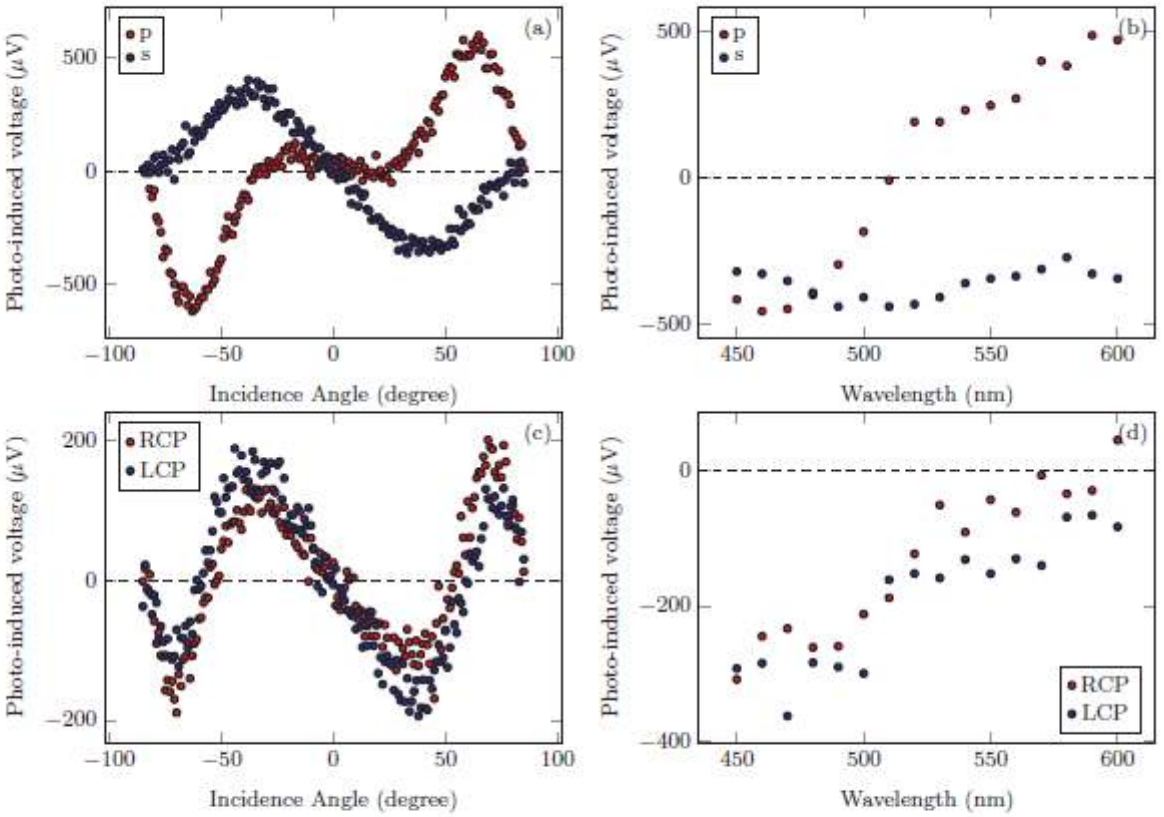

Fig. 5. (a) Angle resolved LPIV for 580 nm, p- and s- polarized light. (b) Wavelength resolved LPIV for +50° incidence angle, p- and s- polarized light. (c) Angle resolved LPIV for 580 nm, circular polarized light. (d) Wavelength resolved LPIV for +50° incidence angle, circular polarized light.

光のスピンホール効果

Luo, …, Zhou,
円偏光の向きによって分離

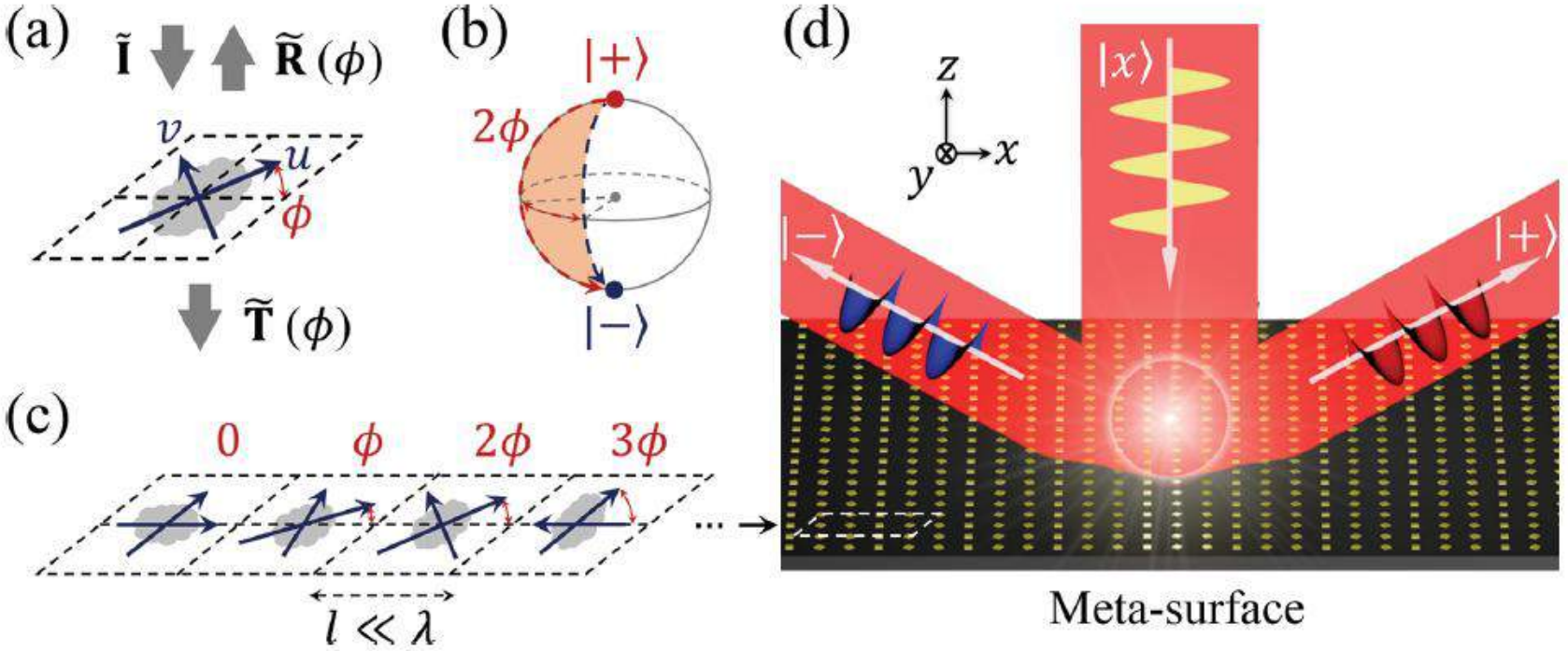

対称性を保った場合

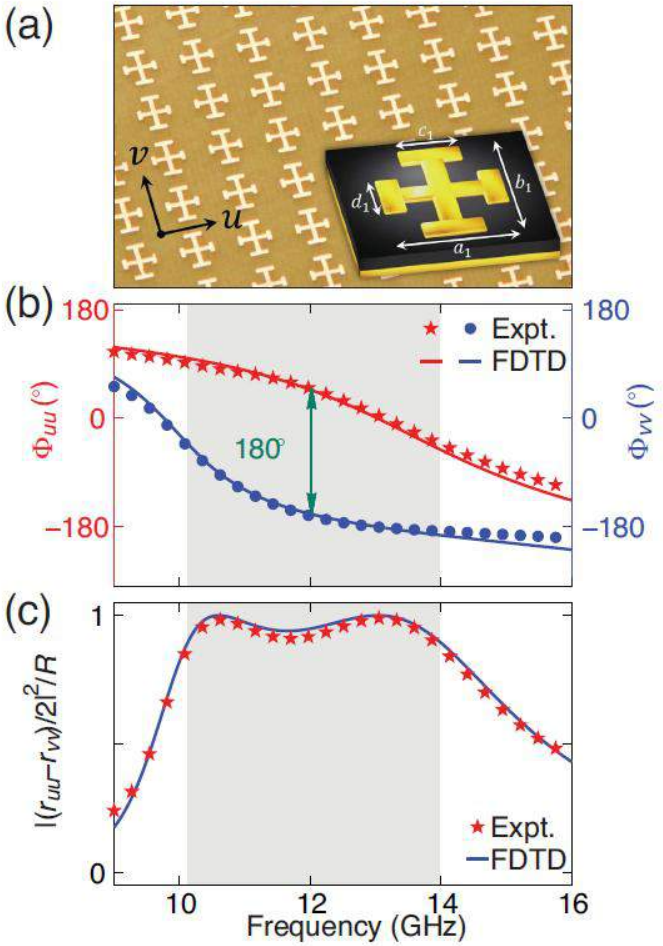
(a)
v
u
c_1
b_1
d_1
a_1
(b)
180
0
−180
Φ_{uu} (°)
Φ_{vv} (°)
180°
Expt.
FDTD
(c)
1
0
$|(r_{uu}-r_{vv})/2|^2/R$
Expt.
FDTD
10
12
14
16
Frequency (GHz)

反転対称性がない場合

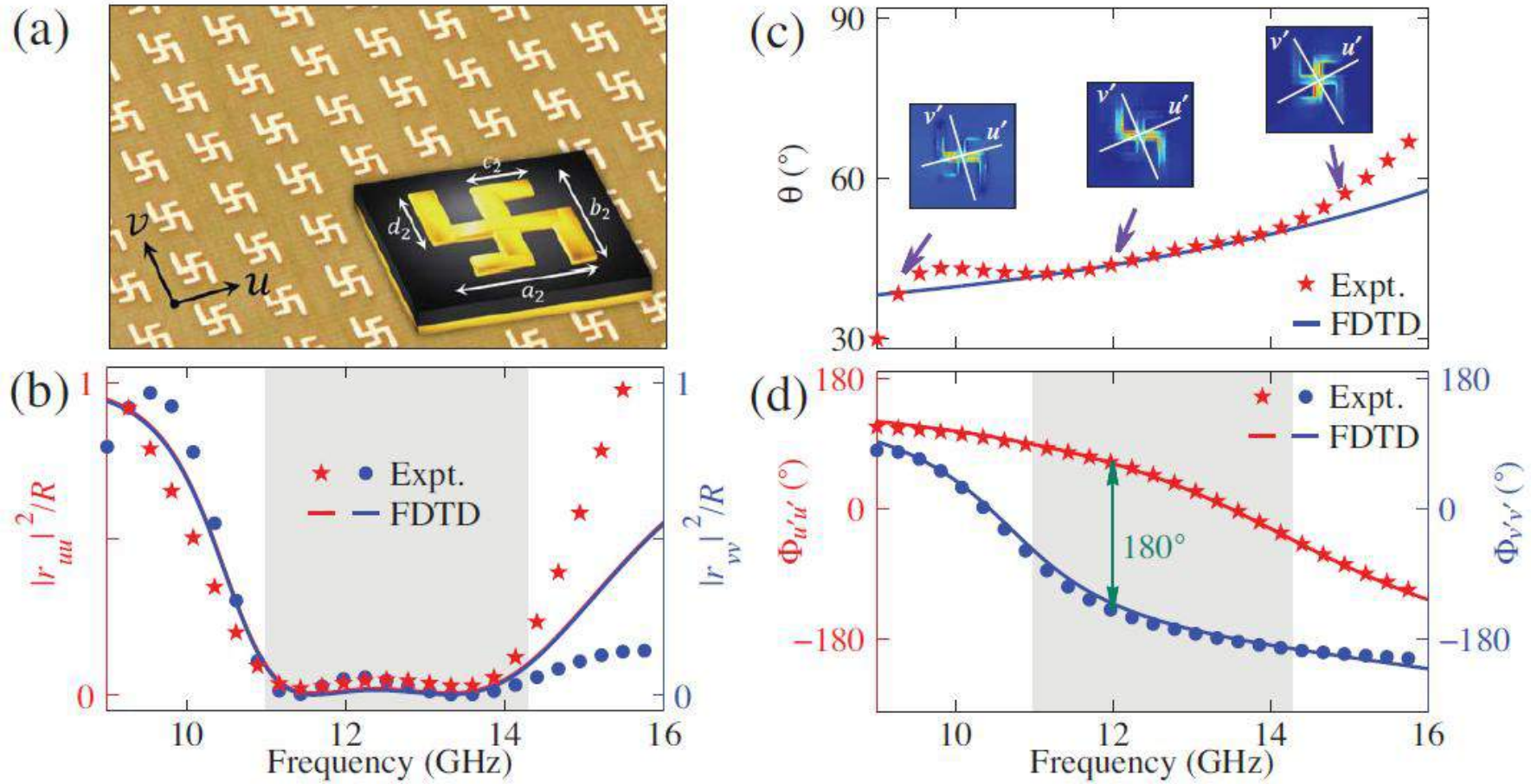

「反射」角度と効率

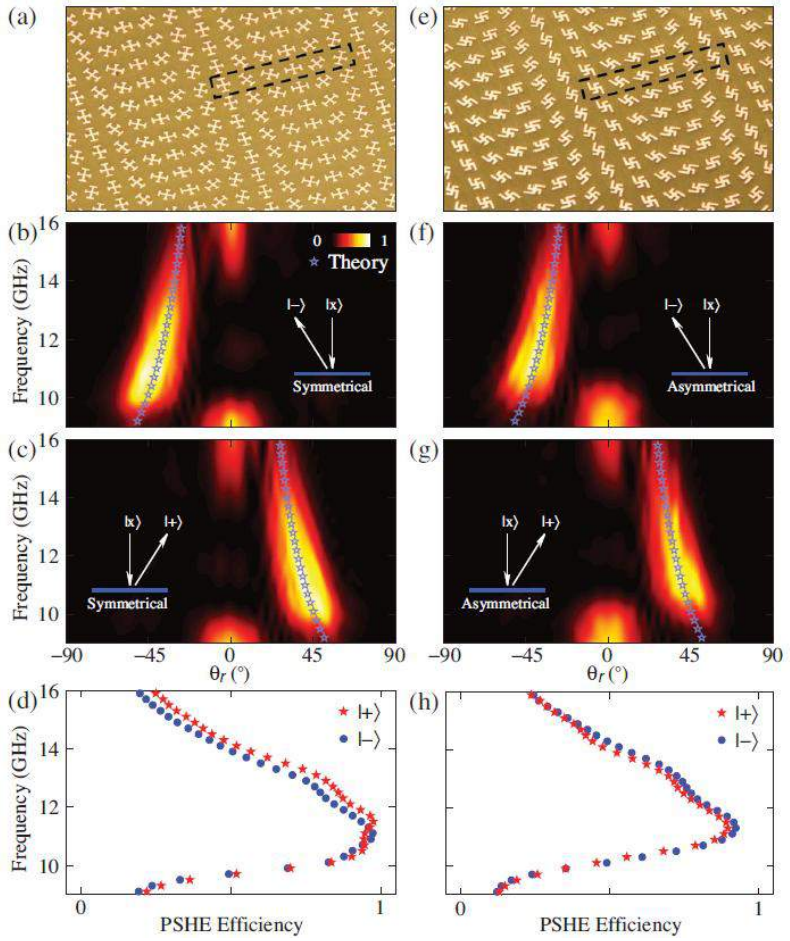
(a)
(e)
(b)
(f)
(c)
(g)
(d)
(h)
Frequency (GHz)
16
14
12
10
0
1
Theory
|–⟩
|x⟩
Symmetrical
Asymmetrical
|+⟩
–90
–45
0
45
90
θr (°)
PSHE Efficiency

入射角度依存性

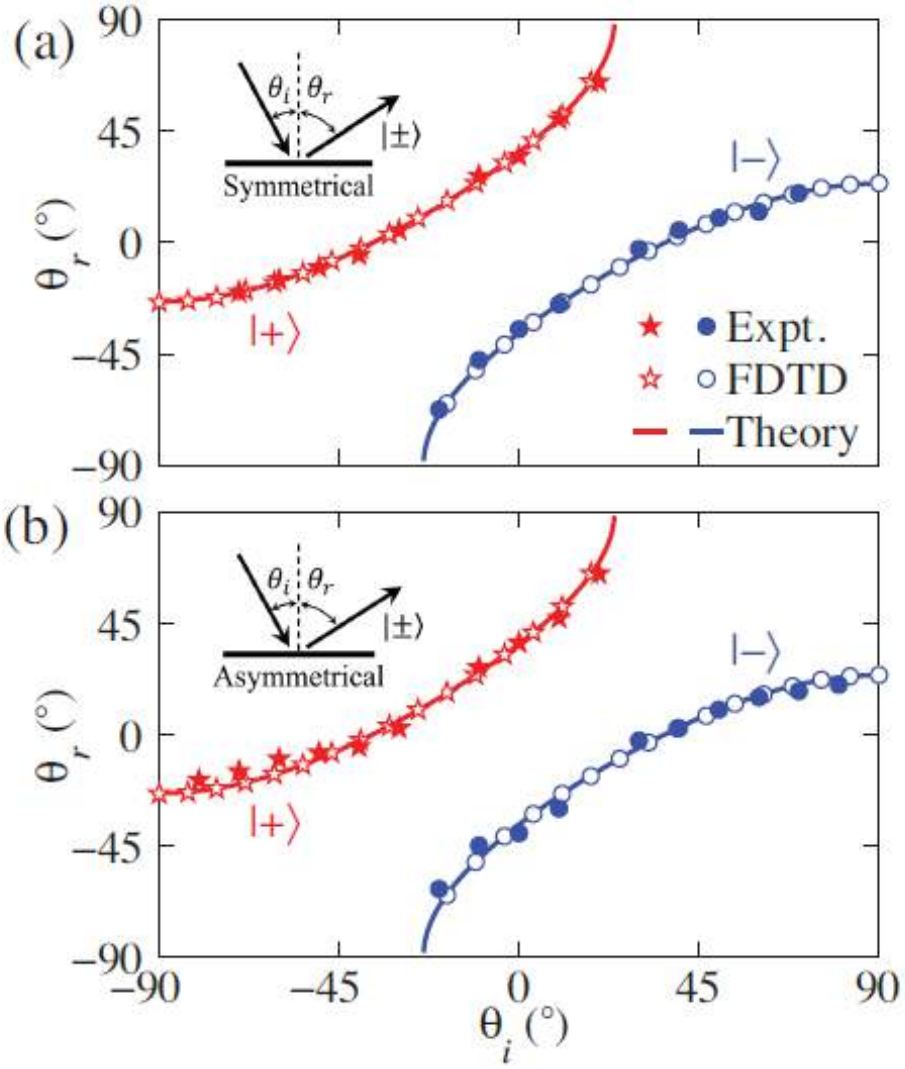
(a)
(b)
90
45
0
−45
−90
θ_r (°)
θ_i (°)
θ_i θ_r
|±⟩
Symmetrical
Asymmetrical
|+⟩
|−⟩
Expt.
FDTD
Theory

まとめ

1. 波長より小さな構造体のデザインを工夫すると電気応答、磁気応答を決める誘電率、透磁率を変えることができる。
2. 誘電率と透磁率が同時に負であると、波の進行方向とエネルギーの流れが逆向きとなり、屈折率は負となる。
3. 誘電率、透磁率が同時に-1の平板では、解像度に制限のない完全レンズができる。
4. 誘電率と透磁率の両方を制御すると、反射なしに、屈折するような物質を作ることができる。
5. 座標変換を用いて、任意に光の進路を制御する手法がある。
6. 異方性のあるメタマテリアルでは大きな波数が実現でき、サブ波長構造を作製するリソグラフィーに応用できる。
7. 多孔性金属薄膜の光整流はプラズモニクスとエレクトロニクスを橋渡しする。
8. メタマテリアルは多くの新概念を生み出す、有効なパラダイム。これらから新しい応用と物理が生まれることが期待される。

近刊予定

「メタマテリアルハンドブック」

講談社サイエンティフィック

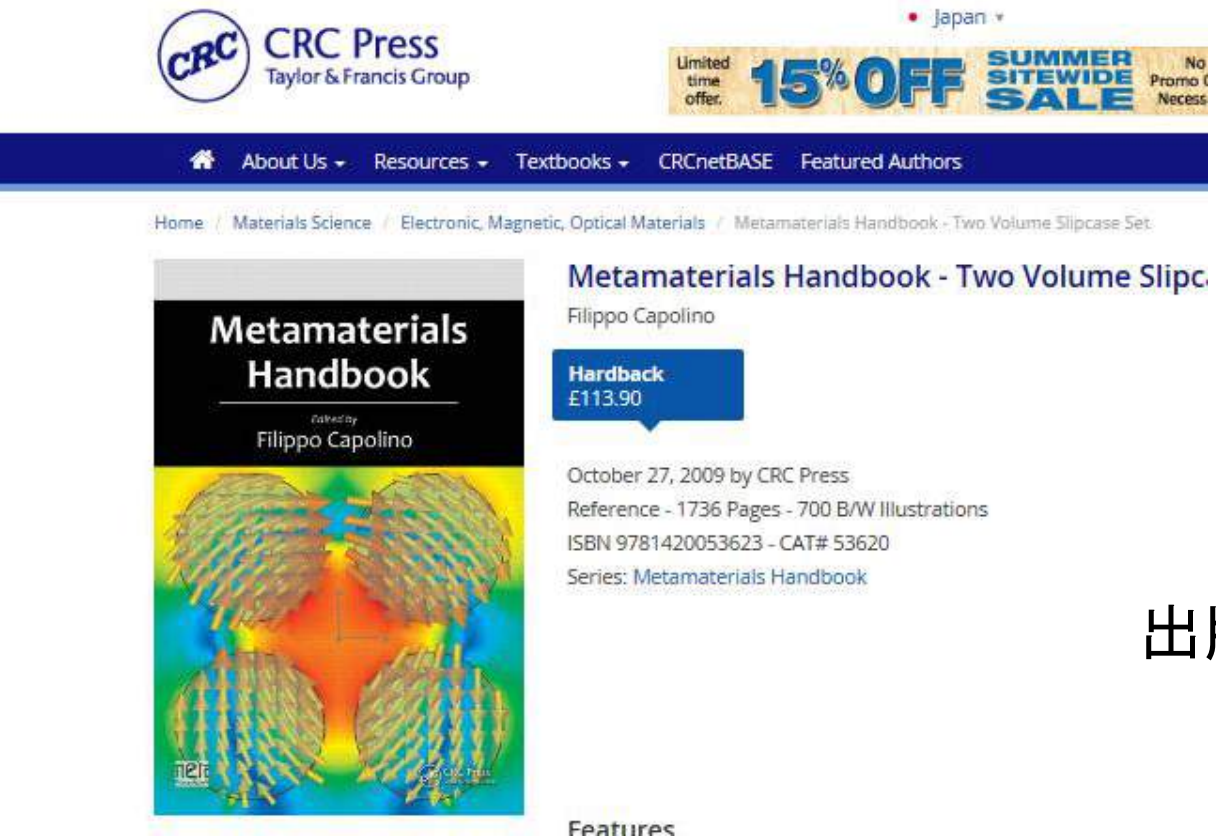

出版予定日　11月10日

電磁場シミュレーション

CST Studio Suite, student edition

種々の制限がつくが、無料で利用可能。

メタマテリアルの木

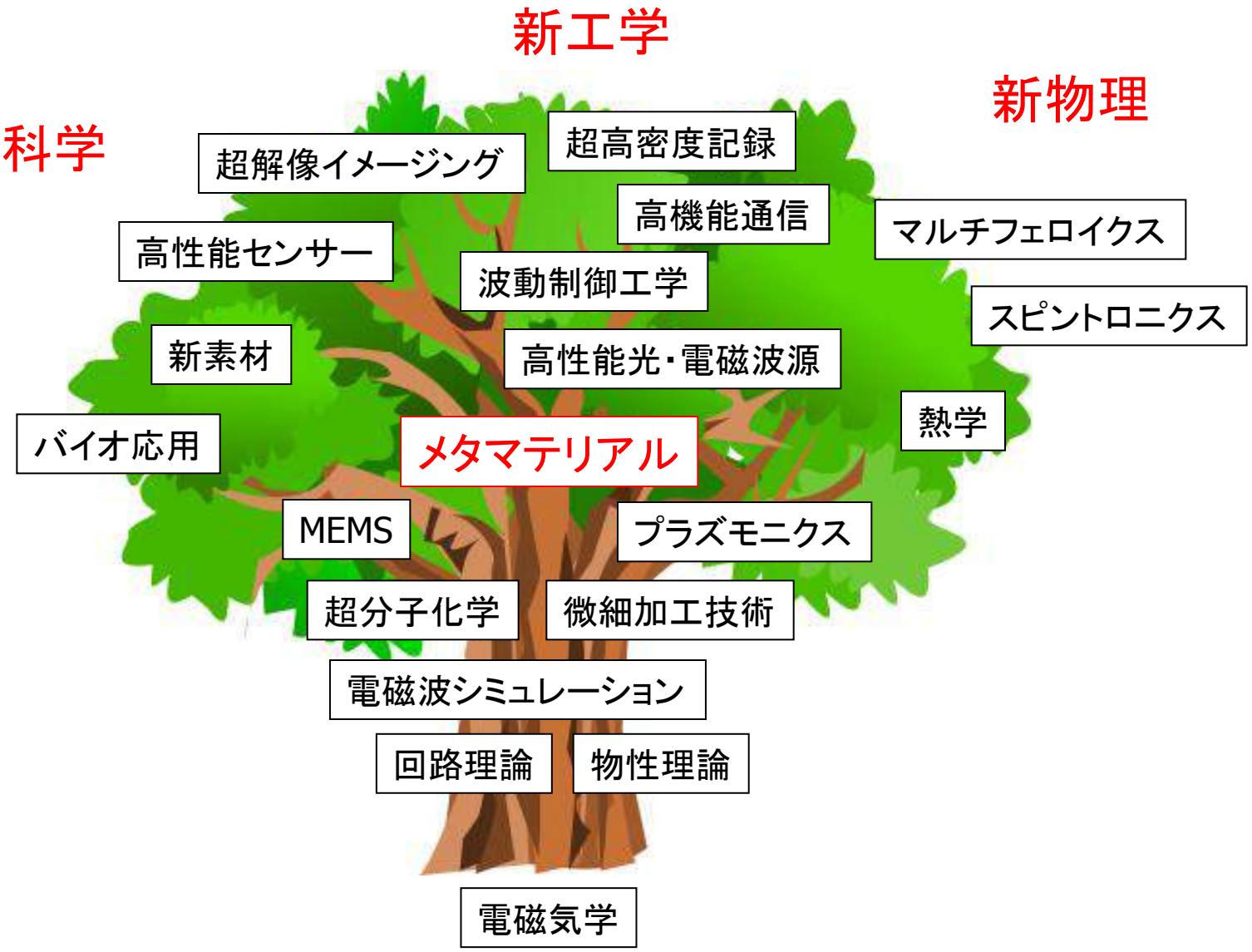
新工学
新物理
新物質科学
超高密度記録
超解像イメージング
高機能通信
マルチフェロイクス
高性能センサー
波動制御工学
スピントロニクス
新素材
高性能光・電磁波源
熱学
バイオ応用
メタマテリアル
MEMS
プラズモニクス
超分子化学
微細加工技術
電磁波シミュレーション
回路理論
物性理論
電磁気学

講義終了

ご清聴ありがとうございました。